THE PENNSYLVANIA STATE UNIVERSITY
SCHREYER HONORS COLLEGE

DEPARTMENT OF ENGINEERING SCIENCE AND MECHANICS

INVESTIGATION OF MAGNETOSTRICTIVE COMB TRANSDUCERS FOR GUIDED WAVE PIPE INSPECTION

MATTHEW D. WALLER
SUMMER 2015

A thesis
submitted in partial fulfillment
of the requirements
for a baccalaureate degree
in Engineering Science
with honors in Engineering Science

Reviewed and approved* by the following:

Joseph L. Rose
Paul Morrow Professor, Department of Engineering Science and Mechanics
Research Adviser

Clifford J. Lissenden
Professor, Department of Engineering Science and Mechanics

Bernhard R. Tittmann
Schell Professor, Department of Engineering Science and Mechanics

Judith Todd
P.B. Breneman Department Head
Honors Adviser

* Signatures are on file in the Schreyer Honors College.

ABSTRACT

Modern society relies on vast networks of pipelines to transport essential commodities including crude and refined fuels for transportation and heating, chemicals destined for refiners and manufacturers, and agricultural fertilizers. Since many of these substances are potentially hazardous to the environment and humans alike, pipeline integrity is an important concern for safety as well as economic reasons. Pipelines are subjected to various stresses throughout their service lives, the most common of which is corrosion. To protect pipes from corrosion and other damaging effects, pipelines are frequently buried underground or sealed with thick coatings. While these steps are intended to protect the pipe, they make inspections for damage especially difficult. Ultrasonic guided waves (UGW) are a promising solution for pipeline inspection because of the demonstrated capability to inspect long ranges, detect defects hidden underneath coatings, and to reliably characterize defects. Specifically, the use of shear waves excited and received by magnetostrictive transducers has shown promise for in-service inspection. To investigate magnetostrictive comb transducers for guided wave pipe inspection, a prototype of a new inspection system available at FBS, Inc. was obtained. The goal of the research was to optimize various instrumentation, actuator, and receiver parameters to see what kinds of inspection problems may be studied with this system. In this thesis, sources of pipeline damage are reviewed, basic elastic guided wave theory is introduced, and magnetostrictive transducer technology is described. A computational model of guided wave propagation is studied and a sample problem is presented. Ribbon cables and MsS circuits of various shapes and apertures were used to excite and measure the SH_0 guided wave mode via the pulse-echo technique in several pipes including a control pipe with targets, a pipe with simulated corrosion, a pipe with real pitting corrosion, and a pipe with a viscoelastic coating. The experimental results are presented and used to compare the different ribbon cables, MsS circuits, and apertures based on performance in detecting and resolving defects for different inspection problems. Raw data is presented, as well as signal amplitude comparisons created using MATLAB.

TABLE OF CONTENTS

LIST OF FIGURES

LIST OF TABLES

ACKNOWLEDGMENTS

First of all I would like to thank my research adviser, Professor Joseph Rose, for introducing me to the field of guided wave ultrasonics and for his support and encouragement throughout my research. I must also thank all of the employees at FBS Inc., as I have enjoyed learning from each of them. In particular I would like to extend my gratitude to Steven Owens for giving me the freedom to pursue an interesting R&D project during my internship, as well as to Dr. Cody Borigo for giving me essential guidance and advice throughout my work. Fellow intern and graduate student Christopher Hakoda assisted me with data collection and analysis for some of the experimentation presented in this thesis. His questions and observations helped deepen my understanding, and I hope he will find this work to have been a learning experience as well. Last but not least I give thanks to my parents for their kindness and support throughout my education.

Chapter 1 Introduction

1.1 Problem Statement

Just as the cardiovascular and lymphatic systems transport vital nutrients and remove waste throughout the human body, pipelines transport the lifeblood of industrialized society. Furthermore, pipelines range in size from large interstate lines to much smaller pipes leading to end consumers, in the same way that blood vessels range from large arteries to tiny capillaries. Since many pipelines transport hazardous materials such as natural gas, pipeline structural integrity is a safety as well as environmental concern. For example, in 2014, 19 fatalities and 95 serious injuries, as well as nearly 300 million dollars in property damage, resulted from pipeline incidents in the United States alone [1]. As of 2008, the natural gas distribution network in the United States contained 305,000 miles of pipeline (including over 8,000 miles in Pennsylvania), according to the U.S. Energy Information Administration [2]. The current network of natural gas pipelines in expected to grow even further, especially in Pennsylvania due to increased production from the Marcellus formation [3]. Recent highly publicized pipeline incidents include the explosion of a 20" diameter natural gas pipeline is Sissonville, West Virginia in 2012 and the explosion of a 30" pipeline in San Bruno, California that resulted in eight deaths and registered as a magnitude 1.1 earthquake [4].

Figure 1: The explosion of a 30 inch natural gas pipeline in Sissonville, West Virginia on December 11, 2012 destroyed several homes and damaged Interstate 77. Amazingly, no one was killed. The National Transportation Safety Board (NTSB) determined that the pipe failure was due to external corrosion and lack of inspections [5].

1.2 Maintaining Pipeline Integrity

To prevent catastrophic accidents like the explosion in Sissonville, the oil and gas industry relies on both inspection and prevention to ensure structural integrity. Inspection for initial defects caused by manufacturing processes, transportation, or assembly occurs as the pipeline is being constructed. At this time, the pipeline is easily accessible and inspection personnel can use a variety of methods, including visual, liquid penetrant, radiographic (x-ray), magnetic particle, eddy current, and ultrasound techniques to inspect pipe segments and their adjoining welds for defects [6]. Material selection, the use of special corrosion inhibitors, protective coatings, and cathodic protection are common strategies to prevent corrosion of pipelines. Despite these best efforts to protect pipes from the corrosive effects of their environment, pipelines are inevitably exposed to environmental factors as well as to other stresses throughout their service lives. Potentially harmful environmental factors include atmospheric and/or soil exposure, moisture, the freeze-thaw cycle, and seismic events. In addition to external corrosion, internal erosion-corrosion and/or flow accelerated corrosion (FAC) on the inner surface of the pipe can also lead to wall-thinning and failure. The possibility of post-construction damage accumulation due to these factors leaves two safe options: either pipelines must be replaced regularly, on a very conservative schedule to ensure a margin of safety, or regular inspections must be conducted using techniques that can reliably detect, locate, characterize, and size defects. The first option is known as schedule or time based maintenance, and the second option is known as condition based maintenance. Regular inspection can often be accomplished by skilled technicians using non-destructive evaluation (NDE) techniques or, in some cases, by sensor laden robotic "pigs" which travel inside the pipeline. As the name suggests, NDE is the process of evaluating materials for discontinuities and other differences in material characteristics without altering the microstructure or otherwise damaging the material [7]. Structural health monitoring (SHM) is another maintenance scheme which incorporates NDE techniques, but uses permanently embedded sensors to detect changes from an undamaged, or baseline, state. SHM offers near continuous monitoring, and can be advantageous over NDE for complex structures, where it may be very difficult to detect and recognize a defect without comparing to baseline data.

.

Table 1: Differences between NDE and SHM. Adopted from Rose [8]

NDE	SHM
• Offline evaluation	• Online evaluation
• Find existing damage	• Determine structural health and remaining service life
• Cost and labor of inspection	• Reduced cost and labor
• Baseline not required	• Baseline required
• Less frequent evaluation	• Environmental data compensation methods required

The field of NDE encompasses a multitude of techniques, each of which has its own advantages and disadvantages. A good overview of current NDE techniques is presented in chapters three through thirteen of the Handbook of Nondestructive Evaluation [9], and some of these techniques are also reviewed in Chapter 2 of this thesis. However, before studying the many available NDE techniques, it is helpful to have at least a basic understanding of the "defects" that these techniques are designed to detect.

1.3 Material Discontinuities and Defects

All engineering materials are made up of discrete pieces, and do not maintain homogeneity at the submicroscopic level. For example, steel is made of many small crystals (or grains), which are composed of atoms arranged in orderly, repeated three dimensional structures (called crystalline lattices), which are in turn composed of protons, neutrons, and electrons. A theoretical physicist might go even further and include elementary particles such as quarks, neutrinos, and the Higgs boson – although that's not necessary for a basic understanding of steel's structure. Inside steel there are grain boundaries, various types of imperfections in the crystalline lattice (vacancies, interstitials, dislocations, etc.), impurities, voids, and possibly phase boundaries. These abrupt deviations from homogeneity and material continuity are known as discontinuities [9]. Despite these discontinuities which are known to exist on the micro-structural scale, engineering materials can usually be well approximated as continuous and homogeneous media for problems concerned with sufficiently large length and time scales [10]. This principle is the foundation of continuum mechanics, and it applies to both solid and fluid media.

In a sense, calculations based on the theory of continuum mechanics do indeed take into account micro-structural discontinuities, since the "sizes, shapes, dispositions, amounts, and character of these microscopic inhomogeneities" influence the properties of engineering materials (stiffness, density, rigidity, etc.) which are used in continuum mechanics calculations [9]. However, especially numerous or large discontinuities do upset the apple cart of continuum mechanics when they go unaccounted for. For example, say an engineer is evaluating a bridge built with A36 structural steel that *in theory* has a yield strength of 220 MPa. If, unbeknownst to the engineer, this particular batch of steel has a high number of slag impurities from poor processing, then the actual yield strength may be significantly less than 220 MPa. If the beam has a large crack, its cross sectional area is reduced, and the stress is increased on the intact part of the beam. Either way, calculations made using the assumed yield strength of 220 MPa and the assumed crack-free geometry could grossly overestimate the strength of the bridge! Hence, it is important for engineers to be able to detect and quantify defects that are large or numerous enough to significantly alter component geometry or degrade material properties.

1.4 Defects: Genesis and Classification

The majority of structural engineering components, including most pipes, are made from metallic alloys such as steel. In a nutshell, producing steel begins with separating iron from ore (a mix of rock and metal that is mined from the Earth), heating the iron to remove impurities, adding the right amount of carbon to create a steel alloy, and finishing with strengthening and/or hardening techniques to achieve the desired material properties. In addition to carbon, iron can also be alloyed with other elements such as chromium to create corrosion-resistant "stainless" steel or with chromium and molybdenum to create chro-moly steel. The microstructure of the resulting steel alloy, and thus the intensive properties of the steel such as strength, hardness, and ductility all depend on the chemical composition of the steel as well as various processes used during manufacturing (cold work, annealing, tempering, etc.) [11], [12]. Discontinuities can be introduced during these processes or at any point in the service life of the final part. An excellent description of how different types of discontinuities are introduced during the manufacture and processing stages of alloys is available in Chapter 2 of Hellier [9]. The time of origin is one way of classifying discontinuities: those that originate during original production of an alloy are called "inherent discontinuities," those introduced during the forming or finishing steps are called "processing discontinuities," and those born during the intended use of a component are "service discontinuities" [9]. The following sections provide a brief overview of some common discontinuities that are particularly relevant to pipe inspection

1.5 Fatigue Cracks

A crack is defined as a planar breach in a material that had previously been continuous [9]. Fatigue cracks are caused by repeated (cyclic) applied loads which induce tensile stresses below the ultimate tensile stress (and sometimes even below the yield stress) of the material [13]. Fortunately, the durability of a material can be evaluated by fatigue testing a large sample of specimens to failure and plotting the resulting data to make what is called an S-N curve (S corresponds to mean stress and N to cycles-to-failure) [12]. With S-N data, cumulative damage and uncertainty models such as Miner's Rule and Weibull analysis can be used to estimate service life [14], [15]. Cracks always initiate on the surface, usually at a point of stress concentration and/or material weakness. Abrupt changes in geometry such as scratches, threads, dents, and notches often serve as stress concentrators and thus as crack nucleation sites [12]. After a fatigue crack is born, it grows incrementally with each stress cycle, gradually reducing the effective cross-sectional area of the part. When the cross-section is reduced beyond a critical point, the part can no longer support the load, and rapid ductile tearing or fast fracture ensues. Viewed through the lens of a powerful microscope, fatigue cracks may be identified by marks called "beach marks" or "clam shell marks" and "striations" that are left on the crack surfaces. Each striation represents the growth from a single loading cycle, while beach marks/clam shell marks represent some break in the fatigue cycle (e.g. equipment being turned off each night and run during the day) [12]. An example of fatigue crack progression viewed under a scanning electron microscope (SEM) is given in Figures 2 and 3. By counting striations or beach marks, it may be possible to estimate the number of cycles to failure.

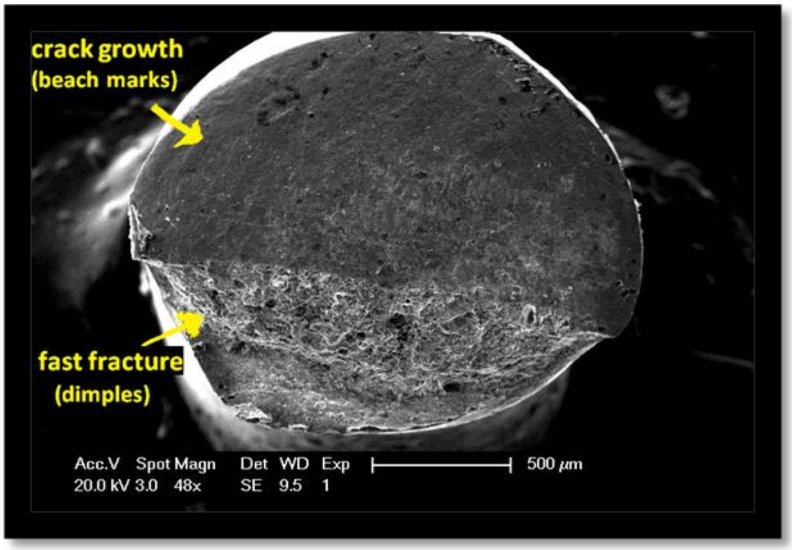

Figure 2: Scanning electron microscope (SEM) image of the fracture surface on a stainless steel bicycle spoke. The distinct crack growth and fast fracture regions indicate failure due to fatigue cracking.[1]

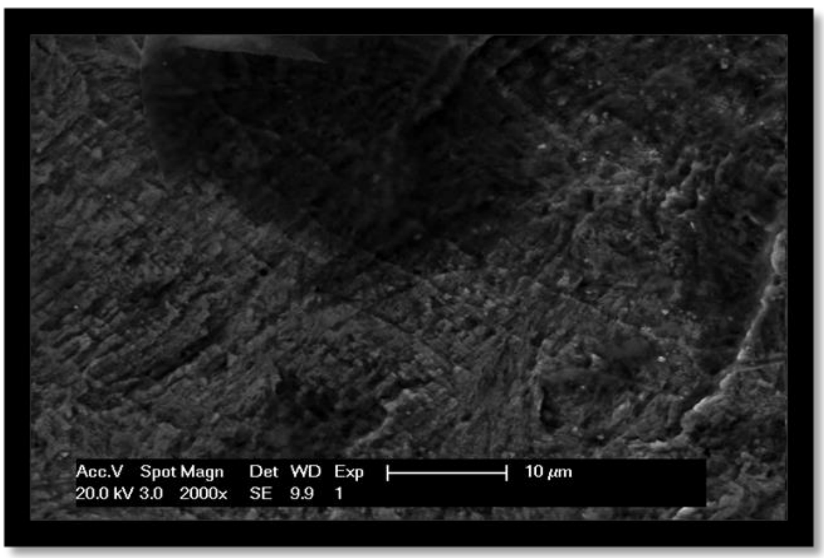

Figure 3: Higher magnification SEM image shows striations due to high-cycle fatigue crack growth on stainless steel spoke.[1]

[1] The images in Figures 3 and 4 were taken with assistance from Penn State ESM Department Research Technician Scott Kralik.

Although fatigue failure is more well-known for its occurrence in moving parts, fatigue is also a serious issue for pipelines and pressure vessels. When pressure is variable, cyclic tensile stresses are induced, and pressure cycle fatigue failure can occur in pipelines, as well as in other pressure vessels. Pronounced temperature gradients can also lead to tensile stresses and cracking – for example, pouring ice cold water into a very hot glass could cause it to shatter, as the author has learned from personal experience. In the same vein, repeated cycles of heat up and cool down can lead to thermal fatigue crack growth. Further, hot water tends to float on top of cooler water in pipe flows leading to a difference in the temperature of the pipe on top of bottom – this temperature stratification, combined with cyclic temperature changes, has contributed to thermal fatigue crack growth in nuclear power plant piping [16].

1.6 Corrosion Pitting

Corrosion is an electrochemical process that frequently occurs on the surface of metals. The effects of corrosion can be so deleterious that corrosion is often referred to as an "attack." Although corrosion prevention may not be the most glamorous branch of engineering, it is certainly important – it is estimated that roughly 5% of an industrialized nation's income is spent on corrosion prevention or on repairing/replacing products damaged by corrosion [12]. Corrosion is actually the combination of two chemical reactions – oxidation and reduction. For example, if iron is exposed to water and oxygen, the iron will give up some of its valence electrons (that is, it will oxidize) and the free electrons will then combine with oxygen that is dissolved in the water (that is, the oxygen will be reduced). The oxidized iron then combines with hydroxyl (OH) ions in the water to form iron oxide, or rust. The net result of this is the conversion of iron to iron oxide, which is undesirable. Corrosive environments are known to decrease the fatigue life of alloy components [12].

A common defect that arises from corrosion is pitting. Pitting is a local attack that occurs when corrosion is concentrated in one area. This localized attack takes place when one area becomes anodic (that is, it is an area where oxidation takes place) relative to the rest of the pipe (which becomes cathodic, that is, where reduction takes place) [9]. Pitting reduces the thickness of the material – in pipes this is referred to as wall thinning – and roughens the surface, which increases stress concentrations.

Figure 4: An example of localized pitting due to external corrosion on a steel pipe.

1.7 Stress Corrosion Cracking

As if the wall-thinning effects of pitting were not pernicious enough on their own, the stress concentrations provided by pitting also act as suitable initiation sites for crack growth. Cracks that originate from pitting are referred to as stress corrosion cracks (SCC), and they may propagate along grain boundaries (intergranular), across grains (transgranular), or both [9]. Similar to ordinary fatigue cracks, stress corrosion cracks may grow due to cyclic loadings and lead to structural failures.

1.8 Flow Accelerated Corrosion and Erosion-Corrosion

Flow accelerated corrosion (FAC) and erosion-corrosion are similar, yet distinct, processes that both lead to wall thinning of the pipe interior. In FAC, the oxide layer which normally shields the pipe surface is dissolved by the pipe flow, which leaves the pipe surface exposed to a corrosive environment. Electrochemical corrosion is then the primary mode of wall thinning. Although FAC can occur anywhere inside of a pipe, it is often localized in areas of high turbulence [17], such as in or near an elbow. Fortunately, FAC can be prevented by using stainless steels [17].

Erosion-corrosion is the combined effect of mechanical abrasion from the pipe flow and simultaneous corrosive attack. Erosion is most likely to occur for two-phase pipe flows due to either cavitation (bubbles in a liquid flow) or liquid impact (liquid droplets in a gas flow), but it can also occur in single-phase flows if the flow velocity is sufficiently high [17] or if abrasive contaminant particles are present in the flow. Wall thinning occurs due to both mechanical wear (erosion) and corrosion. Like FAC, erosion-corrosion is most common in regions of turbulent flow such as bends and elbows [12].

1.9 Welding Discontinuities

Welding is an assembly technique which creates a metallurgical bond between two components. In pipelines, circumferential welds are used to bond adjoining pipe segments in what is called a “butt joint” [18]. Welding is a science in and of itself with many different techniques available such metal inert gas (MIG), tungsten inert gas (TIG), oxyacetylene welding, plasma welding, as well as brazing and soldering [18],[19]. For pipelines, MIG welding is typical. Although pipeline welding is governed by codes, no two welds are exactly alike. Weld characteristics vary depending on the style of the welder and the conditions of the environment. The extreme heat used to melt metal during the welding process also affects the area of the work-piece near the weld joint – this area is termed the heat-affected zone (HAZ). Steel that is located in the HAZ may exhibit a variety of negative effects from the heating and cooling process, including recrystallization and grain growth, residual stresses, phase transformations, and increased susceptibility to corrosion [12]. Some of these effects in the HAZ may be reduced by pre-heating or undone by post-weld heat treatment (PWHT) [9].

The weld itself may also have different structure and resulting material properties than the rest of the pipe. For example, the 316L industrial austenitic stainless steel weld is transversely isotropic (isotropic only in the Θ-Z plane) [20]. In general, welds are often inhomogeneous and anisotropic, whereas the steel in the rest of the pipe is considered homogeneous and isotropic. This discontinuity and the directional material properties of welds must be taken into account when doing finite element or other engineering analyses.

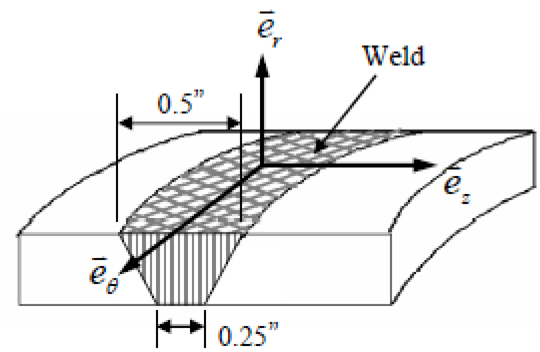

Figure 5: Diagram of a 316L austenitic stainless steel weld in a pipe wall. The weld is isotropic in the Θ-Z plane with anisotropy in the radial (r) direction.2

Besides the micro-structural discontinuities that develop at and near welds, macro-scale discontinuities may also arise. Examples include notches or protrusions along the weld surface from incorrect crown height, lack of fusion or disbonding, contaminations, and lack of penetration [9]. The presence of any of these conditions adversely affects weld strength, and notches/protrusions also serve as stress concentrators for crack growth. Before pipes are welded together with butt joints to form a pipeline, welding may have already taken place during the manufacture of the pipe. Originally, all stainless steel pipes were constructed seamlessly using piercing processes such as the Mandrel mill process or Mannesmann mill process [21], but owing to improvements in welding technology, pipes with welded seams have become more popular [22]. Welds from manufacturing are done in a more controlled environment than those done in the field, so greater quality control can be expected. Pre-heating and PWHT techniques

[2] Used with permission from L. Zhang [20].

that might be difficult to perform in the field may also be done at the factory to reduce detrimental effects in the HAZ. Preliminary NDE techniques such as eddy current or radiographic testing are also sometimes employed at the factory to ensure quality control of seam welds [22]. Despite these efforts, the possibility for defects at welds always remains, and the properties of welds must be considered on a case-by-case basis. For those more interested in either the practical or scientific aspects of welding, ample information is available in the literature (see [9], [12], or [19]) as well as on the World Wide Web (see [18], [22]).

Chapter 2 Overview of Nondestructive Evaluation (NDE) Techniques

The aim of this chapter is to provide a synopsis of some common NDE techniques and highlight their advantages and deficiencies. Particular attention is afforded to the most common methods as well as those with the greatest viability for pipe inspection. For readers interested in a more detailed overview of various NDE techniques, the *Handbook of Nondestructive Evaluation* by Hellier [9] is an excellent resource.

2.1 Visual Inspection

Visual inspection is likely the oldest NDE technique, and it remains a useful option. When the inspector has an unobstructed view of the part, the most important piece of equipment is simply the human eye. This is referred to as “direct” visual inspection, even when visual aids such as microscopes and measuring tools are used to locate and size defects. When an unobstructed view of the part is not unavailable, other tools can be used to gain visual access.

This is termed “indirect” visual inspection. Examples of tools used for indirect visual inspection include the borescope (which was originally developed to inspect the bores of rifle and cannon, hence the name) and remotely controlled camera probes [9]. Although visual inspection is simple in principle, various optical effects (light intensity, reflectance, surface texture, temperature effects, etc.) as well as human factors of the viewer, can affect the results and therefore must be considered [9].

The advantages of visual-inspection are its low cost and good reliability for locating, characterizing, and sizing large surface defects. Access is a primary limitation – many surfaces are simply not accessible to the human eye or to other equipment which could deliver an image to the human eye. Visual inspection is also limited to spotting surface defects, and inspection of large structures with a high level of scrutiny would be time-consuming and impractical. Given that pipelines are often very large structures, and that the pipe surface is often obscured by a protective coating or subterranean location, visual inspection is not a well-suited technique for inspecting pipelines. However, visual inspection does retain usefulness for checking welds for defects prior to a pipeline being coated and/or buried.

2.2 Liquid Penetrant Testing

Liquid penetrant testing (PT) is believed to have been originally developed by the railroad industry in the 1800s [9]. During this time, what was referred to as the “oil and whiting” method was used. This method involved four simple steps: soak the surface of the part to be inspected in dirty oil, clean the surface off, apply a chalky powder to the surface, and wait for oil to seep out of defects and reveal their locations with stains in the chalk [9]. Although the materials and the process have been refined over the years, the procedure remains the same: clean the surface, apply a penetrant, give the penetrant time to flow into the defects (known as “dwell time” or “soak time”) , clean excess penetrant from the surface, and apply a developer to increase the visibility of stains left by bleeding penetrant [23]. Since penetrant testing is really a clever way to make surface defects visible to the human eye, perhaps it should be classified as an advanced visual inspection technique.

Advantages of PT are speed, simplicity, and low-cost. For steel, the required dwell time is typically 30 minutes or less [24], and the examination can be carried out with minimal equipment - a few rags and spray cans of cleaner, penetrant, and developer are usually all that is required [23]. PT is also well-suited to examining parts with complex surface geometries. Just like visual inspection, PT is limited to surfaces that are accessible, is impractical for inspecting large areas, and is restricted to detecting surface-connected defects. For these reasons, PT is not well-suited to pipeline inspection.

2.3 Magnetic Particle Inspection

Magnetic Particle Inspection (MPI) is a NDE technique suitable for detecting surface defects in ferromagnetic components. The basic principle of MPI is that material discontinuities cause variations in the magnetic flux density of magnetized regions, which can then be observed by applying magnetic particles (either dry or suspended in a liquid carrier) to the surface [25]. The first steps of MPI are to clean and magnetize the part. Magnetization can be accomplished by applying electric current or an external magnetic field. To enhance portability for field testing, batteries may be used as the power source. In order for a material to be susceptible to magnetization, it must naturally consist of many smaller regions, or domains, which are inherently magnetized. Magnetic domains can be thought of as many small bar magnets, which each have a north and a south pole. This theory of magnetic domains was originally developed by physicist Wilhelm Weber, and materials which contain magnetic domains are known as ferromagnetic [9] since they often contain iron. When a ferromagnetic material is in a demagnetized state, its magnetic domains are oriented randomly, hence their magnetic fields cancel each other out and there is no net magnetic field. When an external field or electric current is applied, the domains align, their magnetic fields add together, and the part acts as a single large bar magnet. This process is known as magnetization. The strength of the magnetic response exhibited by a ferromagnetic material exposed to an external field or electric current is quantified as permeability, or relative permeability when compared to a vacuum. A material in which the magnetic domains align more completely to form a strong magnetic field under a given external field or applied electric current is considered to have greater permeability than a material which exhibits a weaker magnetization response [9]. To make analogies between magnetism and electricity, permeance is to magnetism as conductance is to electricity; reluctance is to magnetism as resistance is to electricity; and magnetic flux is to magnetism as current is to electricity.

When discontinuities such as cracks are introduced to a magnetized material, the magnetic field lines, or flux, are altered. Just as electrical current follows the path of least resistance, magnetic field lines follow the path of least reluctance – which means they will usually remain inside the ferromagnetic material (with its high permeance and low reluctance) and bend around a defect rather than jump through the air to go across a defect [9]. However, ferromagnetic materials can only support a certain flux density – this is known as saturation. If a discontinuity is sufficiently large, the regions near the edges of the defect become saturated and cannot support any more field lines. This results in a leakage field, which is when some of the field lines “jump” out of the part and bridge across the defect through the air [9]. The regions of increased flux density which result from distorted fields and leakage fields are the key to MPI because they attract any small magnetic particles, such as iron filings or dust, thus providing visual indication of surface defects.

Like any NDE method, MPI has advantages and disadvantages. Obvious disadvantages include an inability to inspect non-ferromagnetic materials (including austenitic stainless steels), to detect subsurface defects, or to give information on the depth of surface cracks [26]. MPI may also give false-indications of defects due to changes in magnetic permeability across the part, for example at the interface of weld and base material [26] or at sharp changes in geometry such as corners and threads [9]. When applied electric current is being used to magnetize the part, care must be taken to not apply too much current for risk of overheating or otherwise damaging the material. Advantages of MPI include the short test time, reliability of detecting surface cracks that are perpendicular to the magnetic flux lines, and relatively simple interpretation of results. Although MPI can certainly be useful for inspecting welds or other local areas, it is very limited for other aspects of pipeline inspection. Since MPI has only short range (it is a spot-checking technique), inspecting an entire section of pipeline would be time-consuming and impractical. The inability to detect subsurface defects, as well as defects on the inner surface of the pipe wall, is also problematic.

2.4 Radiographic Inspection

Radiographic inspection is the use of x-rays or gamma radiation to create images of subsurface regions. The high frequency of x-rays and gamma rays allows penetration of materials which are opaque to visible light, making subsurface imaging possible. As radiation passes through material, it is attenuated due to various effects (Compton scattering, photoelectric effect, pair production, etc.) which result from collisions between photons and the atomic structure of the material [27]. When a component is irradiated, regions which are thinner or less dense absorb less radiation because there are fewer collisions between photons and atoms. If a film is placed on the opposite side of the component from the radiation source, the more absorbent regions will cast a lighter shadow since they transmit less radiation [9]; for example, in x-ray images of the human body, bones appear to be white with a dark background. This is because the bones absorb more radiation than does the soft tissue. This same principle, which is well-known for medical imaging, also lends itself to industrial applications. Thinner or less dense sections, such as voids and pores, will cast darker shadows and (hopefully) become apparent to the inspector.

One interesting observation is that radiographic testing is considered to be a nondestructive technique in industrial applications, yet we know from experience that x-ray radiation may cause tissue damage to living organisms. High frequency radiation is more harmful than visible light because it is more energetic, as described by the Planck-Einstein relation (Eq. 2.1), which relates energy (E) and radiation frequency (ν) by Planck's constant (h). X-rays and gamma rays are energetic enough that when they interact with matter, they disturb electron configurations and therefore may alter chemical bonds. It is logical to ask, "How can radiographic testing be a NDE technique if it alters chemical bonds?" This apparent contradiction is reconciled by the fact that metals and living organisms have different structures with different chemical bonds; hence they are affected differently by radiation exposure. Organic materials are held together primarily by covalent bonds (that is, by sharing electron pairs) and these bonds are easily broken by high-energy radiation [28]. In metals, the electrons may also be dislodged by irradiation, but there is a "sea" of free electrons ready to immediately replace any bonding electrons which are displaced [28]. In short, the same radiation that can be so destructive to organic materials has little effect on the structure of metals. Fortunately, inspection personnel can be protected from radiation by new system called SafeRad which uses radiation shields built from highly attenuative material, as well as a focused beam which minimizes stray radiation [29].

Eq. 2.1 $$E = h\nu$$

Radiographic inspection has several advantages. It is reliable, fast, and characterizes the size of defects – that is, it is a volumetric method [9], [29]. Perhaps most importantly, radiographic inspection is capable of detecting subsurface defects. Disadvantages include safety concerns (especially when the new SafeRad system is not used), high cost of equipment, possibility of artifacts from film processing, and limitations on inspection depth due to attenuation [9]. Another disadvantage is that since radiographic inspection projects an image of a three dimensional area onto a two dimensional film, it is difficult to judge the depth of defects [26]. Radiographic testing is well suited to inspecting welds, and for this reason it is widely used in pipeline inspection. However, radiographic inspection is not a long-range technique, and is therefore impractical for inspecting long sections of pipe.

2.5 Eddy Current Testing

The operating principle of eddy current testing (ECT) is electromagnetic induction. The famous Maxwell-Faraday equation (Eq 2.2) states that a time-varying magnetic field can induce a spatially dependent electric field in a conductor, and vice versa. For ECT, an alternating current is passed through a conducting coil located near the test specimen. This alternating current produces a time-varying magnetic field, which induces an electric field in the test specimen. The electric field in the test specimen causes current to flow in loops within the specimen, hence the name eddy currents. The eddy currents produce their own time-dependent magnetic field, which is 180° out of phase with the magnetic field produced by the coil. This phase difference is in agreement with Lenz's law, which states that an induced current will generate a magnetic field which opposes the magnetic field which created it. Discontinuities and variations in material properties (namely conductivity and permeability) disrupt the flow of eddy currents, which in turn disrupts the magnetic field induced by the eddy currents. This disruption alters the magnetic field coupling between the test specimen and the coil, and is indicated by an impedance change in the coil [30]. A more detailed description of the theory behind ECT is available in the literature [9], [30].

Eq. 2.2
$$\nabla \mathbf{x} E = -\frac{\partial B}{\partial t}$$

Advantages of ECT include the availability of lightweight and portable equipment for field inspection, the ability to test a specimen without special surface preparation, the ability to inspect coated specimens, speed of inspection, and the ability to characterize defect depth [9], [32]. General limitations include short penetration depth, inability to inspect nonconductive materials, and inability to reliably detect subsurface defects in ferromagnetic materials [9]. ECT is widely used in the aerospace industry because it is well-suited to detecting cracks in thin sheets [32]. However, for pipeline inspection, the effectiveness of ECT is hindered by an inability to inspect both the near and far sides of thick-walled pipe due to limited penetration depth [32]. Despite this, Olympus NDT is currently marketing a semi-automated eddy current array system designed to detect outer surface cracking in pipelines [33]. The system consists of multiple coils attached to encoders which traverse the pipe axially and circumferentially [33].

2.6 Ultrasonic Inspection

After visual inspection, the use of sound is probably the second oldest NDE technique. For thousands of years craftsmen have been tapping on castings, glassworks, masonry, grinding wheels, and other structures and listening intently for changes in pitch indicative of cracks. Although the technique is ancient, the “tap test” technique was still widely used in the railroad industry well into the 20th century. Skilled workers called “wheeltappers” were employed to check train wheels for cracks by tapping them with a hammer and listening carefully to the pitch of the ring [34]. Unfortunately for the wheeltappers, the human ear is only sensitive to relatively low frequencies, ranging from approximately 20 Hz to 20 kHz – this is known as the audible range. When an object is struck as is done during a tap test, the resulting vibrations depend mostly on the geometry of the test specimen and where is it struck [35], and vibrations indicating small cracks may exist at frequencies outside the audible range. Over the past century, advances in electronics and transducer technology (a transducer is a device that converts energy from one form to another, for example from electrical to sound and vice-versa) have made inspections at frequencies outside the audible range possible. Sound at frequencies above the audible range (>20 kHz) is known as ultrasonic or ultrasound. Owing to its higher frequency and shorter wavelength, ultrasound can be directed in a beam that is less affected by the geometry of the part than the traditional tap test [35], and is also sensitive to much smaller defects.

2.6.1 Review of Acoustics

Before delving further into ultrasonics, it may be helpful to first review the basics of sound, as a good understanding of sound is crucial to comprehending the following chapters. Kinetic energy may pass through a gas, liquid, or solid medium by vibrating the particles of matter in a wave motion. This type of energy transfer is known colloquially as sound, and the science of sound is acoustics. Unlike electromagnetic (EM) waves or gravity waves, sound waves require a medium (gas, liquid, or solid) to propagate – without a medium, there are no particles to vibrate. For this reason, sound is absent in outer space, since most celestial space is a near vacuum. Although sound waves are different from EM waves in this regard, they do share many other wave characteristics. EM waves and sound waves can both generally be described by Eq. 2.3, where c is the wave speed (typically a constant for a given medium), λ is the wave length, and f is the frequency. From Eq. 2.3, it is clear that there is an inverse relationship between wavelength and frequency.

Eq. 2.3 $$c = \lambda f$$

Just as electrical conductors present some resistance to the flow of current, elastic mediums have some opposition to the flow of sound waves. This property is known as acoustic impedance. When a sound wave confronts a change in acoustic impedance, some of the sound energy is reflected and some is refracted. For example, air and steel have different levels of acoustic impedance, so when a sound wave travelling down a steel pipe confronts a cavity that is filled with air, some of the sound energy will be reflected and some will be refracted. The reflection and refraction of sound due to discontinuities in acoustic impedance is the operating principle of ultrasonic NDE.

2.6.2 Longitudinal and Transverse Waves

Sound waves can be divided into two basic types: longitudinal and transverse. In longitudinal waves, particle displacement is in the same direction as wave propagation. Each particle oscillates about its initial position while the wave passes as an alternating series of compressions and dilations. In seismology, longitudinal waves are referred to as “primary waves”, or “p-waves”. In transverse waves, particle displacement is perpendicular to the direction of wave propagation. Transverse waves are commonly called “shear waves” and are referred to as “secondary waves” in seismology because, during an earthquake, their slower wave velocity means that they arrive sometime after the primary waves. Transverse waves can only propagate in mediums that can support shear forces, i.e. solids and extremely viscous fluids. In non-viscous, or *ideal* fluids such as gases and “thin” or “light” liquids such as water, only longitudinal sound waves are possible. In solids, both longitudinal and shear waves may exist, often simultaneously. For this reason, the acoustics of solids is very different, and arguably more complicated, than that of ideal fluids such as air and water. In addition to longitudinal and transverse waves, sound waves in solids can be further described as either bulk or guided waves, as is explained in the following section.

2.6.3 Bulk vs. Guided Waves

Bulk waves, as the name suggests, are sound waves which travel in the bulk of the material. In bulk wave problems, the medium is considered to be infinite; therefore boundary conditions are not considered. The use of sound navigation and ranging (SONAR) in the ocean is an example of bulk wave propagation since the waves travel through the bulk of a very large medium. Unlike bulk waves, ultrasonic guided waves (UGW) require boundaries to propagate [36]. In fact, the boundaries act as guides for wave propagation. Examples of natural wave guides include plates, rods, pipes, and interfaces [36]. Many structures can act as wave guides provided that the wavelength is sufficiently large relative to the dimensions of the structure – otherwise bulk wave propagation takes place [36]. For NDE of pipelines, guided waves offer several advantages over bulk waves as well as over other NDE techniques. Since guided waves may travel long distances along a waveguide, it is possible to inspect long sections of pipe quickly with a probe mounted at a single point. Guided waves can be used to detect surface as well as subsurface defects, may inspect the outer and inner walls of a pipe simultaneously, and may detect surface defects that are hidden underneath paint or other coatings. For these reasons, guided wave ultrasound is very promising for the inspection of pipelines.

2.7 Acoustic Emission Testing

In both the bulk and guided wave variations of ultrasonic NDE, transducers are used to send energy into the structure of interest, and to listen for reflections indicative of defects. These are referred to as “active” methods since energy must be put into the structure. A third acoustic NDE method, acoustic emission testing (AET), which is passive rather than active, has also been developed. When cracks or other discontinuities in a structure are subjected to loading, they may emit energy in the form of sound waves at ultrasonic frequencies [9]. Transducers may be used to listen for noise indicative of cracks or high pressure leaks, or even to monitor the change in noise as cracks grow [9]. Because of the potential ability to monitor structural changes (fatigue crack growth, creep, etc.), AET is well suited to structural health monitoring (SHM) schemes.

2.8 Comparison and Summary of NDE Techniques

The past century has seen a tremendous growth in NDE techniques beyond the age-old visual inspection and tap-tests. New and improved methods such as radiographic inspection and ultrasonic guided waves have been made possible by increased knowledge of fundamental science and mechanics, advances in hardware and electronics, and the advent of the computer age. In addition to the many different NDE techniques, within each technique there exist countless variations and sub-techniques – modern NDE truly is a vast field! Despite the multitude of inspection techniques available, there are still many challenges, unsolved problems, and improvements to be made across the field of NDE. Pipeline inspection presents a particular set of challenges: pipelines are large structures, and they are usually coated or even buried underground. Ultrasonic guided waves hold great promise as a practical solution for pipeline inspection because of their long range, ability to detect defects hidden underneath coatings, and ability to see defects on both the inner and outer surfaces of the pipe wall. A general comparison of ultrasonic guided waves with the other basic NDE techniques overviewed in this chapter is provided briefly in Table 2.

Table 2: General comparison of NDE techniques for in-service pipe inspection.

	Visual	Liquid Penetrant	Magnetic Particle	Radiographic	Eddy Current	Acoustic Emission	Ultrasonic bulk waves	Ultrasonic guided Waves
Detects surface defects	✓	✓	✓		✓	✓	✓	✓
Detects subsurface defects				✓		✓	✓	✓
Detects defects under coatings			✓	✓	✓	✓	✓	✓
Long range inspection								✓
Volumetric				✓		✓	✓	✓
Fast Inspection time								✓

Chapter 3 Ultrasonic Guided Waves

As stated in Chapter 2, ultrasonic waves are sound waves which oscillate at frequencies above the audible range, that is, above 20 thousand cycles per second, or 20 kHz. Bulk waves travel through media which are very large relative to their wavelength, and therefore may be modeled as infinite media. Hence, for bulk waves, boundary conditions are not a factor. When the wavelength is not miniscule relative to the dimensions of the medium, interactions between the wave and the boundaries of the medium occur – this gives rise to guided waves. This chapter provides a basic overview of guided wave propagation with emphasis given to the wave type used in this thesis. More thorough descriptions of guided waves are available in the literature; see Krautkramer [35] or Rose [36].

3.1 Governing Equations

Both bulk and guided waves are governed by the same set of partial differential equations [36]. Plane waves are governed by the famous wave equation (Eq. 3.1), where u is the particle displacement, c is the wave velocity, and t is time.

Eq. 3.1
$$\nabla^2 u = \frac{1}{c^2}\frac{\partial^2 u}{\partial t^2}$$

In general for three-dimensional considerations, guided wave solutions for isotropic media must satisfy Navier's displacement equations of motion (Eq. 3.2), where μ and λ are Lamé constants [36].

Eq. 3.2
$$\mu\nabla^2 u(x,t) + (\lambda+\mu)\nabla\nabla\cdot\mathbf{u}(\mathbf{x},\mathbf{t}) = \rho\frac{\partial^2\mathbf{u}(\mathbf{x},\mathbf{t})}{\partial\mathbf{t}^2}$$

By using Navier's wave equation with specific boundary conditions, the strain-displacement relations, and generalized Hooke's law; as well as assumed harmonic solutions, one can attempt to solve guided wave problems [36]. However, in most cases it is difficult or impossible to solve guided wave problems analytically, so numerical methods such a finite element analysis (FEA) or semi-analytic finite element methods (SAFE) are used.

3.2 Elastic Wave Speed and Dispersion

The simplest way to understand elastic wave velocity is to make an analogy with a familiar model, such as a mass-spring system. When an elastic wave propagates through a material, the atoms oscillate about a mean position, similar to a mass on a spring. For elastic waves, the restoring forces are provided by stretched and compressed atomic bonds, which behave like microscopic springs. Just as springs are made with varying degrees of stiffness, different materials also have different levels of stiffness (or more properly, *elasticity*) as a function of their atomic bonds. The response of solids to resist stretching and compression from elastic waves is quantified by the Young's Modulus of Elasticity (E) [9], which engineers are familiar with as the slope of the stress-strain curve in the linear-elastic region. In solids, elastic waves may propagate as longitudinal (compression) waves or as transverse (shear waves). Shear wave propagation is possible in solids, but not in ideal fluids, because solids have a restoring force to counteract shear strains, while ideal fluids do not. This property is quantified as the Modulus of Rigidity (G), and it is similar to the Young's Modulus, except it describes a material's response to shear strain rather than to normal strain.

In order for an elastic wave to propagate, of course there must be a medium consisting of many atoms. The wave velocity, known colloquially as the "speed of sound" is the rate at which kinetic energy moves through the medium. Instead of a single mass-spring system, a medium for wave propagation can be thought of as a series of many individual masses connected by springs. In this model, the masses represent atoms and the springs represent inter-atomic bonds. The stiffer the springs, the faster the wave will travel because less displacement of each spring is necessary to build up sufficient energy to push the neighboring atom [9]. For this reason, wave speed is positively correlated with Young's Modulus for longitudinal waves and with shear modulus for transverse waves [9]. In addition to the stiffness of the springs, wave speed is also affected by the size of the masses attached to the springs. For a given applied force to a lighter material, the rate of wave propagation will be increased [9]. In the same vein, elastic waves will propagate faster when the atoms are lighter, as in less dense materials. For longitudinal waves, velocity is also dependent on a third variable called Poisson's ratio, which is a measure of how much a material thins when it is stretched, or thickens when it is compressed. The equation for the velocity of bulk transverse (shear) waves is given in equation 3.3, where G is the modulus of rigidity and ρ is the density of the medium. It is worth noting that the shear wave velocity is generally about 50% of the longitudinal wave velocity.

Eq. 3.3: $$V_s = \sqrt{\frac{G}{\rho}}$$

While the velocity concepts covered thus far are sufficient for describing bulk waves, ultrasonic guided waves involve two more interesting concepts: group velocity and phase velocity. In ultrasonic testing, sound energy is typically sent in repeated short bursts or pulses.

The velocity that the entire pulse, or wave-packet, propagates through the material is known as the group velocity. The group velocity is the velocity of energy transport [36]. Since pulses are of finite length, they must contain some spread of frequencies, known as frequency bandwidth or spectra. Pulse waveforms are in fact a superposition of many perfect sine waves at similar frequencies [36]. Lord Rayleigh, one of the early pioneers of acoustics, keenly observed that the velocity of individual waves within a group is not always equal to the group velocity [36], since velocity is frequency dependent. This phenomenon is called *dispersion* and it gives rise to two distinct measures of velocity: group velocity and phase velocity. Phase velocity is the velocity of individual sine waves, or harmonics, within the wave packet, while group velocity is the velocity of the wave packet as a whole. Dispersion occurs only for certain guided wave modes in certain media (called *dispersive media*) primarily due to the boundary effects where the phase velocity is a function of frequency [37]. In dispersive media, the shape of a wave pulse may spread due to the differences in velocity of various harmonics within the packet [37]. More detailed explanation of group and phase velocity concepts is provided in Chapter 2.8 of Rose [36].

3.3 Guided Wave Modes

In order to understand guided wave modes, it is helpful to first consider how guided waves are formed from bulk waves. When an elastic bulk wave is excited by a transducer at a specific angle and frequency in a natural waveguide such as a pipe or plate, ultrasonic waves reflect back and forth inside the plate, giving rise to interference phenomena [36]. In some places the interference is totally destructive; in others it is totally constructive or intermediate.

The guided wave that results is the superposition of all the reflecting bulk waves – it is the result of interference phenomena. Points of constructive interference represent guided wave modes. By tuning the frequency and angle of incidence, many different sets of constructive interference, or guided wave modes, can be produced [36].

Before attempting a guided wave experiment, it is suggested to solve for guided wave modes analytically or numerically, since doing so provides useful information on mode and frequency selection. By solving Navier's equations with the appropriate boundary conditions, as well as using the theory of elasticity and equations of solid mechanics, one can determine the points of constructive interference corresponding to guided wave modes [36]. Typically, modes are plotted on a graph of either group velocity (c_g) or phase velocity (c_p) vs. frequency. These plots are called dispersion curves because they illustrate the frequency dependence of guided wave velocity. Example phase velocity and group velocity dispersion curves are provided in Figures 6 and 7.

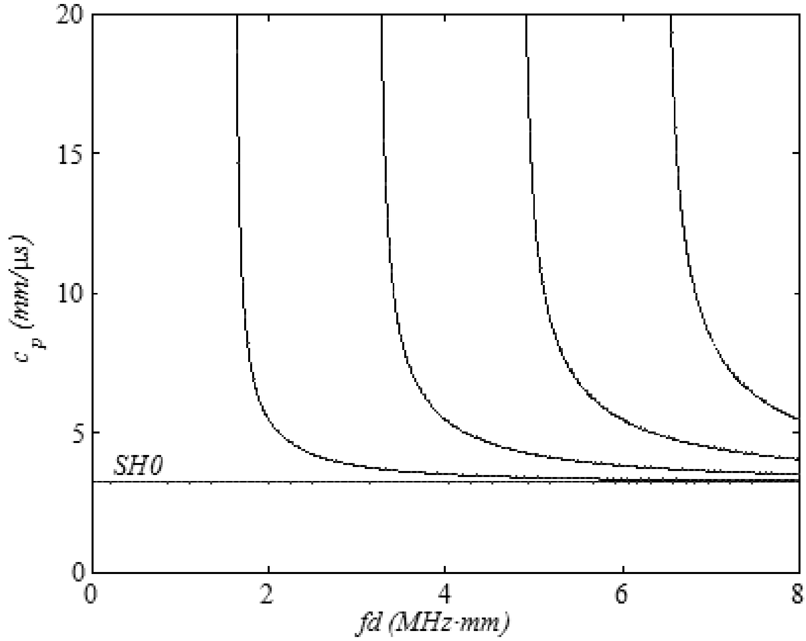

Figure 6: Example phase velocity dispersion curve. Each line represents a guided wave mode.[3]

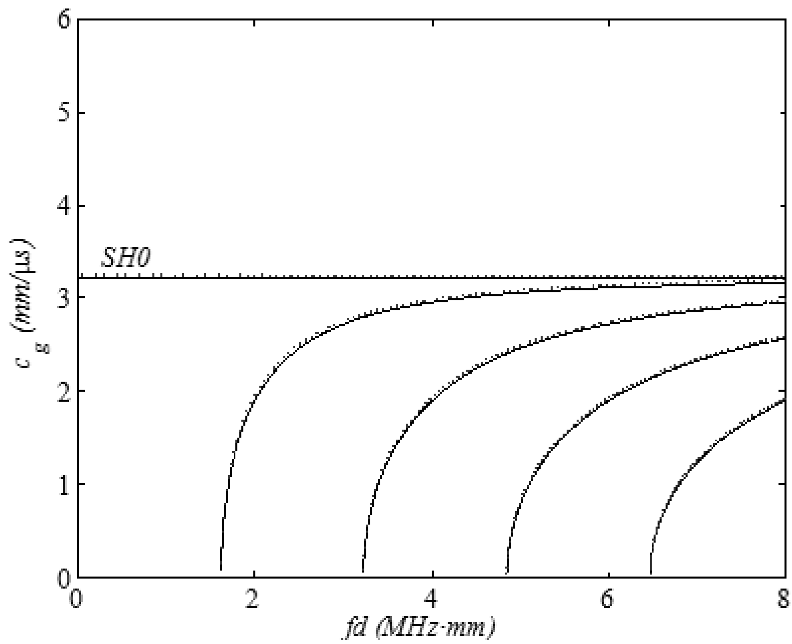

Figure 7: Example group velocity dispersion curve.[2]

[3] Images used with permission from Rose [36].

3.3.1 Mode Conversion

Dispersion curves are helpful for choosing the appropriate frequency to excite a desired guided wave mode. Unfortunately, once a mode is excited, energy may convert to other modes before it reaches the receiver. In guided wave testing, mode conversion occurs anytime a particular mode and frequency encounters a defect. Since boundary conditions must be satisfied, the resulting modes that are reflected and transmitted can be found on the appropriate dispersion curve along a vertical line at the frequency used, with the amount of each mode generated dependent on the boundary conditions at the defect. In practice, mode conversion is typically seen as additional reflections that are delayed or advanced slightly from the main reflection of an interface of defect. These mode-converted signals arrive slightly before or slightly later than the original mode does because of their different wave velocities, as can be seen on a dispersion curve.

3.4 Shear Horizontal and Torsional Modes

Transverse waves that are polarized in a plane parallel to the surface are called shear horizontal (SH) waves when they occur in flat plates, and torsional (T) waves when they occur in cylinders or pipes due to axisymmetric loadings. There are several reasons why shear horizontal or torsional modes may be advantageous for NDE. Compared to longitudinal modes, shear/torsional modes are less affected by non-viscous fluids on the surface, since ideal fluids cannot support shear stresses. As a result, less energy leakage takes place when using a SH or T than a longitudinal mode on a plate or pipe immersed in an ideal fluid [36]. This property is especially useful for in-service pipeline inspection, where the interior of the pipe is typically filled with liquid. Mode conversion may also be reduced by using SH or T modes. For interfaces that are parallel to the direction of polarization, such as welds, mode conversion is expected to be reduced because there is no oblique incidence [38]. Torsional modes in pipe are also volumetric, allowing for inspection of the entire cross section.

3.5 Pulse-Echo Technique

Two of the most common techniques for sending and receiving ultrasonic signals during NDE are through transmission (sometimes referred to as "pitch-catch") and the pulse transit-time method, more often known as the "pulse-echo" technique. For through transmission, one transducer is placed at each end of the test specimen. The transmitting transducer converts a sinusoidal electrical signal to elastic waves in the specimen, while the receiving transducer does the inverse. In the pulse-echo method, a single transducer is used to both transmit and receive. The single transducer pulses, and then receives any signals which are reflected. Sources of reflection include the end-wall of the specimen, welds, and possible defects. The pulse-echo method was used for the experiments presented later in this thesis.

Besides the simplicity of only requiring a single transducer, the pulse-echo method offers other advantages over through transmission. To understand these benefits of pulse-echo, it's helpful to compare the operating principles of pulse-echo and through transmission with regard to flaw detection. An excellent example, summarized as follows, is presented in Chapter 10 of Krautkramer [35]: When using through transmission, a flaw is indicated by a reduction in the signal strength at the receiver. If a large flaw, such as a crack, is present, then the amount of energy reaching the receiver should be greatly reduced, since much of the energy is reflected by the crack. To see the limitations of through transmission, consider a case where only a small defect, for example a defect which reflects 5% of the total sound energy, is present. Given that a 5% change in signal is not much (if any) greater than normal variations due to changes in coupling, as well as scattering and interference effects, it would be difficult to positively identify such a minor defect using through transmission. With the pulse-echo method, even a defect which only reflected 5% of the total energy would be apparent because the reflections from the defect would arrive sooner than the reflections from the end wall. Based on the time difference of arrival and the wave speed, the position of the defect could be estimated.

A simple model produced by the author with the finite element analysis software package ABAQUS CAE provides a neat illustration of the pulse-echo method. Figure 8 illustrates shear horizontal wave propagation in a thin plate without defects. Figure 9 shows the A-scan image for the defect free plate; the A-scan image is how a NDT inspector would view the wave form. In the A-scan, the pulse from the main bang is visible on the left, and reflection from the near end wall is visible at about 0.24 milliseconds.

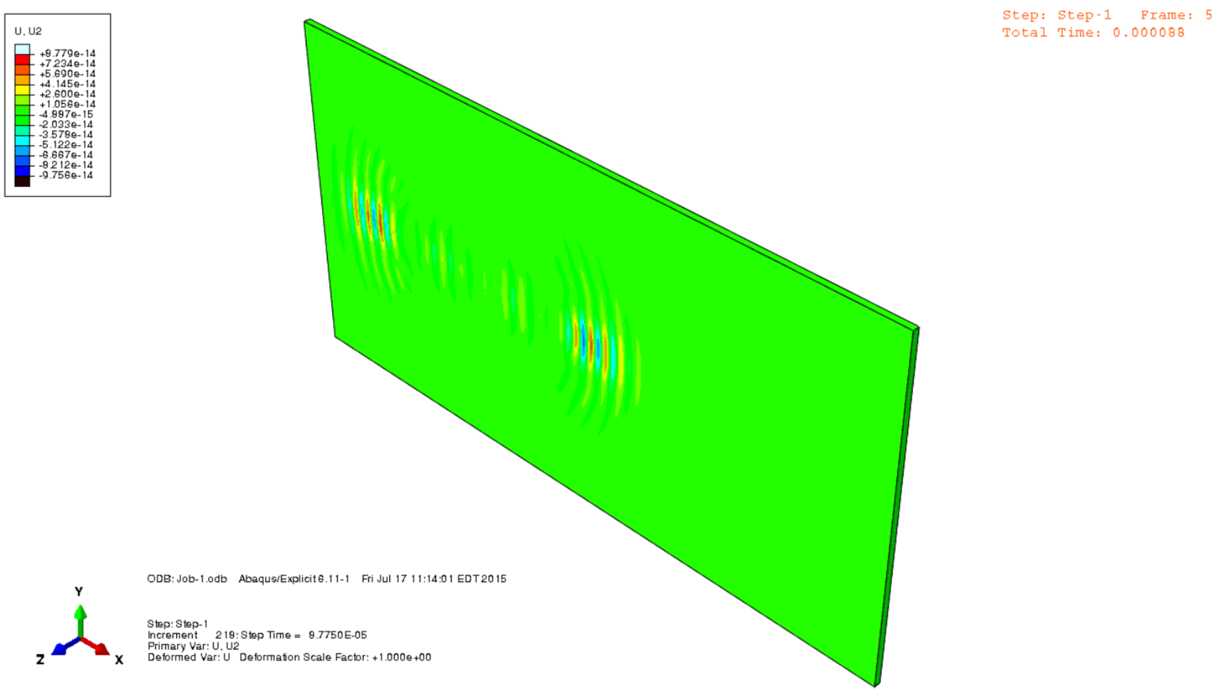

Figure 8: Illustration of wave propagation in a thin plate without defects. The color contours are based on displacement in the Y direction.[4]

[4] Image produced by the author

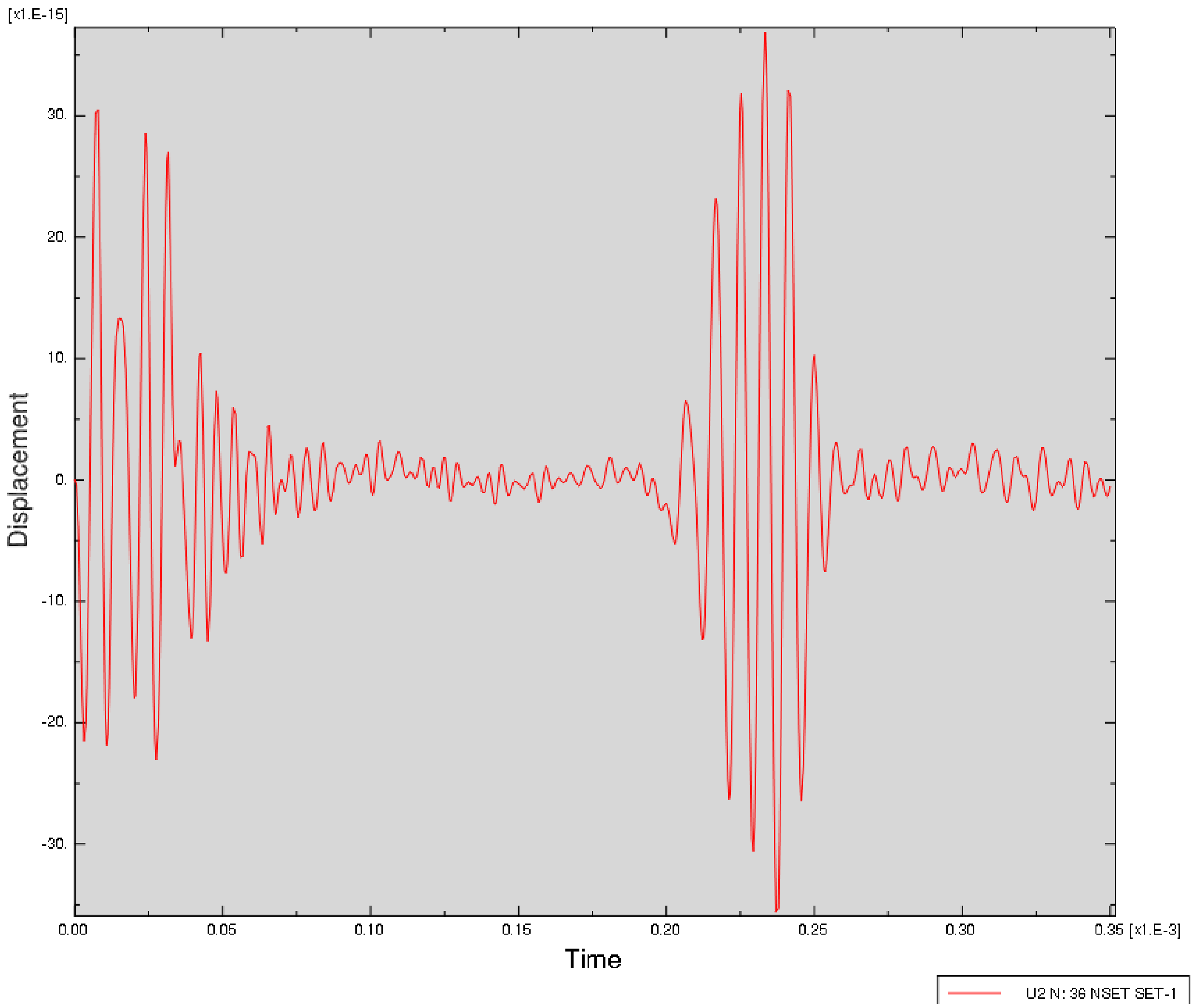

Figure 9: The A-scan image of the defect-free plate shows the reflection from the near end wall arriving at about 0.24 milliseconds.[5]

Figures 10 and 11 show the same shear horizontal wave propagation, but this time in a plate with a large defect. In Figure 10, some of the wave energy can be seen reflecting off the defect, while some of the energy refracts around the defect. The A-scan in Figure 11 shows a strong reflection from the defect being received at about 0.12 milliseconds, which is half the time that defect from the end-wall is expected, based on the A-scan in Figure 9. This principle,

[5] Image produced by the author.

known as time difference of arrival, is how the pulse-echo method is used for determining the distance to defects.

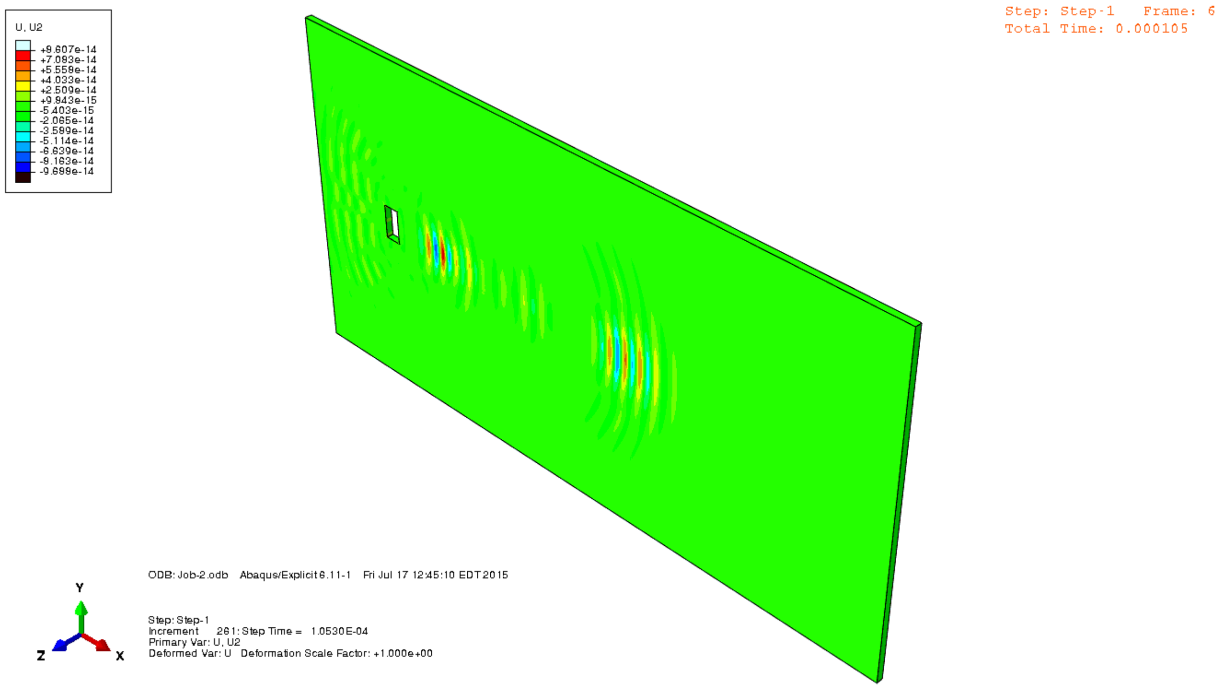

Figure 10: Illustration of wave propagation in a thin plate with a rectangular through hole defect. The color contours are based on displacement in the Y direction. Notice the reflections and refractions due to the defect.[6]

[6] Image produced by the author.

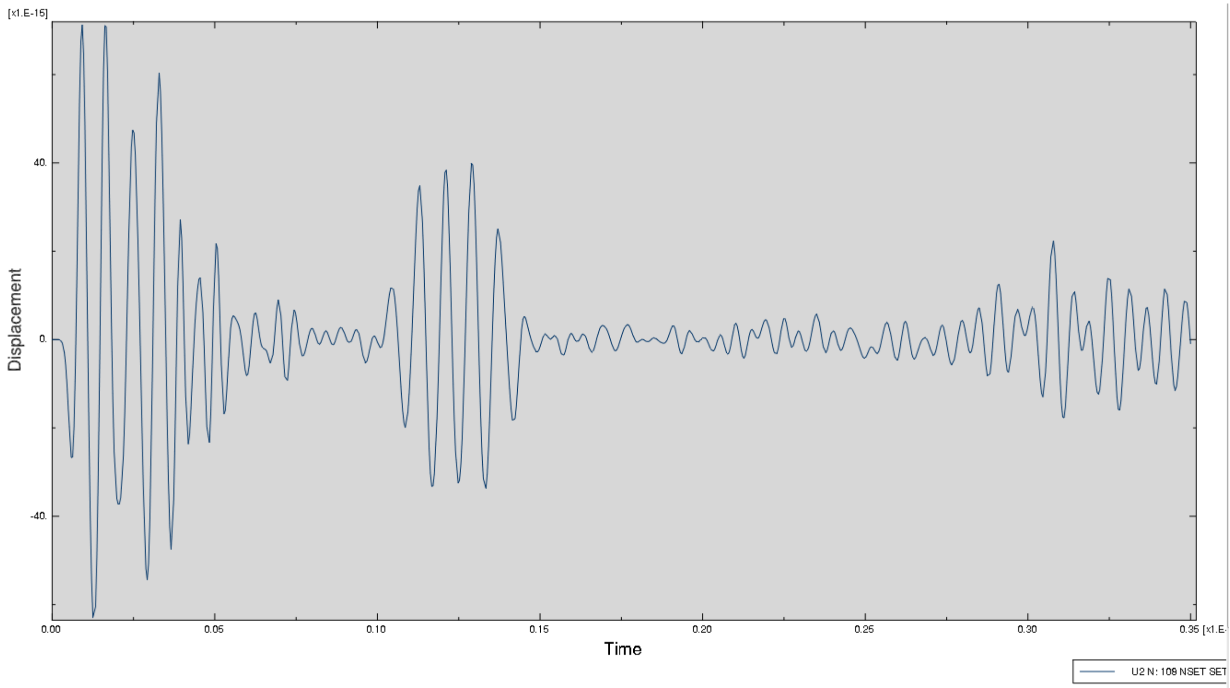

Figure 11: The A-scan image of the plate with a defect shows the reflection from the defect arriving at about 0.12 milliseconds. The reflection from the end wall is also weaker because much of the energy is blocked by the defect.[7]

Figures 12 and 13 show the same SH wave propagation once again, but this time the defect goes through 50% of the plate's depth. This could be a crude model of a corrosion pit. Notice in Figure 12 that the reflection from the defect is weaker than it is when the defect goes all the way through the thickness (as in Figure 11), and the end wall reflection is stronger.

[7] Image produced by the author.

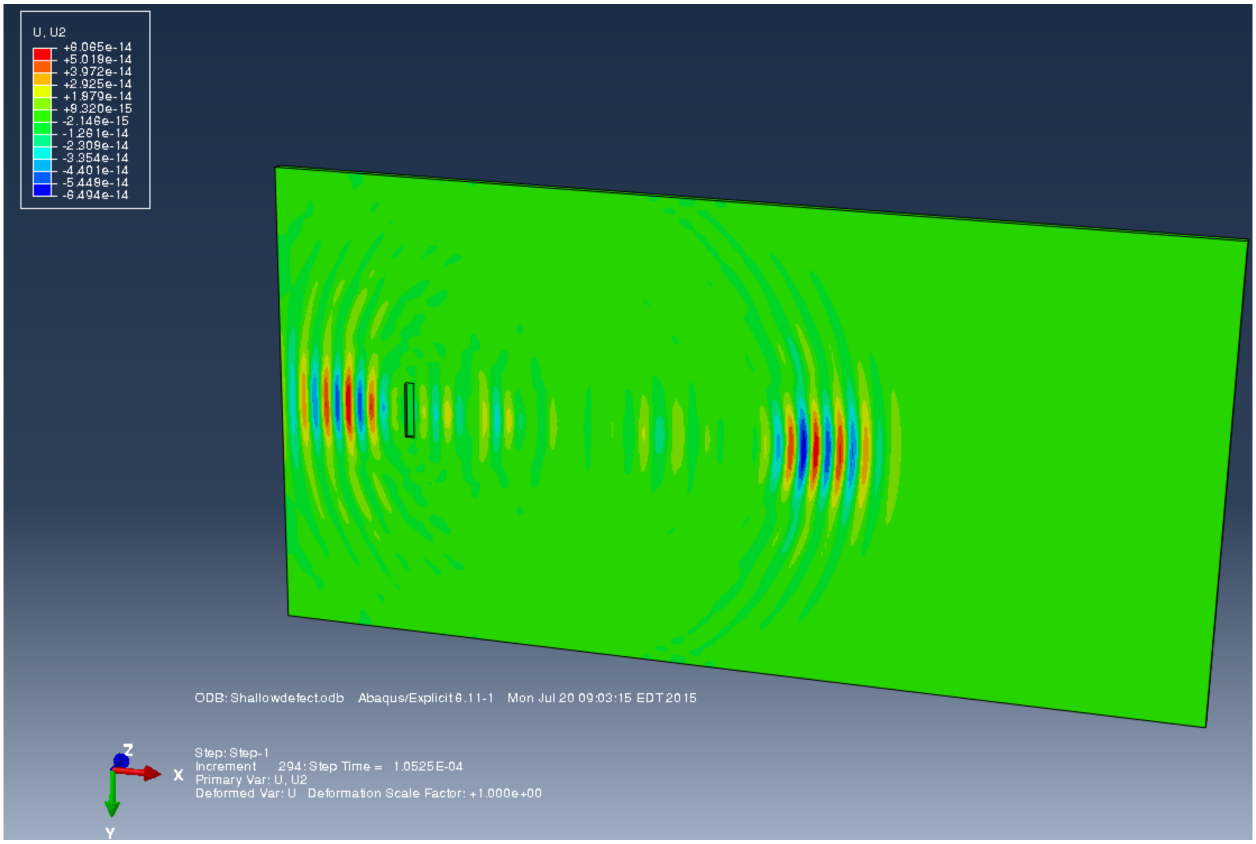

Figure 12: Reflections and refractions from a defect of 50% plate thickness.[8]

[8] Image produced by the author.

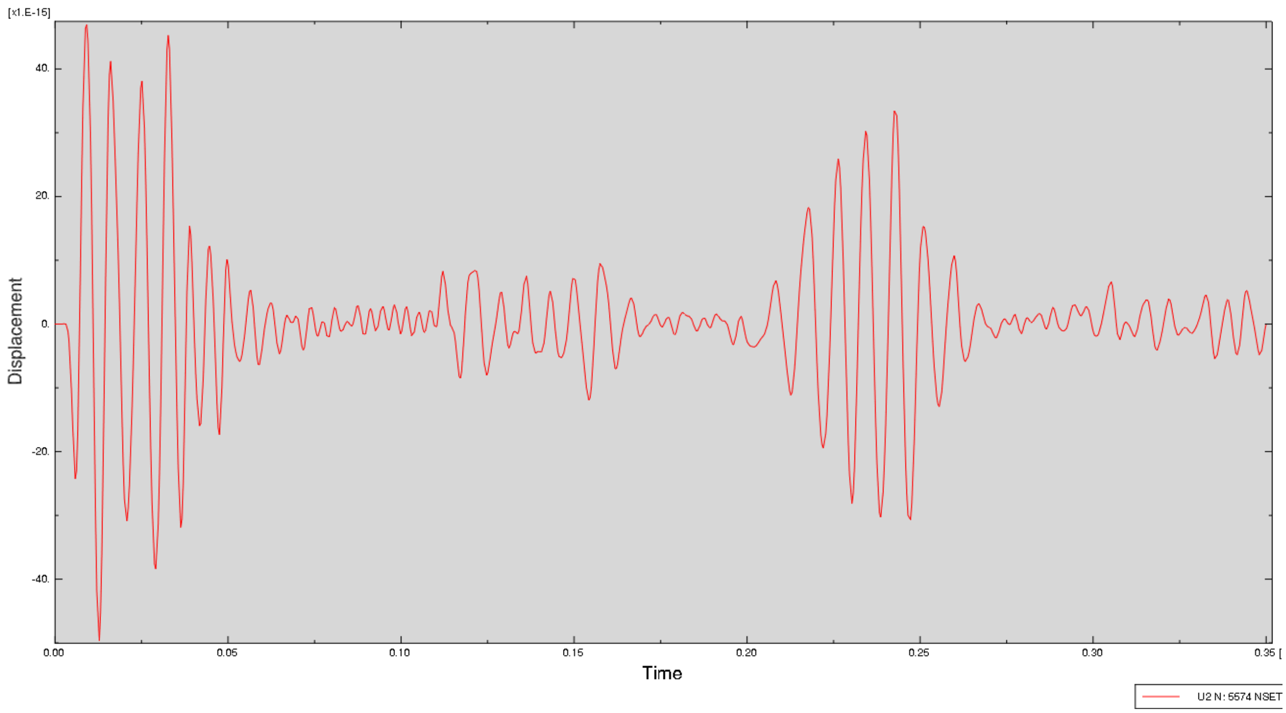

Figure 13: A-scan image of plate with 50% depth defect. Notice the reflection from the defect at about 0.15 milliseconds and the reflection from the end wall at about 0.24 milliseconds.[9]

3.6 Sources of Attenuation

Attenuation is the reduction in intensity of a sound wave with distance. In ultrasonic NDE, attenuation occurs due to four primary sources: beam spreading, scattering, absorption, and leakage. In an ideal material with perfect homogeneity, beam spreading would be the only source of attenuation [39]. However, all real materials have inhomogeneities which result in boundaries where acoustic impedance changes abruptly, leading to scattering [35]. Examples of inhomogeneities responsible for scattering include inclusions, pores, differences in crystal or grain structure, and anisotropy [35]. Scattering due to grain boundaries is negligible when grain

[9] Image produced by the author.

size is 1/1000th to 1/100th the wave length, but is very noticeable when grain size is 1/10th the wave length or greater [35].

Absorption is the conversion of elastic wave energy to heat; it can be thought of as internal friction that affects each cycle of the wave. A common strategy to reduce absorption is to excite waves of lower frequency, which require fewer cycles to travel a given distance. It is for this reason that lower frequencies are typically used for long-range inspections. The downside of using lower frequencies is decreased sensitivity to small defects, as well as decreased axial and lateral resolution.

Leakage occurs when energy travels from the test specimen to the surroundings. For example, when inspecting a pipe filled with water, it would be best to use a mode with dominant in-plane displacement at the inner diameter, since energy would not be able to leak into an ideal fluid. If a mode with dominant out-of-plane displacement was used, substantial amounts of energy could be lost as bulk waves into the fluid. Similarly, mode selection is important for preventing leakage when inspecting pipes with viscoelastic coatings. Exciting the correct mode requires some knowledge of the different available modes (provided by dispersion curves) and transducers capable of generating the desired wavelength and frequency.

Often, to increase signal amplitude and/or signal-to-noise (S/N) ratio, it might be necessary to increase the signal strength by applying greater voltage to the transducer or amplification (gain) at the receiver. However, receiver amplification will also increase the amplitude of noise and other undesirable signals, so amplification is only helpful when the S/N ratio is already favorable.

Chapter 4 Magnetostrictive Transducers

A critical component of any ultrasonic NDE system is the electro-acoustic transducer, which converts energy from an electrical signal to an elastic wave, and vice versa. Common transducer systems include piezoelectric, electromagnetic acoustic (EMAT), and magnetostrictive designs. Optical systems (i.e. lasers) may also be used to generate and detect elastic waves, though this method is far less common in NDE. In theory, the physics of a guided wave problem is identical regardless of the transducer system used. However, in practice, there are many considerations that must be taken into account for choosing the correct transducer to optimize results and improve prospects of commercialization. In addition to being well-suited for generating and receiving guided waves in long cylindrical wave guides [40], magnetostrictive systems offer several advantages over piezoelectric systems. From experience at FBS Inc., advantages of magnetostrictive transducers include:

- Shorter dead zone
- Lower cost
- Less power required
- Smaller and lighter system
- Loading is more axisymmetric
- Improved signal-to-noise ratio

For these reasons, magnetostrictive transducers were the technology of choice for the experiments presented in this thesis. The following sections provide an introduction of the operating principles of magnetostrictive comb transducers.

4.1 Magnetostrictive Effects

Similarly to piezoelectric and EMAT transducers, magnetostrictive systems begin with a signal generator, or pulser, which generates voltage pulses with a specified center frequency, number of cycles, and pulse repetition frequency (PRF). In magnetostrictive systems, the electrical signal is transmitted from the pulser to a coil, which may be either a ribbon cable or MsS circuit (described in Chapter 4.2). The passage of AC current through the coil generates alternating magnetic fields, which couple the coil to a ferromagnetic strip bonded to the surface of the test specimen. The ferromagnetic strip is made out of iron, cobalt, and/or nickel because these elements display magnetostrictive properties; that is a change in shape in response to magnetization. For the experiments in this thesis, a heat treated iron cobalt (FeCo) alloy with trade name "Hiperco 50" was used. Although nearly all ferromagnetic materials possess at least weak magnetostrictive properties (35), which means waves could be generated directly in a steel pipe without a special magnetostrictive strip, a FeCo strip is generally used because its much stronger magnetostrictive properties make for superior wave excitation from lower voltages.

The property of magnetostrictive materials to change shape in response to magnetic fields was first discovered by James Prescott Joule in 1842, and became known as the Joule effect [40]. The inverse of the Joule effect is known as the Villari effect. Waves are generated in the FeCo by the Joule effect and received by the Villari effect. Like other ferromagnetic materials, FeCo consists of grains which each have a magnetic moment in a direction determined by their crystallographic orientation [41]. Since each one of these grains behaves as a microscopic bar magnet, they are referred to as magnetic domains. Normally, these magnetic domains are oriented randomly and there is no net magnetic field. But, by "poling" or "biasing" the material with a permanent magnet, these domains align. When, an alternating magnetic field is applied, the magnetic domains can be aligned and misaligned with the bias field in unison [41], leading to cyclic expansions or contractions, which generates an elastic shear wave.

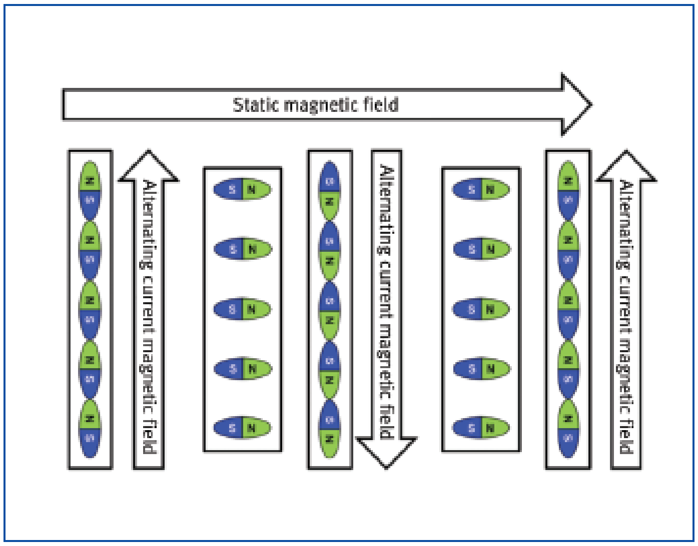

Figure 14: A Conceptual illustration of the magnetostrictive effect.[10]

In order for the elastic wave generated in the FeCo strip to propagate into the test specimen, a strong bond is necessary to attach the FeCo to the specimen. Throughout the experiments presented in this thesis, a consistent procedure was used to ensure sound coupling between the FeCo and the pipes. The pipe surfaces were sanded (to remove any rust or paint) and cleaned with acetone, and the FeCo was also lightly sanded (to provide a more textured surface for the epoxy to adhere to) and cleaned with acetone. Acetone, a strong solvent, was used rather than water because it is better for removing oils and other contaminants. A high strength epoxy, Loctite E-30CL Hysol, was spread onto the FeCo, and the FeCo was then

[10] Used with permission from Rose [42].

secured to the test surface with multiple wraps of electrical tape. The epoxy was then allowed to cure overnight before testing.

4.1.1 Voltage Sign Independence of Magnetostrictive Response

An interesting property of magnetostriction that is often overlooked is that the magnetostrictive response is typically independent of the sign of the magnetic field [35]. For example, cobalt has a positive magnetostriction, and will therefore expand whether the applied magnetic field is positive or negative [35]. As a result of this, the frequency of the expansions/contractions of the magnetostrictive material will be twice the frequency of the AC signal sent through the coil. However, this effect is undone by poling the FeCo strip with a permanent magnet, which aligns all of the magnetic domains, prior to putting the coil in place. In all of the experiments presented in this thesis, the procedure including poling the FeCo with a permanent magnet, so the doubling of frequency effect was not observed. For those interested, a wealth of information on the magnetostrictive effect and its applications is provided by Lacheisserie [43].

4.2 Comb Transducers

In order to use the magnetostrictive effect to generate a guided wave, it is necessary to use a comb transducer. Comb transducers consist of strips of piezoelectric material, or in the case of magnetostrictive comb transducers, a series of conducting wires in comb geometry. Depending on the direction of current flow, each finger of the comb forms either a peak or valley in the electromagnetic field. In the FeCo placed directly under the comb transducer, these peaks and valleys in the electromagnetic field correspond to mechanical expansions and contractions by the Joule effect. When AC current is passed through the comb transducer, a wave can be generated. The wavelength of the ensuing wave depends on the spacing of the comb transducer – the spacing between two fingers that represent peaks or two fingers that represent valleys is the wavelength.

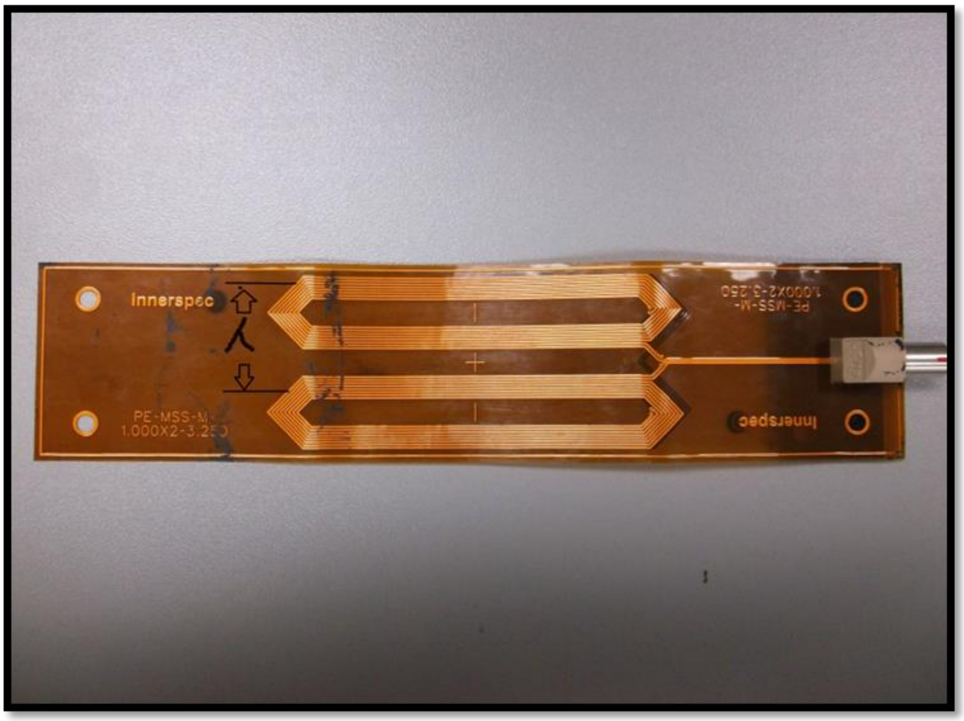

Figure 15: Illustration of finger spacing and wavelength on an MsS circuit type comb transducer.

By choosing the spacing of the comb transducer and the frequency of the AC pulses, a specific guided wave mode, or group of modes, can be excited. Choices in frequency and wavelength are important considerations for NDE. For example, a long wavelength comb transducer pulsed at a low frequency would excite lower order modes, and provide the best penetration power for long range inspection. On the other hand, a short wavelength transducer pulsed at high frequency would provided better sensitivity to small defects. Clearly, comb transducers are useful tools for mode selection, and the correct comb transducer depends on the situation. A thorough description of how comb transducer geometry and mode selection were used in this thesis is given in Chapter 5.1. In addition to finger spacing, the aperture, or circumferential distance covered by a comb transducer is also an important variable. Smaller aperture comb transducers may provide better circumferential resolution (especially when post-processed with the synthetic aperture focusing technique, or SAFT), but at the cost of transmitting less energy into the specimen, which leads to weaker signals.

4.2.1 Ribbon Cables

Ribbon cables are a versatile and inexpensive type of comb transducer for magnetostrictive applications. A two inch wide ribbon cable, such as the one used in this thesis, consists of 40 large wires which are protected inside a plastic coating. Each end of the ribbon cable plugs into a circuit board, which is then connected to a pulser/receiver by a Limo cable. The circuit board controls which wires in the ribbon cable receive voltage; by pulsing some of the wires and leaving others inactive, a comb transducer can be created. The same ribbon cable can be utilized with different circuit boards that are designed to create comb transducers of different spacing.

4.2.2 Magnetostrictive Sensor (MsS) Circuits

Flexible printed circuit boards (FPCB), known by the trade name "MsS" circuits, are a promising alternative to ribbon cables. Although MsS circuits are similar physically to ribbon cables in that they consist of many traces of wire in a comb shape, there are several key differences. MsS circuits use much finer traces of wire, which have greater electrical impedance than the thick traces used in ribbon cables. This increase in impedance makes it easier to impedance match MsS circuits with the pulser, leading to more efficient power transfer and smaller main bangs. In a nutshell, impedance is the opposition to current flow present in AC circuits (similar to resistance in DC circuits), and impedance matching the load (in this case, the comb transducers) to the signal source (in this case, the pulser) enhances power transfer and reduces signal reflection from the load. MsS circuits also offer great versatility in design. The shape of the fingers can be fine tuned for different applications – for example, the fingers could be curved so that they generate a wave with a certain focal distance, as shown in Figure 16.

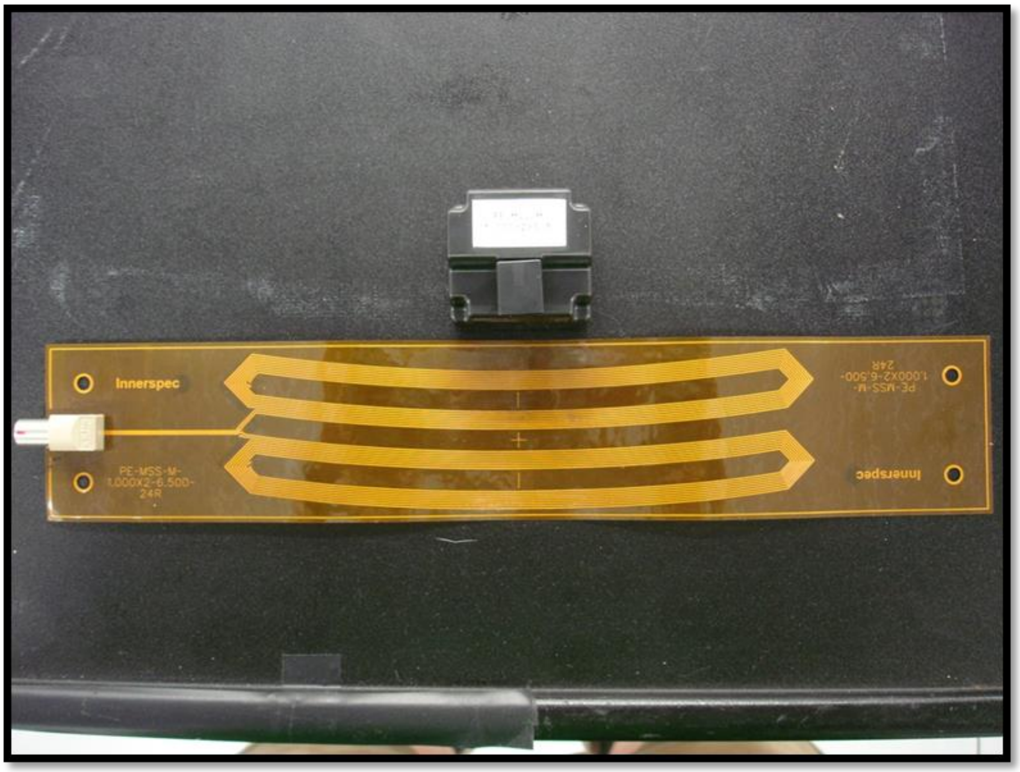

Figure 16: An MsS circuit designed for a focal length of 24 inches.

Chapter 5 Mode Selection and Test Equipment

Given the availability of MsS circuits of different sizes and shapes, as well as ribbon cables which can be used for a range of apertures, an investigation which compares the performance of the different transducer options is logical. In this thesis, several different MsS coils were compared on an 8.5” diameter control pipe, a 10.5” diameter pipe with pitting corrosion, two 16” diameter pipes with saw cuts and simulated pitting corrosion, and a 4.5” diameter pipe with an attenuative tar coating. In the following sections of Chapter 5, the test equipment, mode selection process, and results are presented.

5.1 SH_0 Mode Selection

Proper mode selection is one of the first steps to a successful guided wave experiment. For the experiments in this thesis, the fundamental shear-horizontal, or SH_0 mode, was chosen because it propagates without dispersion, with minimal mode conversion due to circumferential welds and cracks, and without energy leakage (if the pipe were filled with liquid). Typically, SH modes are associated with flat plates and torsional (T) modes are associated with pipes. However, in these experiments, the loading area of the transducer was only a section of the circumference (i.e. the loading was not axisymmetric) so local SH modes were generated in pipes. To determine what wavelength transducer and what pulse frequency would excite the SH_0 mode (and *only* the SH_0 mode), dispersion curves were plotted.

Typically, making a dispersion curve requires root finding because there is no explicit solution for the points of constructive interference which make up guided wave modes. However, for SH modes propagating in a plate, there is an explicit solution, and plotting dispersion curves is therefore a relatively simple process. From Chapter 14 of Rose [36], the equation for phase velocity of SH waves as a function of the frequency thickness product (fd) of a plate is given in equation 5.1, where C_T is the bulk transverse wave speed and n = 0,1,2,3 . . is the mode order.

Eq. 5.1
$$C_p(fd) = 2C_T\left\{\frac{fd}{\sqrt{4(fd)^2 - n^2 C_T^2}}\right\}$$

For the SH_0 mode, n = 0 and Eq. 5.1 reduces to $C_p = C_T$. In other words, the phase velocity is a constant equal to the bulk transverse wave velocity, which is about 3200 m/s in steel. Hence, in order to excite the SH_0 mode it is necessary to use a frequency and wavelength that give a wave velocity of about 3200 m/s. To find a frequency that can be used to excite the SH_0 mode without exciting any other modes, it is helpful to make a dispersion curve by plotting equation 5.1 with several values of n, so that the first few higher order modes are visible along with the SH_0 mode. Since the pipes used in the following experiments all have a wall thickness of about 10 mm, a dispersion curve for d = 10 mm was created – see Figure 17. Note that this dispersion curve is intended for flat plates, and is merely a good approximation for local SH modes propagating axially along a pipe, since the curvature of the pipe likely has some effect.

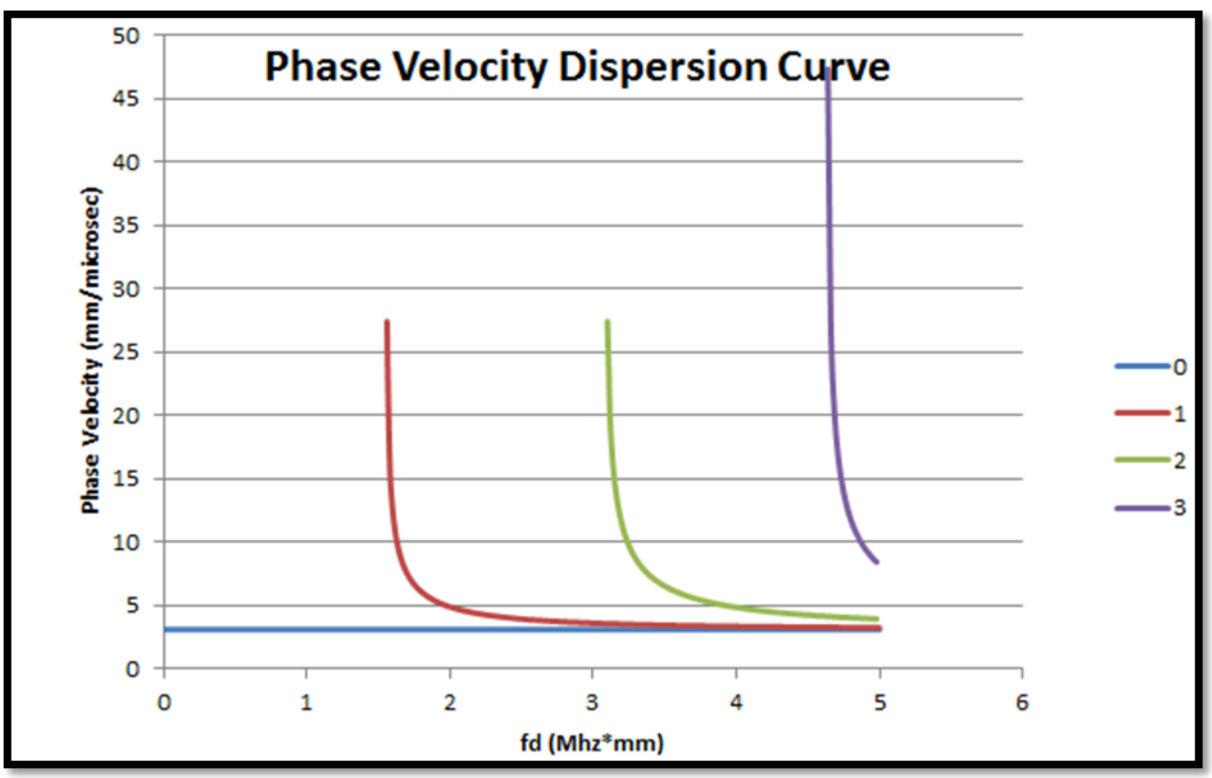

Figure 17: Phase velocity dispersion curve of the first four SH modes in a 10 mm thick plate.[11]

In Figure 17, it is clear that the SH_0 mode travels at a constant phase velocity equal to the bulk transverse wave speed, of about 3200 m/s or 3.2 mm/µs, just as expected. More interestingly, all of the higher order modes have cutoff frequencies where their phase velocities go to infinity. At pulse frequencies less than the cutoff, these modes will not be excited. The closest mode to the SH_0 mode, the SH_1 mode, cuts off at an fd value of about 1.8 Mhz*mm. In a pipe with 10 mm wall thickness, this corresponds to a frequency of 0.18 MHz or 180 kHz. If a transducer of appropriate wavelength is pulsed at a frequency below 180 kHz, say 125 kHz, then the SH_0 mode will be the sole mode generated.

In addition to the phase velocity dispersion curve, the group velocity dispersion curve is also insightful. While the phase velocity dispersion curve provides useful information for wave excitation, the group velocity dispersion curve is helpful for receiving, since wave packets travel at the group velocity. The group velocity dispersion relation for SH modes is given in Chapter 14 of Rose [36] as equation 5.2:

$$C_g(fd) = C_T \sqrt{1 - \frac{\left(\frac{n}{2}\right)^2}{\left(\frac{fd}{C_T}\right)^2}} \qquad \text{Eq. 5.2}$$

From Eq. 5.2, it is apparent that when n = 0, the dispersion relation simplifies to $C_g = C_T$. In other words, the group velocity is equal to the bulk transverse wave velocity, which is equal to

[11] Image produced by the author.

the phase velocity. Plotting Eq. 5.2 for several different values of n gives the group velocity dispersion curve shown in Figure 18.

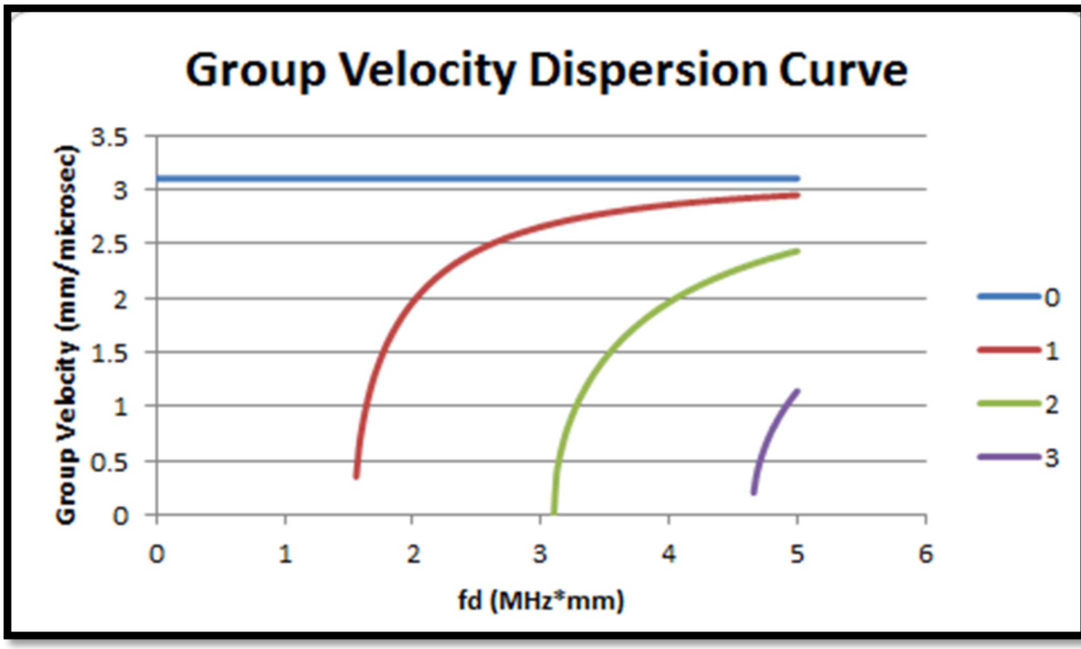

Figure 18: Group velocity dispersion curve for SH modes in 10 mm thick steel plate.[12]

Similar to the phase velocity dispersion curve, the group velocity dispersion curve shows that no wave packets other than the SH_0 mode propagate below an fd value of about 1.7 MHz*mm, which corresponds to 170 kHz in a 10 mm thick plate.

5.1.1 Exciting the SH_0 Mode

From the dispersion curve in Figure 17, it is clear that the SH_0 mode can be excited at any frequency. However, it is best to excite the SH_0 only, so that there is no confusion due to the simultaneous propagation of multiple modes. This is accomplished by keeping the frequency

[12] Image produced by the author.

safely below the cutoff frequencies of all the modes except $SH_{0.}$ For pipes with 10 mm wall thickness, this means keeping the frequency below about 160 kHz. The ribbon cables and MsS cicruits used in the following experiments all have comb spacings of about one inch between fingers with like current directions – which means that the transducers are designed to generate wavelengths of about 1 inch or 2.54 cm. To see what phase velocities a comb transducer can excite at different frequencies, it is useful to draw an excitation line on the dispersion curve, as seen in Figure 19. The slope of the excitation line is the wavelength of the transducer, which is equal to the finger spacing of the comb. In essence, the excitation line is a graphical illustration of equation 5.3. To excite the SH_0 mode, a frequency must be used that gives a wave velocity of 3,200 m/s (since that is the velocity of the SH_0 mode) when used with a wavelength of 2.54 cm. From Figure 19, it is clear that a frequency of 125 kHz is a good choice for exciting the SH_0 mode in a 10 mm thick plate when using 2.54 cm spacing comb transducers.

Eq. 5.3 $$C = f*\lambda$$

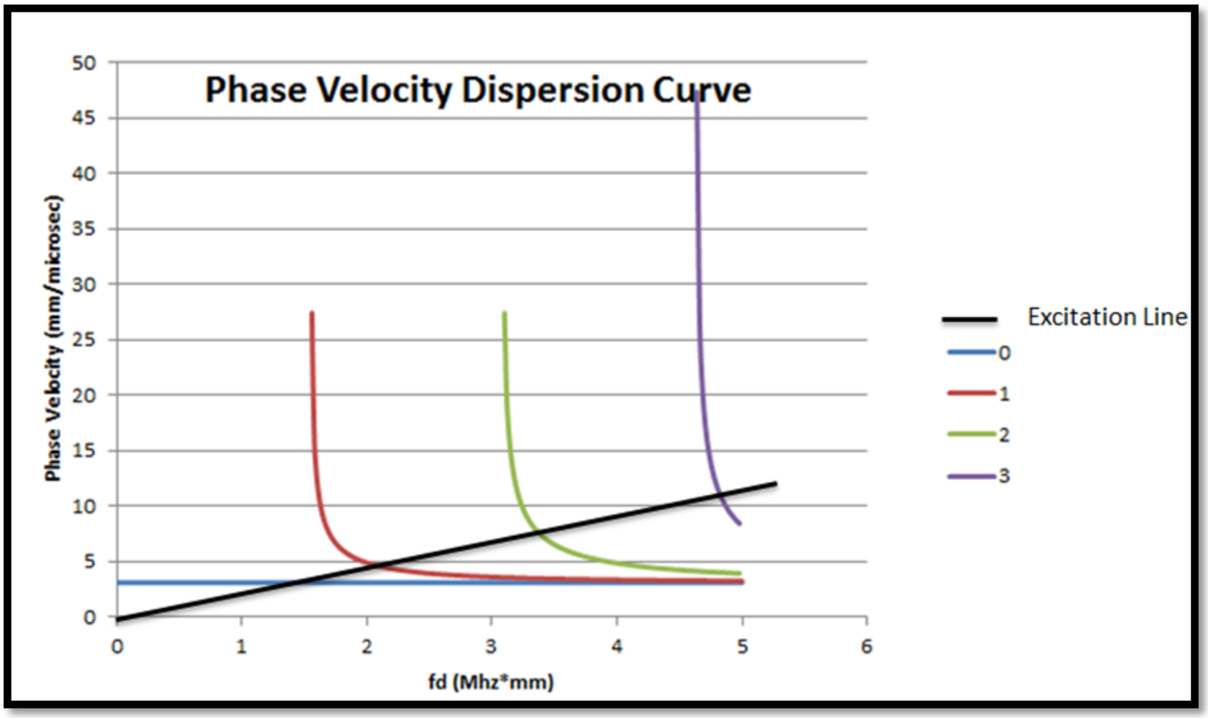

Figure 19: Phase velocity dispersion curve for SH waves in 10 mm thick plate, with excitation line for 2.54 cm spacing comb transducer shown in black.[13]

[13] Image produced by the author.

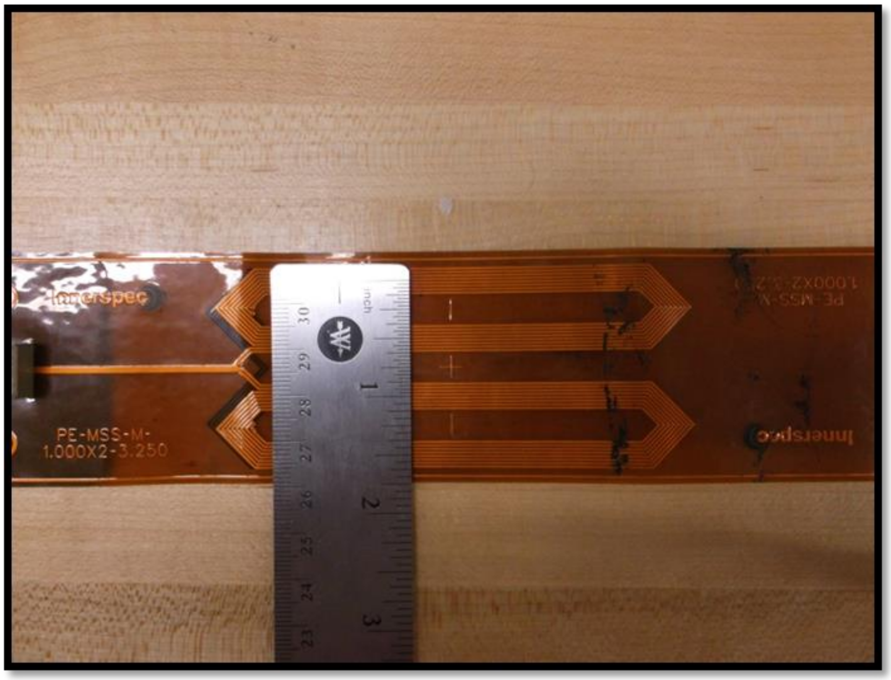

Figure 20: The spacing/wavelength of the MsS circuits used is 1 inch, or 2.54 cm.

5.1.2 Finite Element Model

Finite element analysis (FEA) is a ubiquitous technique used across disciplines to provide approximate numerical solutions to engineering problems governed by partial differential equations. Instead of using an infinite number of differential elements to solve a mathematical model (as done in traditional integral and differential calculus), the finite element method discretizes the domain into a finite number of connected elements. On each element, simple functions (usually polynomials) are used to approximate the exact solution. FEA is well-suited to solving complex problems (which are difficult or impossible to solve analytically) and to generating quick models which can predict or validate experimental results.

To verify that the transducers used in this thesis would in fact generate the SH_0 mode, a comb transducer was modeled on a steel plate using the commercial finite element software package ABAQUS CAE. A plate thickness of 10 mm was chosen to replicate the 10 mm wall thickness of the pipes, and the transducer was 3.25” long, with the same comb spacing as the transducers used in the experiments. Surface tractions in alternating directions were specified on each finger of the comb, and a 4 cycle, 125 kHz tone burst was specified as the frequency – just as was used during the actual experiments. The ABAQUS model shows the SH_0 mode generated as expected, with minimal excitation of other wave modes with out-of-plane displacement.

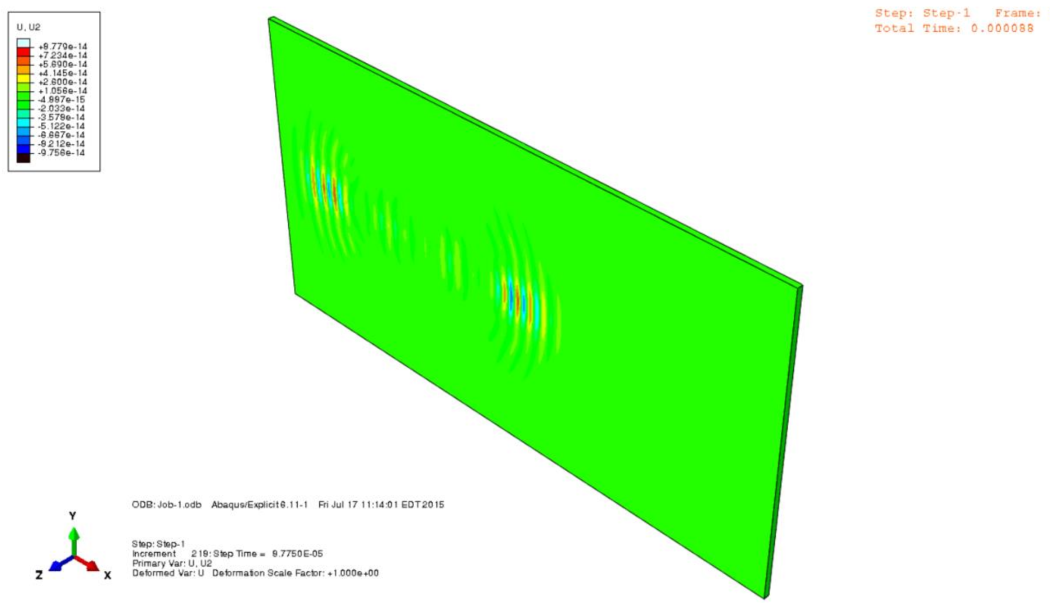

Figure 21 A finite element model made using ABAQUS shows two groups of SH waves propagating away from the comb transducer. The color contours are based on the displacement in the Y (horizontal) direction.[14]

[14] Image produced by the author.

5.2 Innerspec PowerBox H

For the experiments presented in this thesis, a combined pulser/receiver system marketed as the "PowerBox H" was used in pulse-echo mode. Manufactured by Innerspec High Performance NDT Solutions, the PowerBox H is a hand-portable, battery-powered instrument that can be used to generate and receive guided waves in either through-transmission (pitch-catch) or pulse-echo operation. Unlike alternative systems, such as the laptop-based Guided Wave Workstation software, the PowerBox H can operate with a position encoder, which allows for reliable tracking of transducer position during a scan. The PowerBox H system is also much more compact than laptop-based systems, which require a separate pulser/receiver unit to go between the laptop and the transducer. By comparison, the PowerBox H is a self-contained system that weighs only six pounds and can be carried easily in one hand. Data collected with the PowerBox can be saved to a USB thumb drive for analysis on a regular laptop or desktop computer.

Figure 22: The control panel and display of the Innerspec PowerBox H pulser/receiver. Notice the impedance matching module (with the white sticker) which plugs in just above the display.

5.2.1 Settings

The PowerBox H offers a wide variety of settings, including filters, adjustable pulse-rep rate up to 300 Hz, data averaging, and encoder pitches (for when the encoder is used to trigger the pulser.) The following settings were used for the experiments in this thesis:

- MsS circuit frequency: 125 kHz
- Ribbon cable frequency: 128 kHz (dictated by impedance matching modules)
- Pulse rep frequency (PRF): 20 Hz
- Sampling frequency: 10 MHz
- Pulse shape: 4 cycle tone burst
- Spatial averaging: none
- Time averaging: none
- Filter: 100-150 kHz
- Receiver gain: variable, 0 – 10 dB

In order to work with various ribbon cables and MsS circuits of different impedances, the PowerBox H uses small impedance matching modules which plug in directly above the display screen. By reducing the difference in impedance between the PowerBox and the transducer, these impedance modules enhance power transfer and reduce ringing around the main bang. The PowerBox H is very sensitive to impedance differences; without the correct impedance matching network it will not function correctly.

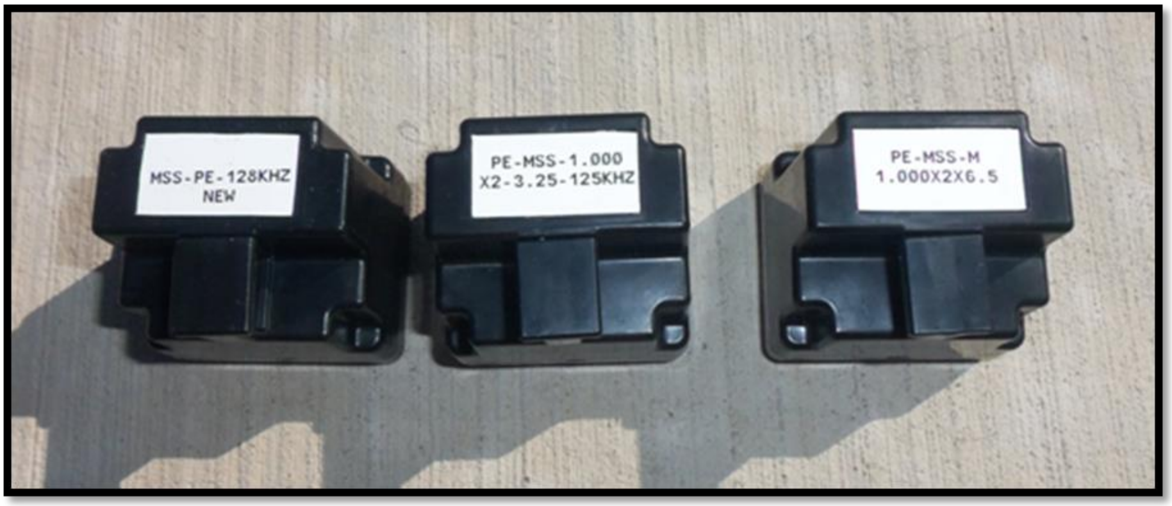

Figure 23: Impedance matching modules for the ribbon cable at 128 kHz, the 3.25" MsS circuit, and the 6.5" MsS circuits.

One downside of the PowerBox H is that the lowest allowed pulse voltage with the manufacturer's settings is 600 Volts peak-to-peak (Vpp). Typically, about 100-200 Volts is sufficient for using magnetostrictive transducers, but since the PowerBox H is designed for other transducers which require more power, namely electromagnetic acoustic transducers (EMATs), it lacks settings for lower voltages. The voltage could potentially be lowered by modifying the internal circuitry or adding a variable resistor in between the PowerBox output and the transducer. Besides depleting the battery, using 600 Vpp for magnetostrictive applications has the effect of de-poling the FeCo, leading to progressively weaker signals unless the FeCo is frequently biased with a permanent magnet (sometimes referred to as a "strip conditioner") in between each test. This effect was observed, and corrected by frequent re-poling, by the author throughout the experiments presented in this thesis.

5.3 MRUT Probe

To move a magnetostrictive transducer smoothly around the circumference of a pipe in sync with an encoder, it is helpful to have a wheel probe which holds both the transducer and encoder side-by-side. The medium range ultrasonic testing (MRUT) probe was designed by Steven Owens and Connor McLaughlin at FBS Inc. to meet this need for pipes with diameters of at least four inches and transducer apertures of 3.5 inches or less. The MRUT can be outfitted with magnetic wheels to help it stick to the pipe, or with rubber wheels to help it roll smoothly over pipes with rough surfaces. The encoder wheel is made out of soft rubber, and the encoder arm is spring loaded to maintain pressure on the wheel – the combined effect is that the encoder wheel has excellent traction on the pipe, and always rolls without slipping.

Figure 24: The MRUT probe mounted above a FeCo strip on a 10.5” pipe. The yellow colored wheel on the side of the MRUT is the encoder wheel. A circuit board for attaching ribbon cables is visible on top of the MRUT, but no ribbon cable is plugged in. On the front of the MRUT, an MsS circuit attached with electrical tape is visible.

5.3.1 Limitations

Although the MRUT works well for most tests, it does have its limitations. Due to the small size of the MRUT, it does not have space to accommodate transducers longer than about 3.5 inches. For this reason, when 6.5” transducers were tested, an alternative set-up had to be devised. A 6.5” strip of rubber was cut for the transducer to be attached to, and the MRUT (sans transducer) was run in parallel around the pipe next to the transducer, in order to collect position data with the encoder. This technique required keeping one hand on the rubber mount with the transducer, and another hand on the MRUT, and trying to keep them synchronized as the pipe was traversed. Obviously, this technique is not perfect, but when done carefully it is possible to keep the transducer and MRUT closely synchronized.

Figure 25: 6.5" length MsS circuit on rubber mount. The MRUT can only accommodate apertures of 3.5 inches or less, so rubber mounts were used for the 6.5" circuits and ribbon cable.

5.4 Transducers

Five different transducers were tested, all of which are designed for a wavelength of approximately 1 inch:

- Ribbon cable (set to various contact lengths, or "apertures")
- 3.25" long MsS circuit (1.00x2-3.25)

- 6.5” long linear MsS circuit (1.00x2-6.50)
- 6.5” long curved MsS circuit w/ 24 inch focal length (1.00x2-6.50 24R)
- 6.5” long curved MsS circuit w/ 36 inch focal length (1.00x2-6.50 36R)

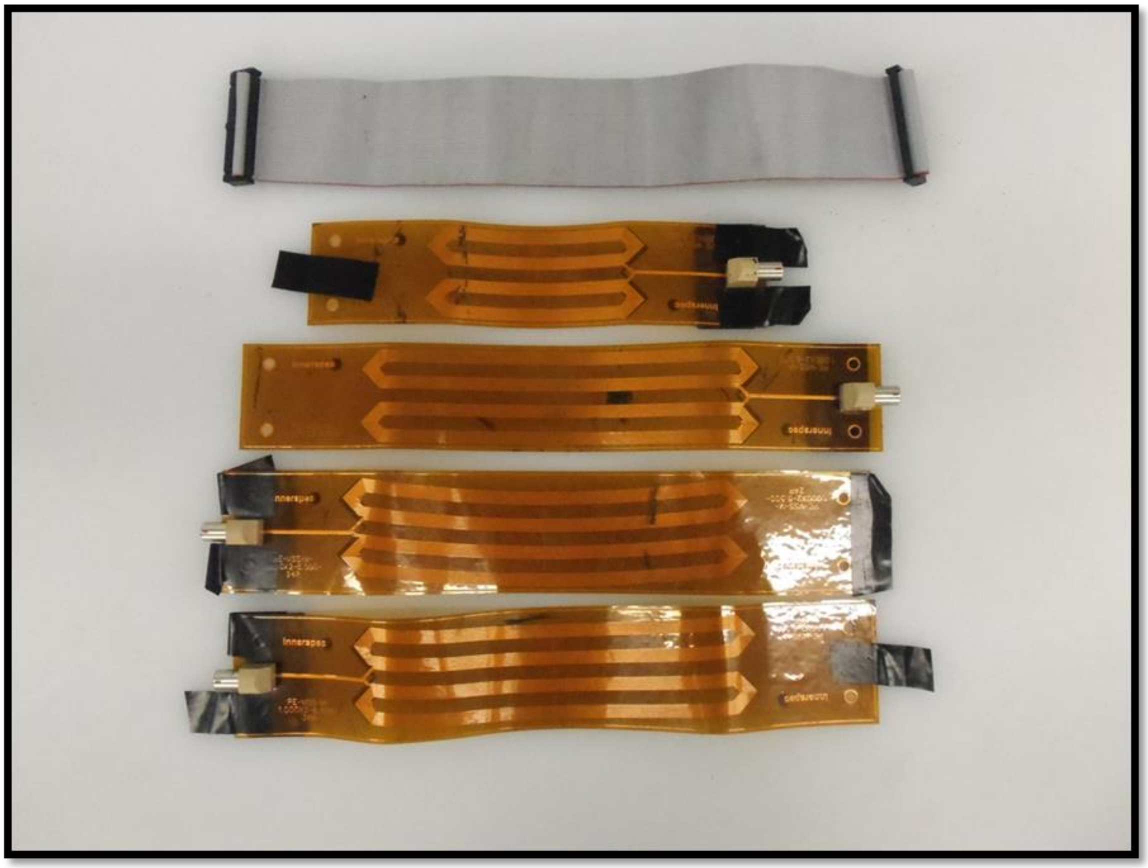

Figure 26: From top to bottom: ribbon cable, 3.25” MsS circuit, 6.5” linear MsS circuit, 6.5” MsS circuit with 24” focal length, and 6.5” MsS circuit with 36” focal length.

5.5 Stainless Steel Test Targets

For some of the tests in this thesis, small stainless steel targets were used instead of conventional defects such as drill holes. The dimensions of each target were 12x6x1.5 mm, and they were bonded to the outer surface of the pipe with epoxy. Compared to drill holes and other permanent defects, targets are advantageous in that they can be added quickly and easily, and can be removed with a chisel when the test is complete. The disadvantage of rectangular targets is that they are directional, which means that variations in the angle of the target leads to oblique incidence and changes the reflections. Another downside of the targets is that they rely on strong acoustic coupling to the pipe in order to have any effect on the guided wave. If the bond is not strong enough, the target may provide only a weak reflection or not appear at all. If extra epoxy is left around the target, it may give a particularly strong reflection. Hence, to ensure consistent results it is best to pay close attention to the angle of the targets and to the type and amount of epoxy used.

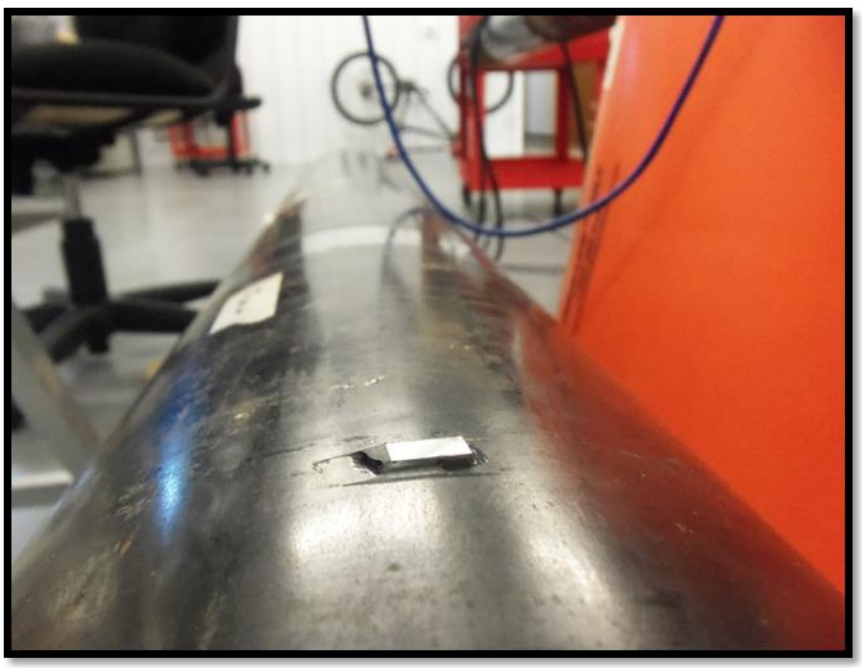

Figure 27: 12x6x1.5 mm stainless steel target bonded to pipe. Notice the excess epoxy on the sides.

Chapter 6 Experimental Results

6.1 8” Control Pipe

Before testing the different transducers on pipes with actual corrosion or other real defects, the different transducers, as well as the PowerBox H and impedance matching modules, were tested on a pipe with stainless steel targets. The point of this first series of tests was to validate the equipment on a pipe that should give reflections that are easy to predict and interpret.

An 8” diameter schedule 40 steel pipe with several targets was chosen as the control. This pipe contains a cluster of four large spherical pits on one side of the FeCo (arbitrarily designated the “reverse” side) and four targets mounted on the forward side. The pits are 15” from the FeCo and the targets are 9”, 17”, 25”, and 33” from the FeCo. The targets wrap around the circumference and each target is separated by approximately 90°. Figure 28 shows the lay-up of the pipe on the right, along with an example display taken with the PowerBox. In the B-scan (the color contour plot on the bottom half of the PowerBox display), the four targets and the pits are clearly visible. The horizontal axis of the B-scan represents circumferential position, and the vertical axis represents axial position. Axial position is shown in units of inches, and is calculated based off a wave speed of 3,200 m/s since this is the speed of SH_0 mode. In the B-scan, amplitude of the signal is indicated by color, with white corresponding to a lack of signal and red corresponding to clipping – dark blue or yellow indicates a strong signal without clipping. The horizontal axis of the A-scan represents axial position, and the vertical axis represents amplitude.

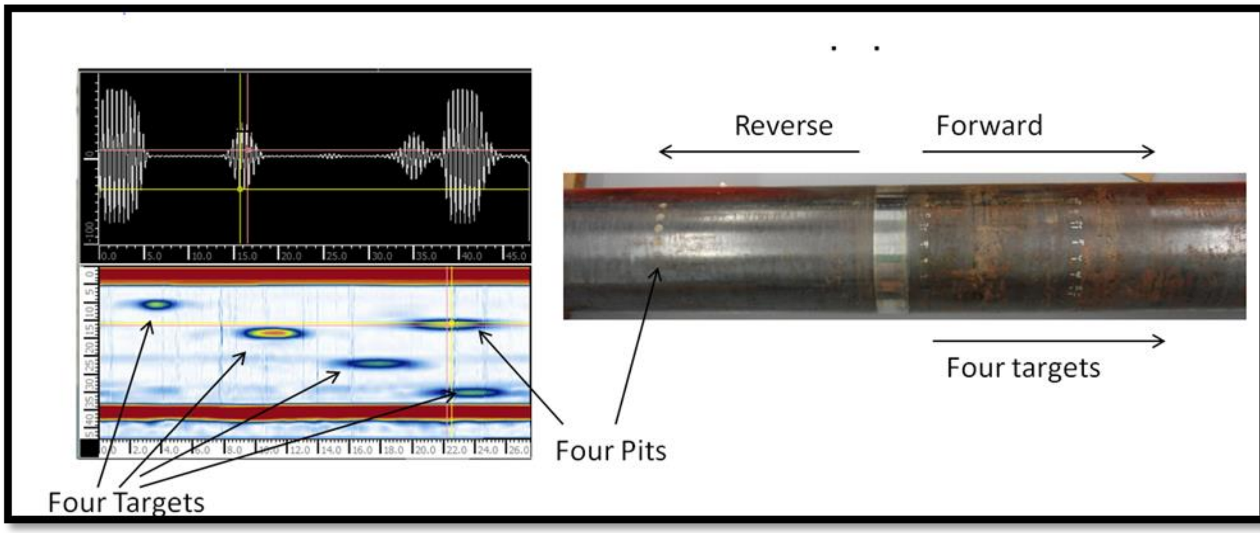

Figure 28: Example A and B scans of the 8" schedule 40 steel pipe with 4 test targets and a cluster of 4 spherical pits.

Since the transducer sends and receives waves in both directions, the cluster of four pits which are in the reverse direction are also visible in the scans. The A-scan image shows the waveform corresponding to the position of the yellow, vertical cursor line on the B-scan. In this example, the yellow cursor is placed on the four pits and the target that is farthest away. Looking at the A-scan from left to right, the wave forms resulting from the main bang, the reflection from the four pits, the reflection from the fourth target, and the end-wall echo are visible.

The results taken on the 8" control pipe with the PowerBox H match results collected on the same pipe with the proven Guided Wave Workstation laptop based system and a ribbon cable transducer.

6.1.1 Ribbon Cable Results

A ribbon cable was tested using both 3.25” and 6.5” apertures. In order to excite the SH_0 mode, a frequency of 128 kHz was used. The signal was strong enough that no gain needed to be applied to the received signal. Results are shown in Figures 29 and 30. Notice the main bang protrudes out to about 8 inches; this is known as a “dead zone” because the system is blind to any defects that are within 8 inches of the transducer.

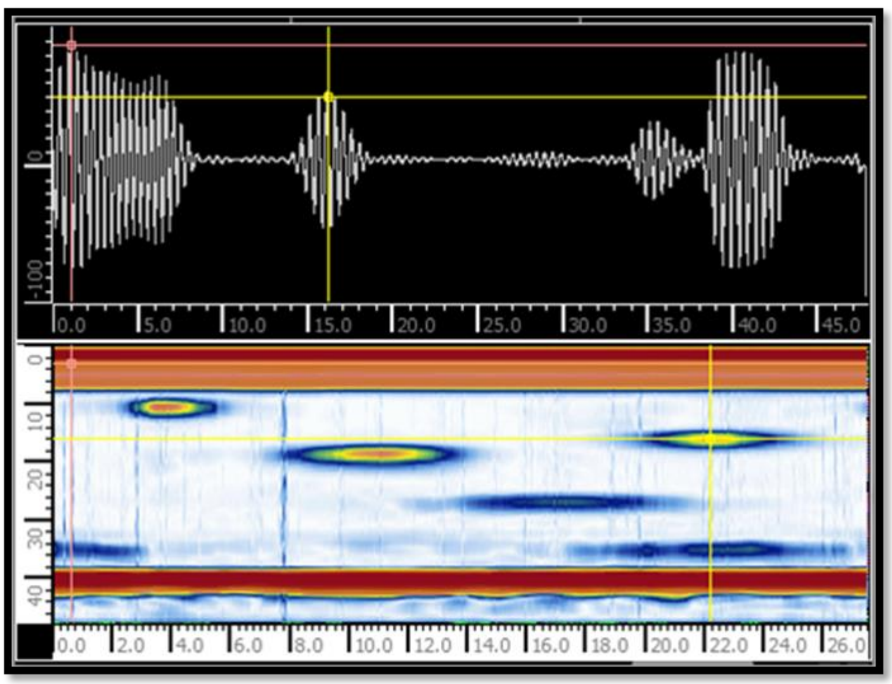

Figure 29: Scan of 8” schedule 40 steel pipe with 3.25” ribbon cable.

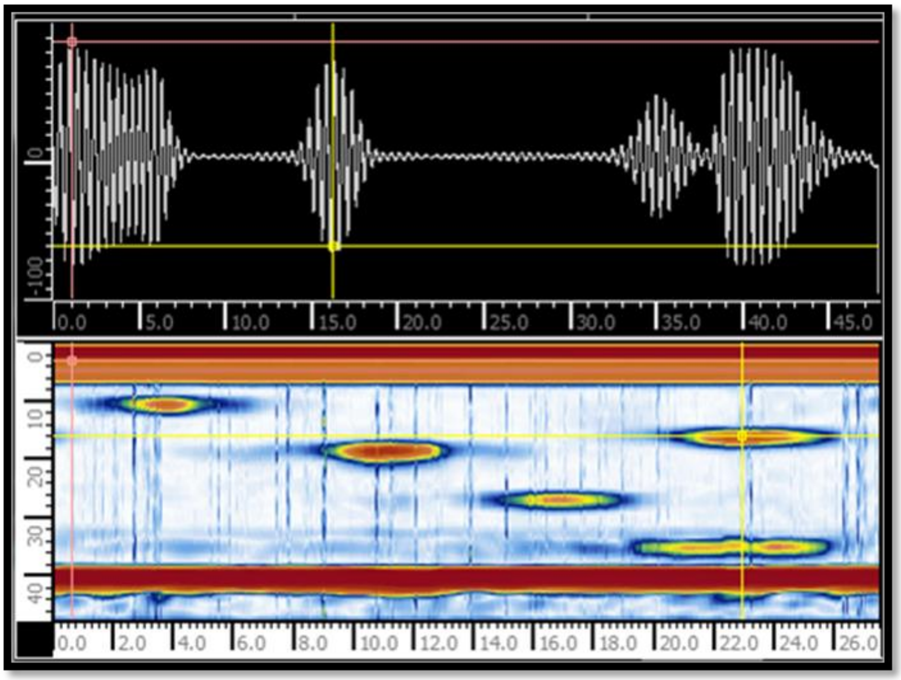

Figure 30: Scan of 8” schedule 40 steel pipe with 6.5” ribbon cable.

6.1.2 MsS Circuit Results

All four MsS circuits were tested on the 8” pipe. Results are shown in Figures 31 through 36. The scan from the 3.25” MsS circuit (Figure 31) looks very similar to the scan taken with the 3.25” ribbon cable (Figure 29), except for one significant difference: when the MsS circuit is used, the dead zone is only about 6 inches, compared to 8 inches with the ribbon cable. For the 6.5” MsS circuits (Figures 32, 33, 34, 35, and 36), the dead zone is further reduced to about 5 inches. This is likely due to differences in impedance matching. Compared to ribbon cables, MsS circuits are easier to impedance match with the PowerBox H because of their higher impedance. By the same logic, longer MsS circuits are also easier to impedance match than short MsS circuits because they have longer traces of wire and thus greater impedance. Impedance mismatches lead to internal ringing in the electronics of the PowerBox, and this is known to contribute to the main bang. For example, if the PowerBox is pulsed when it is not even connected to a transducer, there still appears to be a main bang on the A-scan. Clearly, this main bang is not an acoustic wave; rather it is some sort of ringing inside the PowerBox. By virtue of improved impedance matching, MsS circuits have a reduced dead zone compared to ribbon cables.

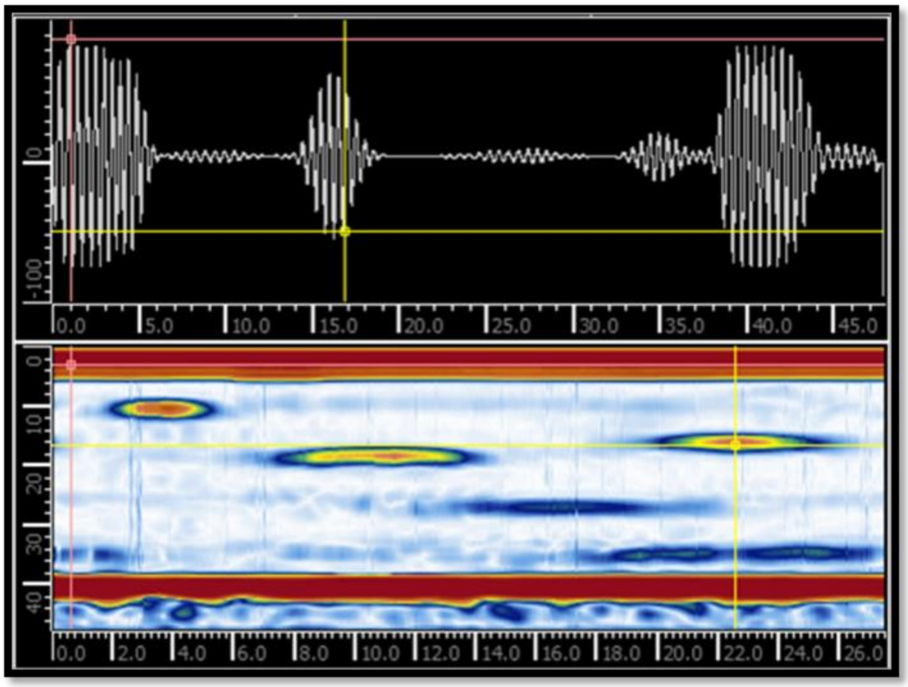

Figure 31: Scan of 8" schedule 40 steel pipe with 3.25" MsS circuit, pulsed at 125 kHz.

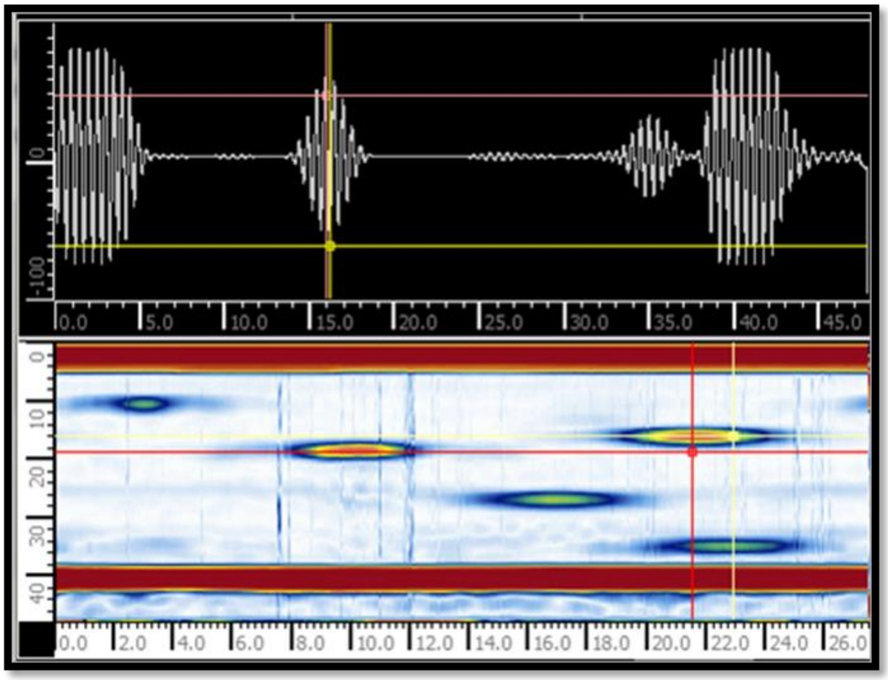

Figure 32: Scan of 8" schedule 40 steel pipe with 6.5" linear MsS circuit, pulsed at 125 kHz.

The focused circuits give interesting results. Even when the transducer is focused in the opposite direction of the targets (see Figure 34 or 36), it still sees the targets, but not as well as when it is focused on them – clearly the focusing does make a difference. The circuit with 24 inch focal length gives excellent results for close range inspection – to see this, compare the strength of the first target (visible in the top left of the B-scan) between the 24 inch focused circuit (Figure 33) and the 36 inch focused circuit (Figure 35) or the 6.5" linear circuit (Figure 32.)

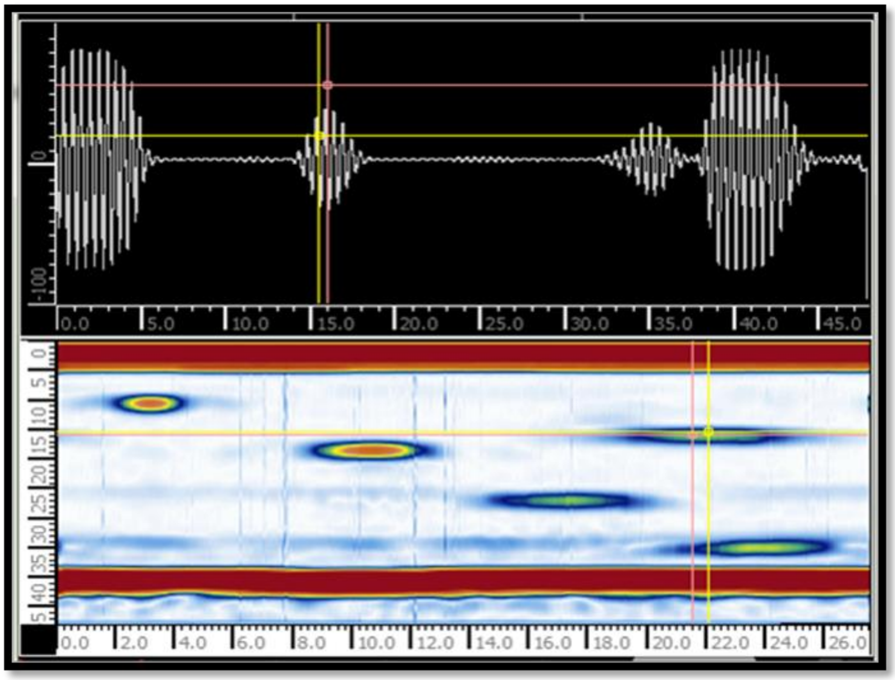

Figure 33: Scan of 8" schedule 40 pipe with 6.5" long MsS circuit with 24 inch focal length. The circuit is focused in the forward direction (towards the targets.)

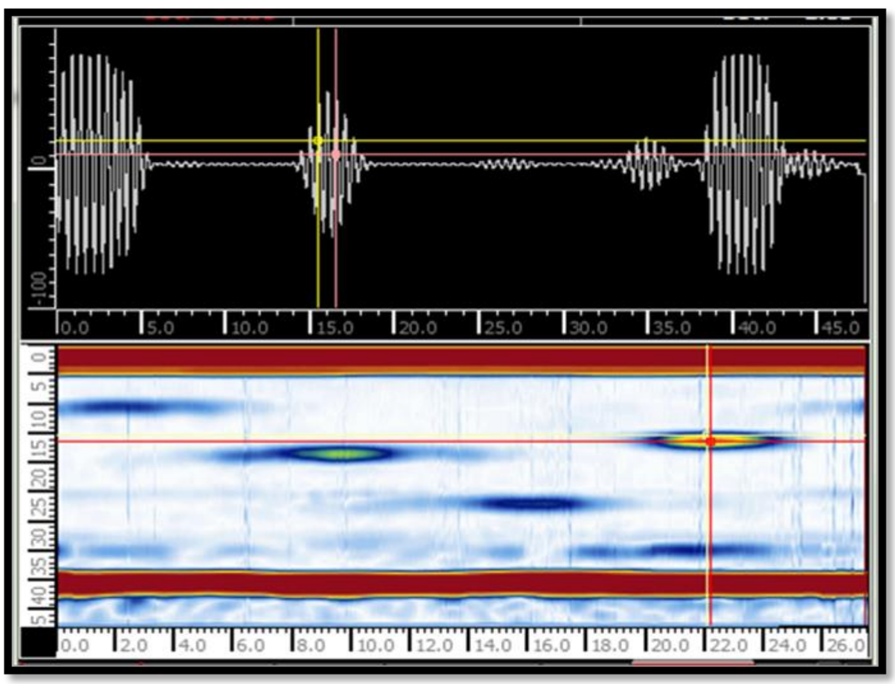

Figure 34: Scan of 8" schedule 40 pipe with 6.5" long MsS circuit with 24 inch focal length. The circuit is focused in the reverse direction (towards the cluster of four pits.)

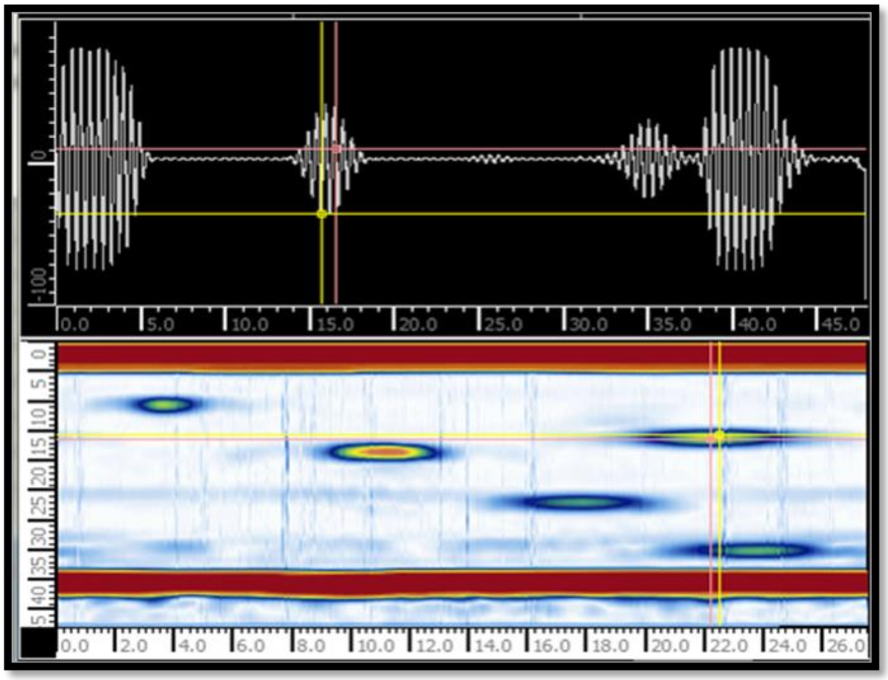

Figure 35: Scan of 8" schedule 40 pipe with 6.5" long MsS circuit with 36 inch focal length. The circuit is focused in the forward direction (towards the targets.)

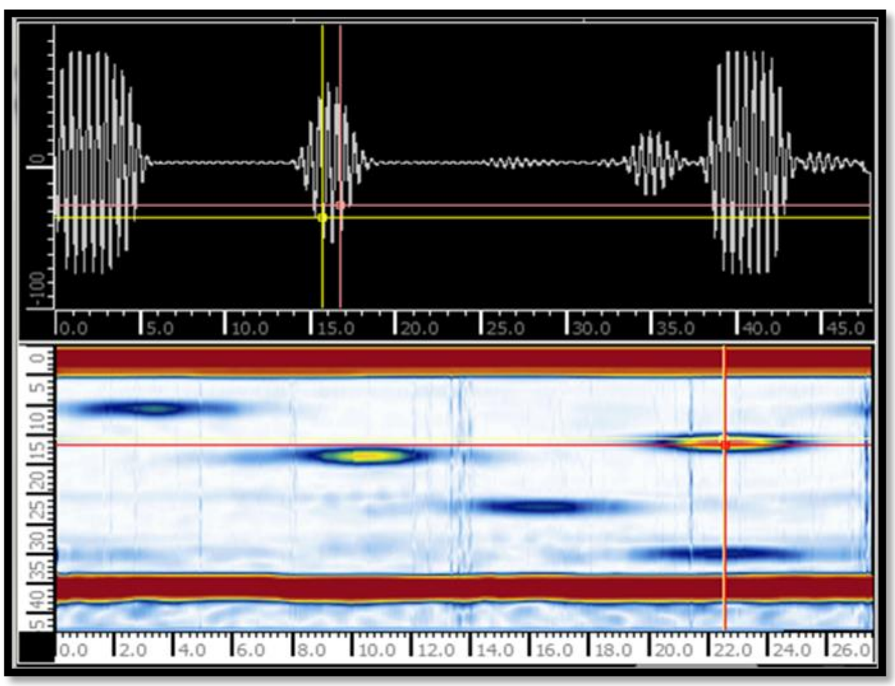

Figure 36: Scan of 8" schedule 40 pipe with 6.5" long MsS circuit with 36 inch focal length. The circuit is focused in the reverse direction (towards the cluster of four pits.)

6.1.3 Target Cross Sections

Plotting the target cross sections is another way to compare the performances of the transducers. Figures 37 and 38 show the cross-section of each target, defined as the length of the reflection in the axial direction, as a function of circumferential position. B-scans are also shown above each cross section plot for reference. The plots were generated in MATLAB using code originally developed by Cody Borigo and modified for data smoothing by the author. The code is available in Appendix A. The 3.25" ribbon cable gives excellent resolution for the first target, but gives wide and weak reflections for the targets which are farther away – possibly due to beam spreading. The 6.5" ribbon gives more consistent reflections for each target, but also shows a wide reflection for the third target. The 6.5" linear (unfocused) MsS circuit shows the 4th target with better resolution than the ribbon cables.

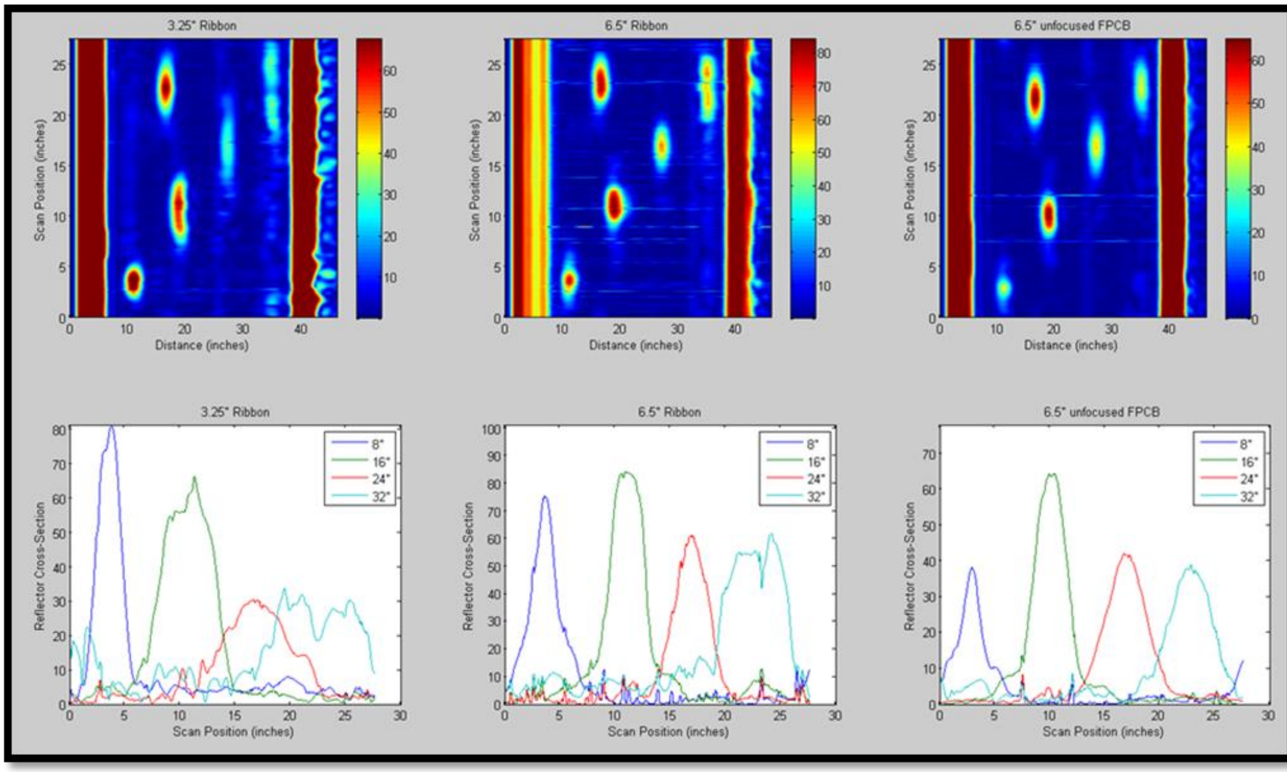

Figure 37: Plots of target cross sections generated from the scans taken with the 3.25" ribbon cable, 6.5" ribbon cable, and 6.5" linear MsS circuit. The blue line corresponds to the target at 8", the green line to the target at 16", the red line to the target at 24", and the turquoise line to the target at 32".

Figure 38 compares the three 6.5" MsS circuits. The 3rd and 4th targets looks almost identical for the three different transducers, suggesting that the focusing does not make much difference at ranges of 20" to 40". Interestingly, the reflection from the first target is significantly stronger when using the circuit with 24" focal length – this matches the results from the PowerBox H display. Also notice that second target gives the strongest reflection, even though the targets themselves are identical. This is most likely due to the fact that there is some extra epoxy around the 2nd target.

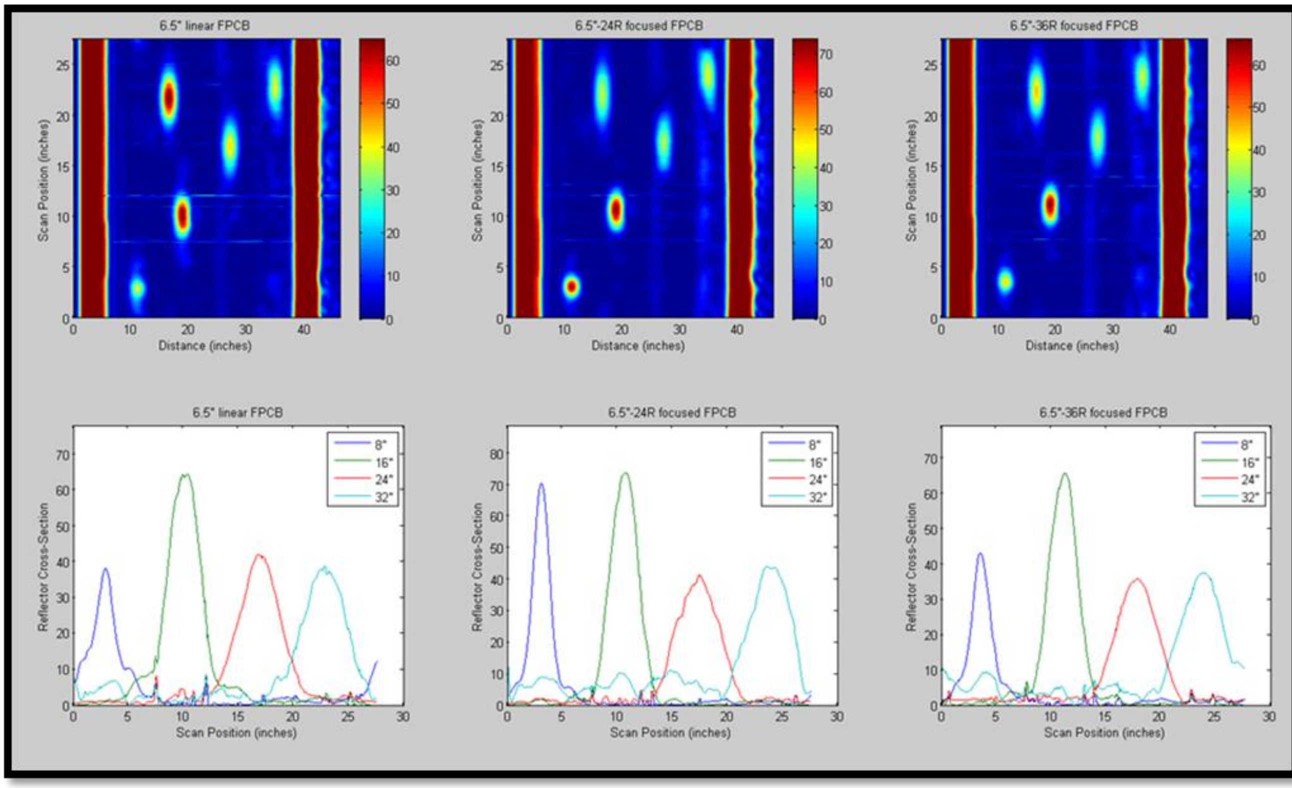

Figure 38: Plots of target cross sections generated from the scans taken with the three 6.5" MsS circuits – from left to right, the linear circuit, circuit with 24" focal length, and circuit with 36 inch focal length. The blue line corresponds to the target at 8", the green line to the target at 16", the red line to the target at 24", and the turquoise line to the target at 32".

6.2 10.5" Pipe with Pitting Corrosion

Once the various transducers and the PowerBox H system were validated on a known pipe, the next logical step was to repeat the tests on a pipe with more realistic defects. A 10.5" diameter steel pipe with pitting corrosion patches was chosen to compare the corrosion detection and mapping abilities of the different transducers. This pipe has distinct corrosion patches located at one axial position around the circumference where a clamp or pipe support was previously attached. A 12x6x1.5mm stainless steel target was also attached to the pipe on the opposite side of the FeCo from the corrosion, so that the amplitudes of the reflections from the corrosion patches could be compared to that of the target.

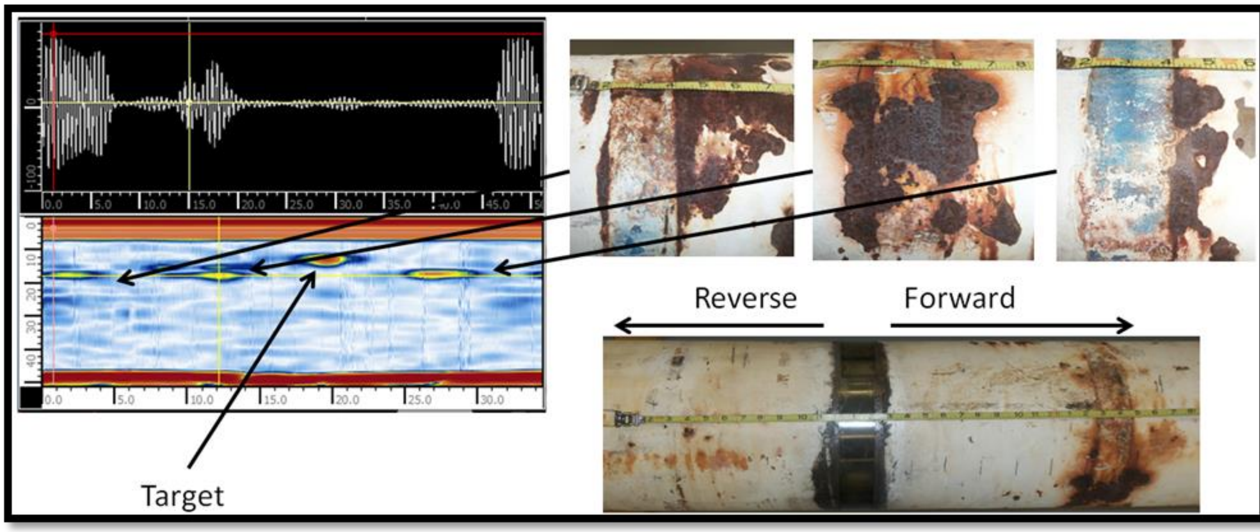

Figure 39: 10.5 inch pipe with pitting corrosion patches around the circumference at the former site of a pipe support. An example display from Powerbox H shows which corrosion patches correspond to which signals on the B-scan.

6.2.1 Ribbon Cable Results

Comparing Figures 40 and 41, it is interesting how the corrosion patches produce stronger signals when using the 6.5" length ribbon cable versus the 3.25" ribbon cable, but the target appears to be roughly the same. One possible explanation is that since the target is a plane reflector, it reflects energy straight back and thus produces a strong signal even with a relatively small aperture transducer. The corrosion pits, on the other hand, are not plane reflectors, and probably produce much more scattered reflections. The 6.5" ribbon cable may do a better job catching these scattered reflections by virtue of its size. It should also be noted that the 6.5" ribbon cable produces waves with less beam spread than the 3.25" ribbon cable. This is because the 6.5” ribbon cable comes closer to exciting a plane wave front, while the 3.25” ribbon cable behaves more as a point source due to its smaller size.

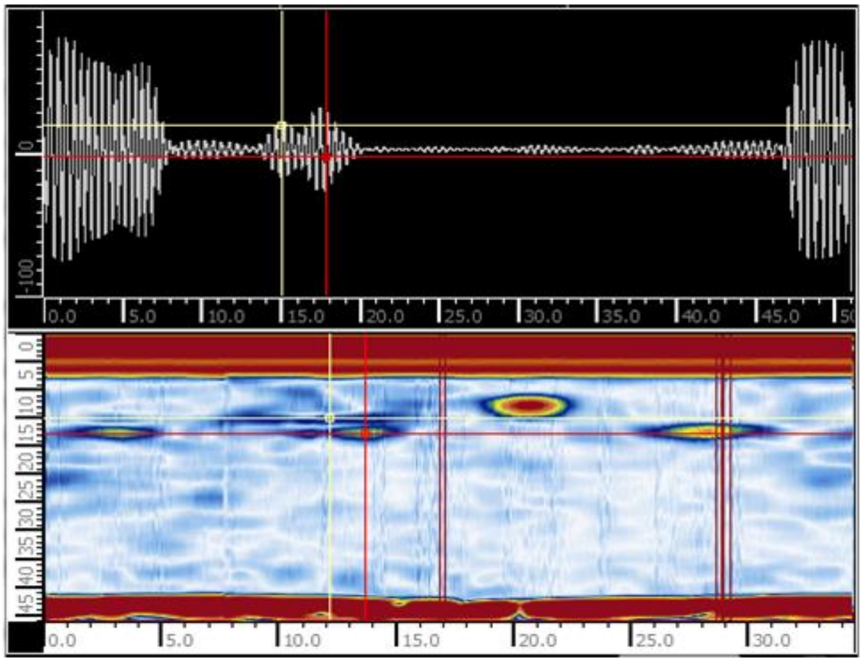

Figure 40: Scan of 10.5” pipe with 3.25" ribbon cable.

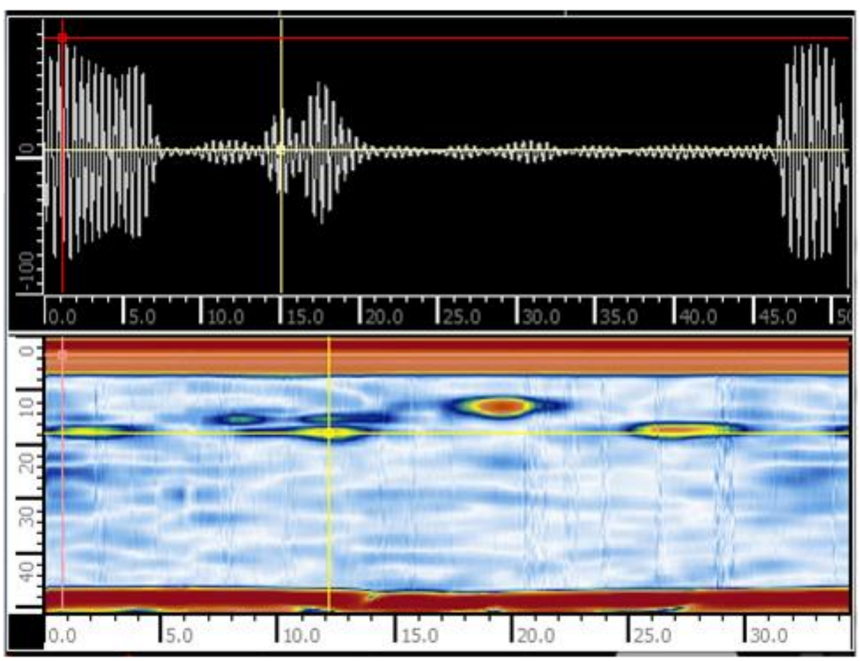

Figure 41: Scan of 10.5” pipe with 6.5" ribbon cable.

6.2.2 MsS Circuit results

The 3.25” and 6.5” linear MsS circuits produce very similar results (see Figures 42 and 43), with only a few differences. The scan from the 6.5” circuit is slightly less noisy, and it also stretches out the corrosion patch that is located between 25 and 30 inches circumferentially on the B-scan. This may be due to the fact that the 6.5” circuit is sending and receiving more energy (by virtue of its greater size), which leads to stronger signals, or it may be due to the size of the 6.5” circuit limiting its circumferential resolution.

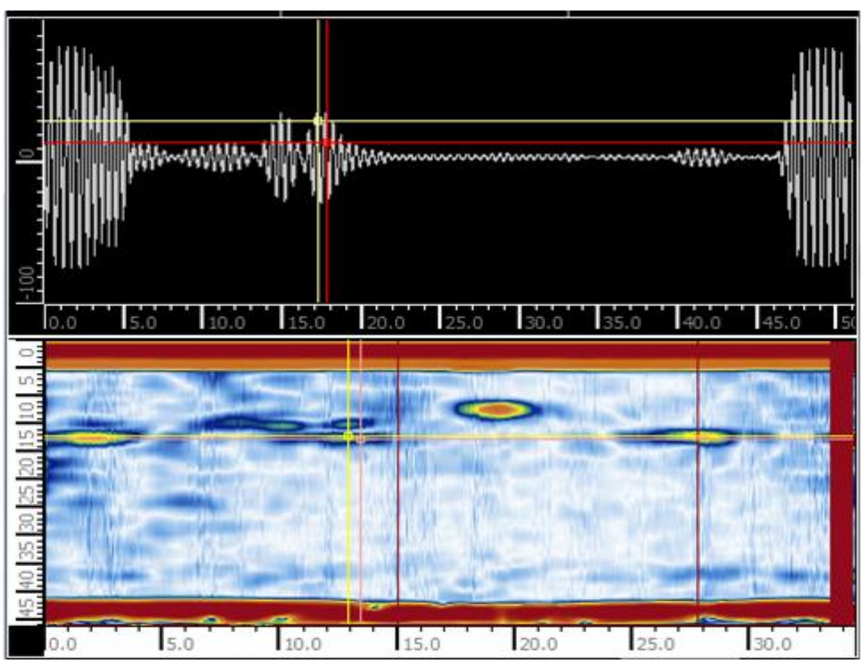

Figure 42: Scan of 10.5” pipe with 3.25" MsS circuit.

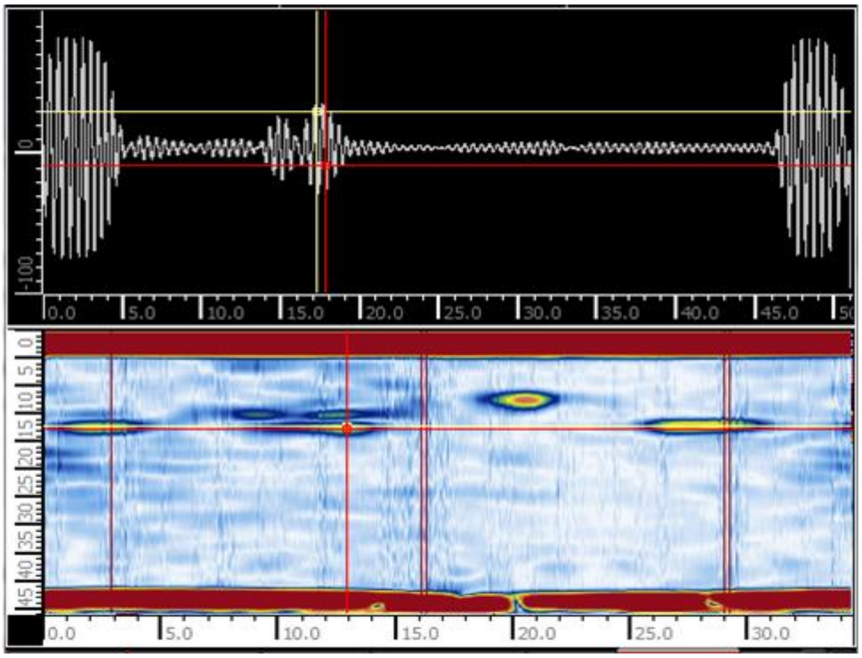

Figure 43: Scan of 10.5" pipe with 6.5" linear MsS circuit.

The 6.5" MsS circuits with focal lengths of 24 and 36 inches probably give the best results on the 10.5" pipe, clearly showing strong signals from each pitting corrosion site. The circuit with 24" focal length does a poor job seeing the target, although the target is in the opposite direction of the focusing. Interestingly, the circuit with 36" focal length does a much better job of seeing the target. Perhaps this is because, just as the 24" focal length circuit would be more focused on a target at 12 inches in the forward (i.e. focused) direction than would the 36" focal length circuit, it is also more out-of-focus than the 36" focal length circuit on a target that is 12" away in the reverse (i.e. unfocused) direction.

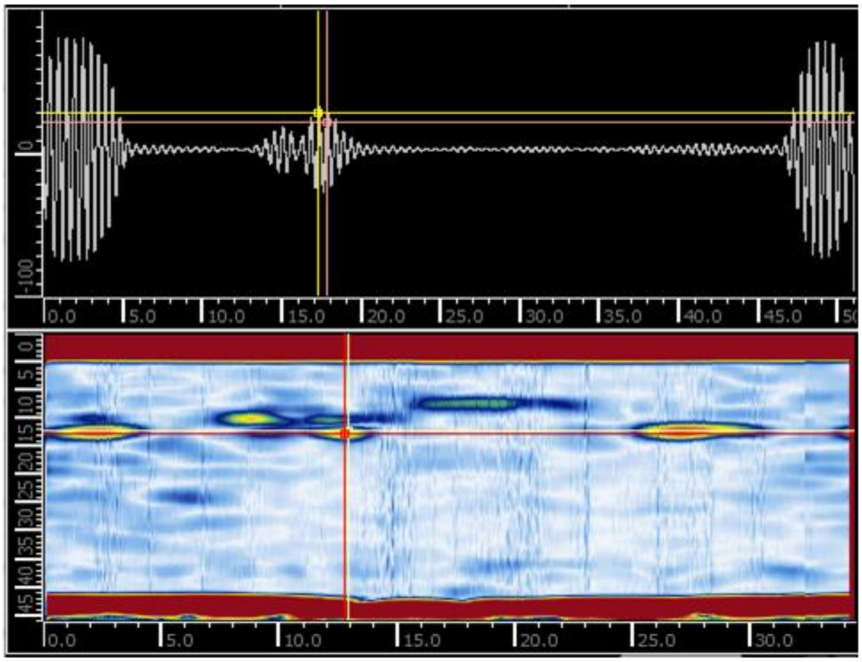

Figure 44: Scan of 10.5" pipe with 6.5" MsS circuit, 24" focal length, focused in the direction of corrosion.

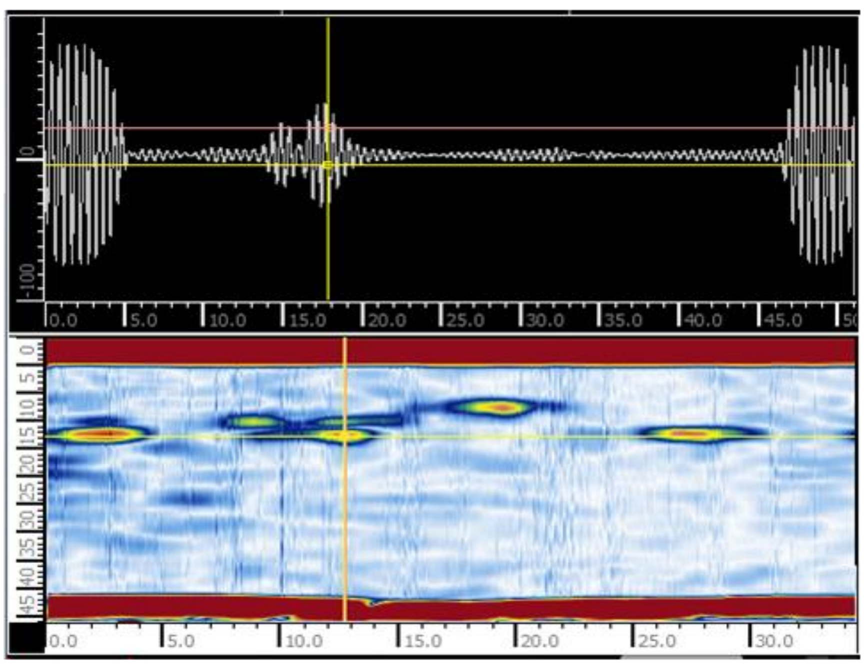

Figure 45: Scan of 10.5" pipe with 6.5" MsS circuit, 36" focal length, focused in the direction of corrosion.

6.3 16” Pipe with Hole and Simulated Pitting

The tests done on the 10.5” pipe demonstrate that the different transducers and the PowerBox H system can map real pitting corrosion that is spread circumferentially around a pipe. While corrosion mapping ability is certainly necessary for any pipe inspection system, another important criterion is the ability to distinguish different defects that are in close proximity. To compare the performance of the different transducers at distinguishing closely spaced defects, a third test was devised using a 16” diameter steel pipe with a small hole that goes completely through the thickness of the pipe wall. A smaller cluster of spherical pits, meant to simulate pitting corrosion, was created about three inches away from the hole using a magnetic drill press. A simulated corrosion patch from a previous experiment was also present in the reverse direction; this is visible as the light blue signal at the bottom of the B-scan. As in the tests on the 10.5” pipe, a stainless steel target was bonded to the pipe in the reverse direction for comparison purposes. Instead of wrapping FeCo around the entire circumference as done on the 8” and 10.5” pipes, FeCo was only wrapped around a 19” arc of the pipe, since this was the entire scan area required for the test.

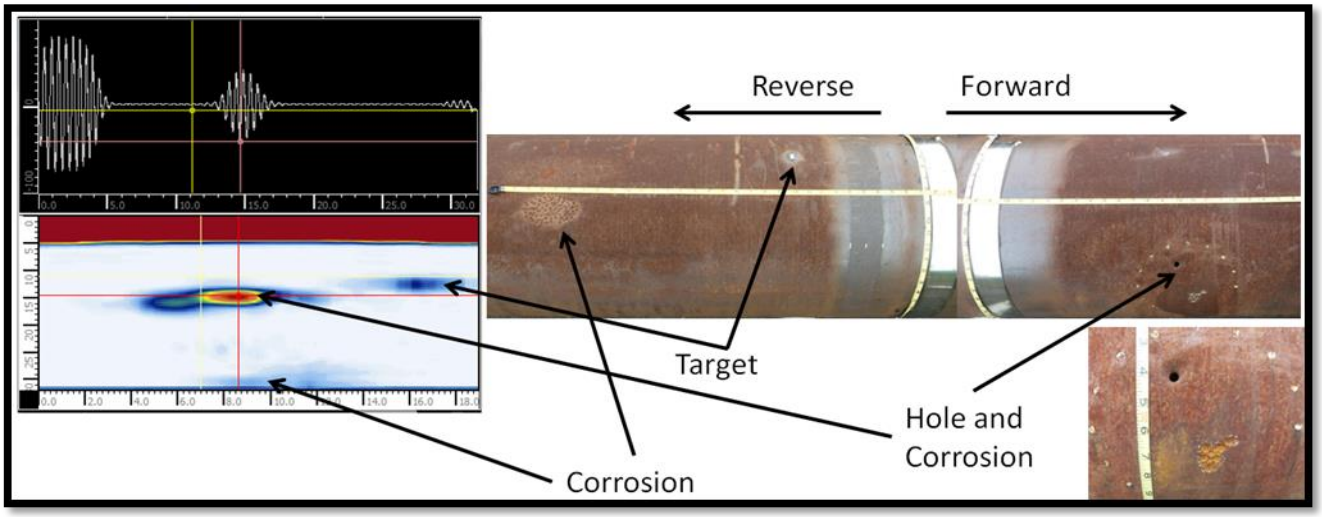

Figure 46 16” pipe with a hole and simulated pitting corrosion in close proximity. The example PowerBox display shows which signals correspond to which defects.

Figure 47: Close-up view of the hole and the simulated pitting corrosion. These two defects are a mere 3” apart.

6.3.1 Ribbon Cable Results

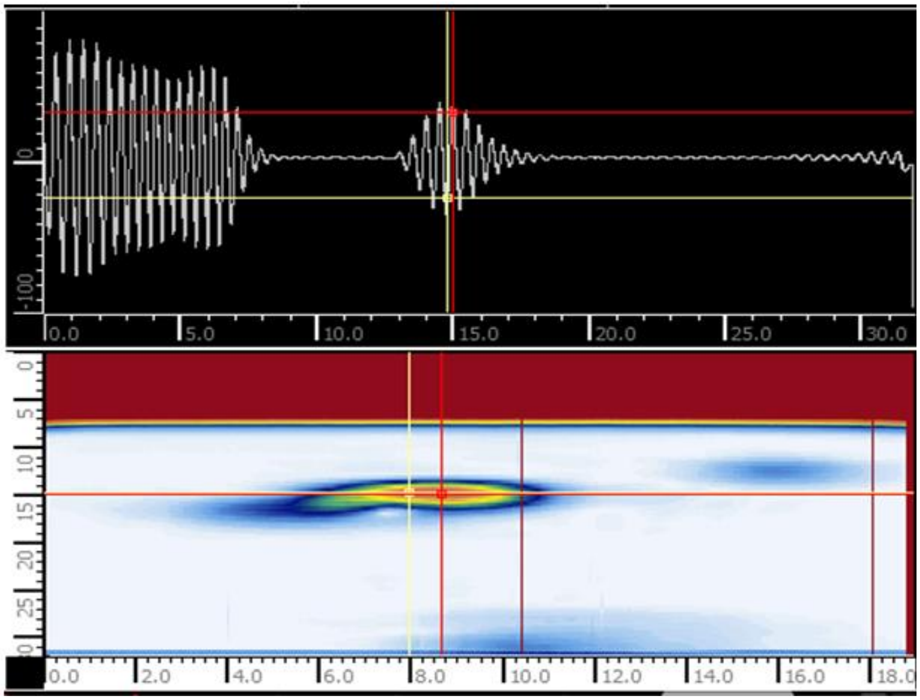

Figure 48: Scan of 16” pipe with 3.25” ribbon cable.

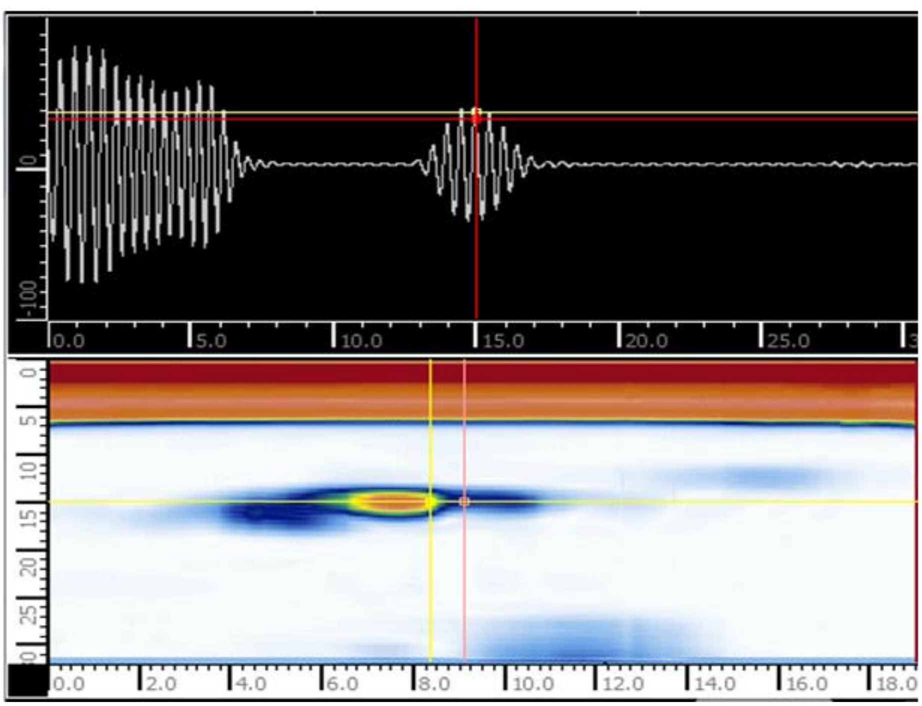

Figure 49: Scan of 16” pipe with 6.5" ribbon cable.

In the scans taken with the 3.25" and 6.5" ribbon cables (Figures 48 and 49, respectively), it is difficult to distinguish the pits from the hole. The hole appears clearly as a bright reflection, with the pits showing up as a second reflection arriving slightly later axially and slightly sooner circumferentially. With the 3.25" ribbon cable, the pits look like a curved tail attached to reflection from the hole. Without prior knowledge of the two defects, an inspector would likely interpret this as a single defect. The scan provided by the 6.5" ribbon cable shows the reflection from the pits as being slightly more distinct, but still somewhat merged with the reflection from the hole.

6.3.2 MsS Circuit Results

In the scans taken with the 3.25" and 6.5" linear MsS circuits (Figures 50 and 51, respectively), it is also difficult to distinguish the pits from the hole. The 3.25" MsS circuit provides the least resolution, and the 6.5" linear circuit provides some indication that there may be two separate defects, but it probably still would not be clear to an inspector without prior knowledge.

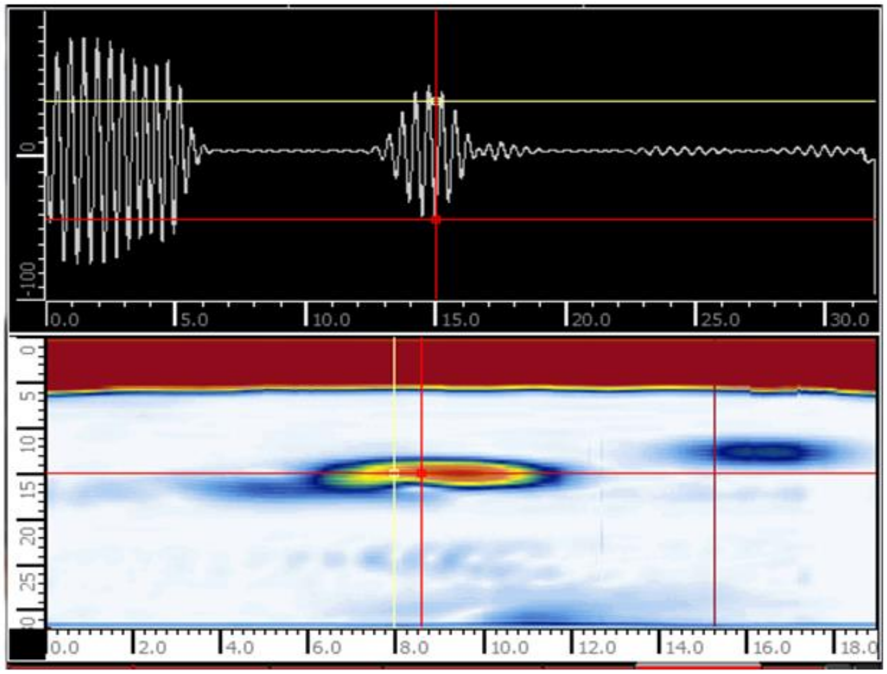

Figure 50: Scan of 16” pipe with 3.25” MsS circuit.

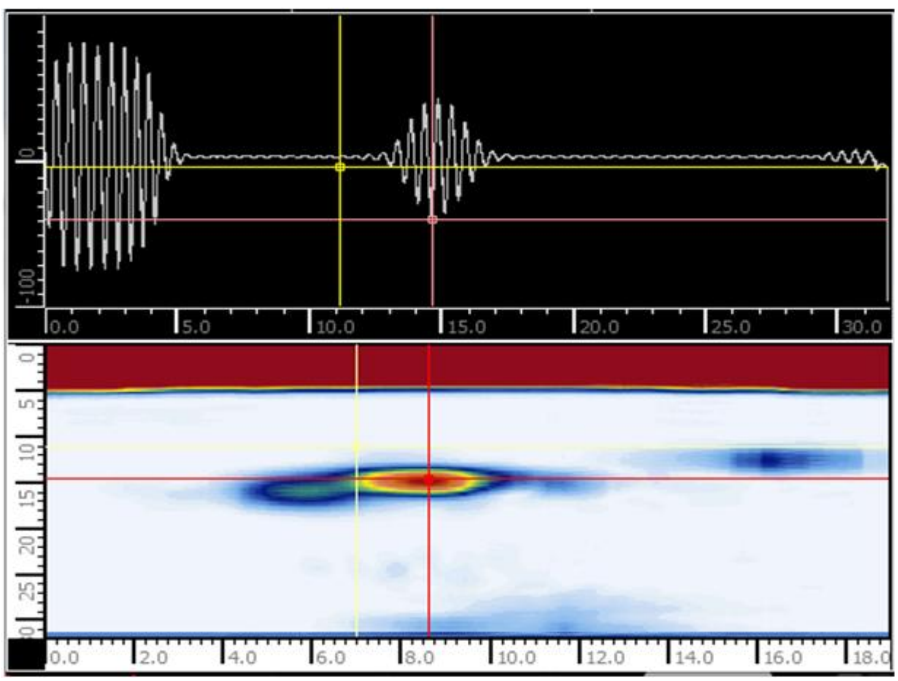

Figure 51: Scan of 16” pipe with 6.5" linear MsS circuit.

The scans taken with the focused MsS circuits provide the best results for distinguishing the pits from the hole. The pits appear as a separate, distinct reflection in both the scan taken with the circuit with 24” focal length (Figure 52) and the scan taken with circuit with 36” focal length (Figure 53). The reflection from the pits is weaker than the reflection from the hole, but this is expected since the pits are a much smaller change in cross sectional area (CSA) of the pipe than the hole is.

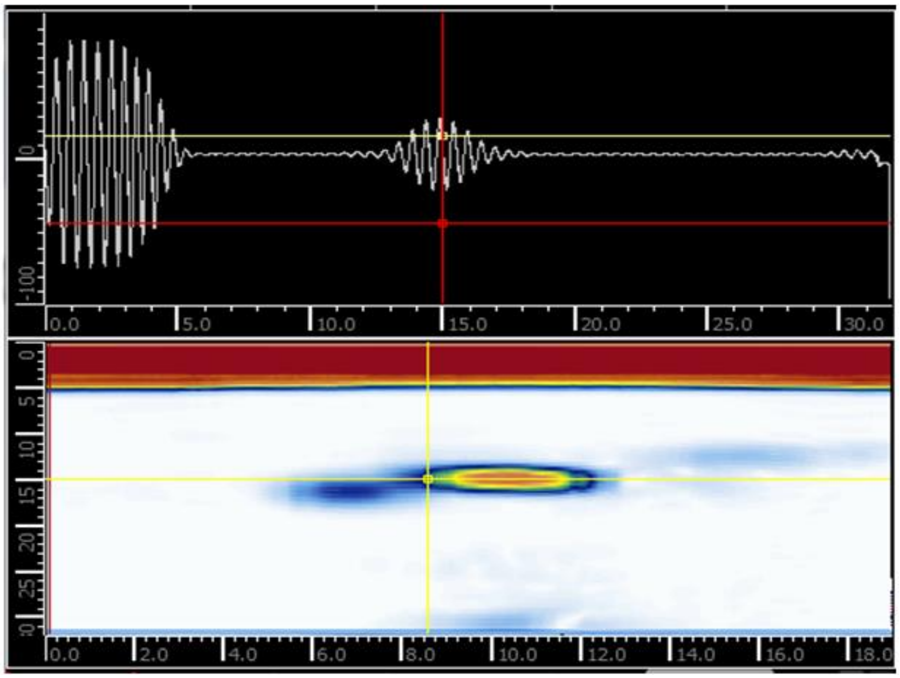

Figure 52: Scan of 16” pipe with 6.5” MsS circuit, 24” focal length, focused in direction of hole and pits.

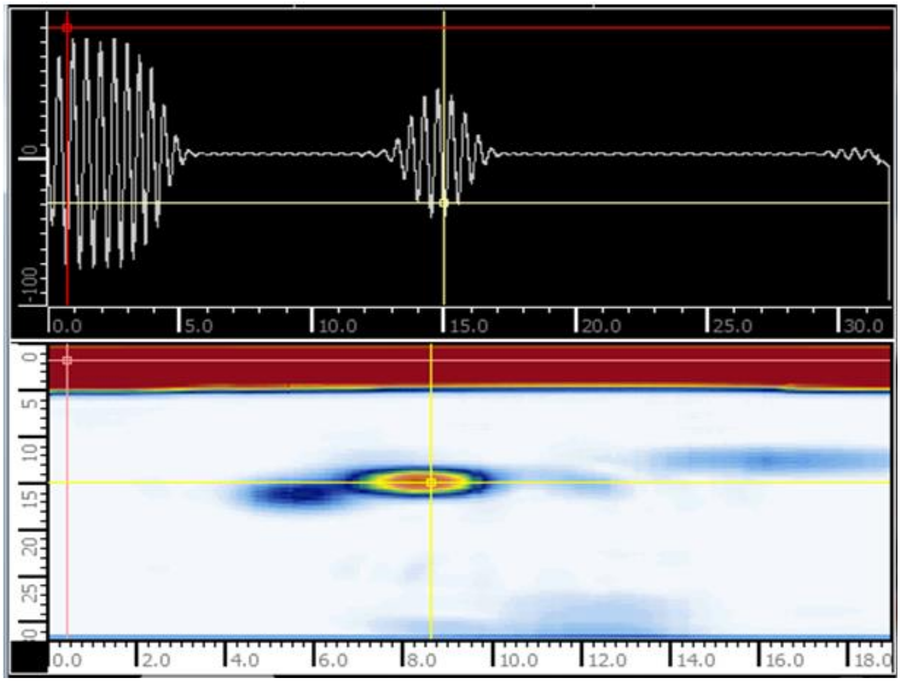

Figure 53: Scan of 16” pipe with 6.5” MsS circuit, 36” focal length, focused in direction of hole and pits.

6.4 16” Pipe with Large Corrosion Patch

The ability to detect and characterize large corrosion patches is an important criterion for pipe inspection systems. The tests done on the 10.5” pipe demonstrated that the different transducers and the PowerBox H can detect pitting corrosion patches, but it did not test their performance at sizing larger corrosion patches. To evaluate the different transducers’ capability to characterize (i.e. size) a large corrosion patch, each transducer was tested on a 16” pipe with a very large simulated pitting corrosion patch – shown in Figure 54. The simulated pitting corrosion patch was created by grinding the outer surface of the pipe to reduce the wall thickness by several millimeters, and then drilling many small, spherical pits into the surface. Prior to testing, it was not known whether such a large corrosion patch would appear on the B-scan as a large defect, or whether the front and back edges of the corrosion patch would appear as separate defects, since the edges are where the most drastic changes in cross sectional area (CSA) occur.

Figure 54: 16" diameter pipe with large simulated pitting corrosion patch, visible to the left of the FeCo strip. The corrosion patch was made by first grinding down the surface to thin the pipe wall, and then drilling many small spherical pits. The grinding reduced the wall thickness by a few millimeters, and each pit is another few millimeters deep.

6.4.1 Results

The scan taken using the 3.25" ribbon cable (Figure 55) gives good results, clearly showing a large series of reflections from the area of the pitting corrosion patch. As expected, the strongest reflections originated from the front and back of the corrosion patch, due to the large change in CSA. However, some reflections also originate from the middle of the corrosion patch due to the pitting, which makes it apparent that there is a large, continuous defect rather than two separate defects.

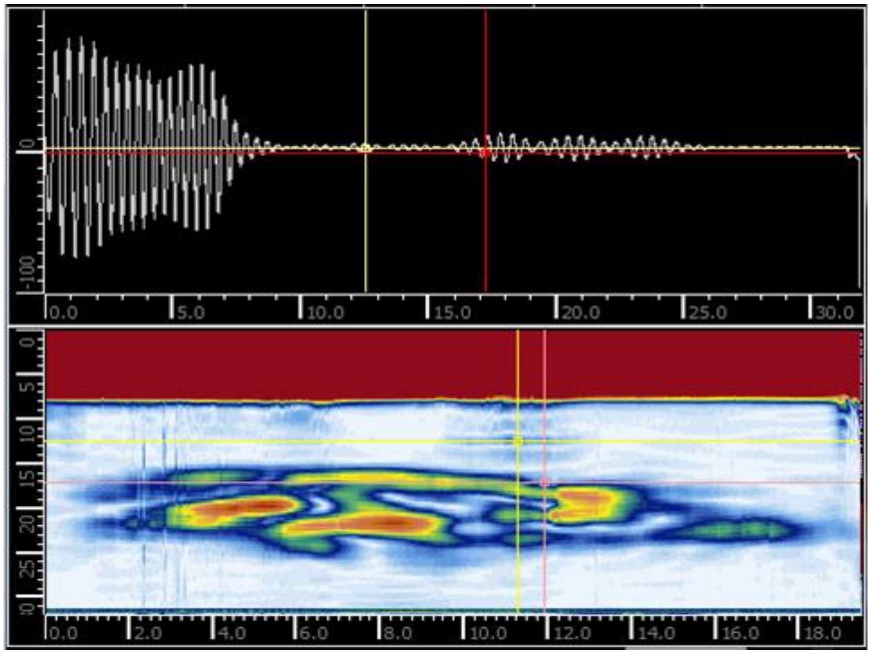

Figure 55: Partial scan of 16" pipe with large corrosion patch using 3.25" ribbon cable.

Unfortunately, the scans taken with the transducers other than the 3.25" ribbon cable show extra ringing after the main bang, as shown in Figure 56. Notice in the A-scan of Figure 56 that the reflection from the pitting corrosion is also very weak. The source of this ringing is not known, but it may be due to the transducer running off the side of the FeCo strip. Since conclusions cannot be drawn from scans with inexplicable ringing, these defective scans are omitted (except for the example in Figure 56).

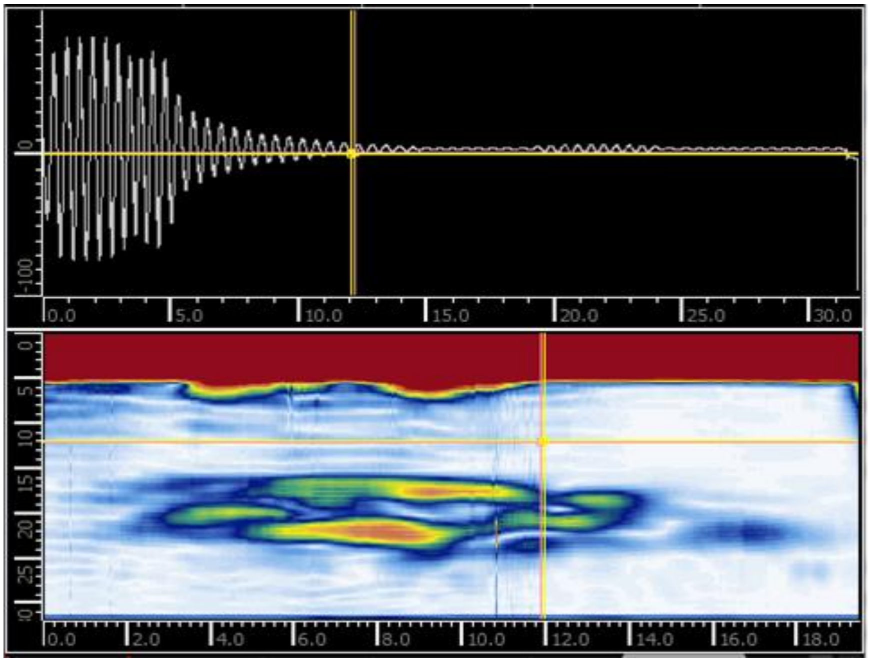

Figure 56: Partial scan of 16" pipe with large corrosion patch using 3.25" MsS circuit. Notice the prolonged ringing after the main bang in both the A-scan and the B-scan.

6.5 4.5” Pipe with Attenuative Coating

To reduce corrosion, many pipes are encased in protective coatings. Coatings rule out the possibility of NDE techniques that require access to the surface, such as visual inspection, liquid penetrant testing, and magnetic particle inspection to name a few. Although ultrasonic guided wave inspection is known to have some capability to detect defects hidden underneath coatings, coatings do present challenges for guided wave inspection. Soft, sticky coatings act as viscoelastic layers coupled to the outer surface of the pipe. Unlike water, viscoelastic materials can support shear stresses, so energy leakage from SH or T modes is likely, resulting in rapid attenuation and diminished range. To evaluate the inspection capabilities of the MsS transducers to detect defects under coatings by exciting the SH_0 mode, a tar wrap coating was applied to a section of 4.5” steel pipe for testing. Small pieces of the tar were then cut away and stainless steel test targets (12x6x1 mm) were added at various positions around the circumference at distances of 8 inches, 12 inches, 16 inches, and 20 inches into the tar-covered section. A small spherical pit (a remnant from previous testing) was also present on the pipe just before the green tar wrap. The tar was very sticky and viscoelastic in nature (as shown in Figure 58) and therefore was expected to increase attenuation.

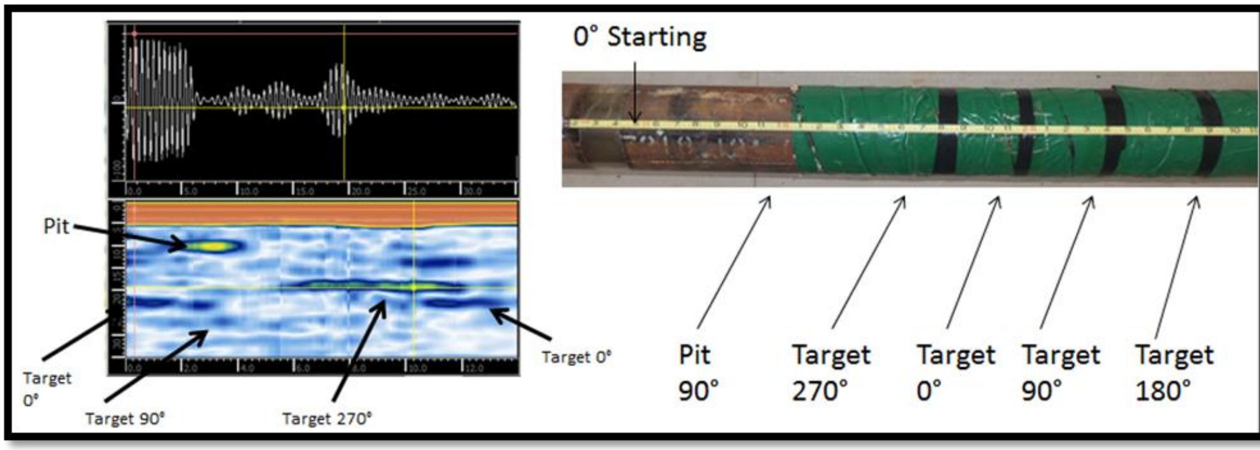

Figure 57: 4.5 diameter steel pipe with tar wrap coating. Four targets were placed underneath the coating, and a small pit was also present just before the tar wrap.

Figure 58: The tar was very sticky and viscoelastic. Notice the air bubbles under the wrap, indicating that the coupling between the tar wrap and the pipe may be highly variable. Adhesion between the tar and pipe should attenuate SH waves due to energy leakage.

6.5.1 Results

The 3.25" MsS circuit was tested first, leading to mixed results as shown in Figure 59. The first and second targets, which are 8" and 12" deep into the tar region, respectively, are clearly visible. The third target, positioned at 90°, is also visible but the signal is faint. Noise is visible throughout the B-scan, possibly due to inconsistent coupling between the tar wrap and the pipe.

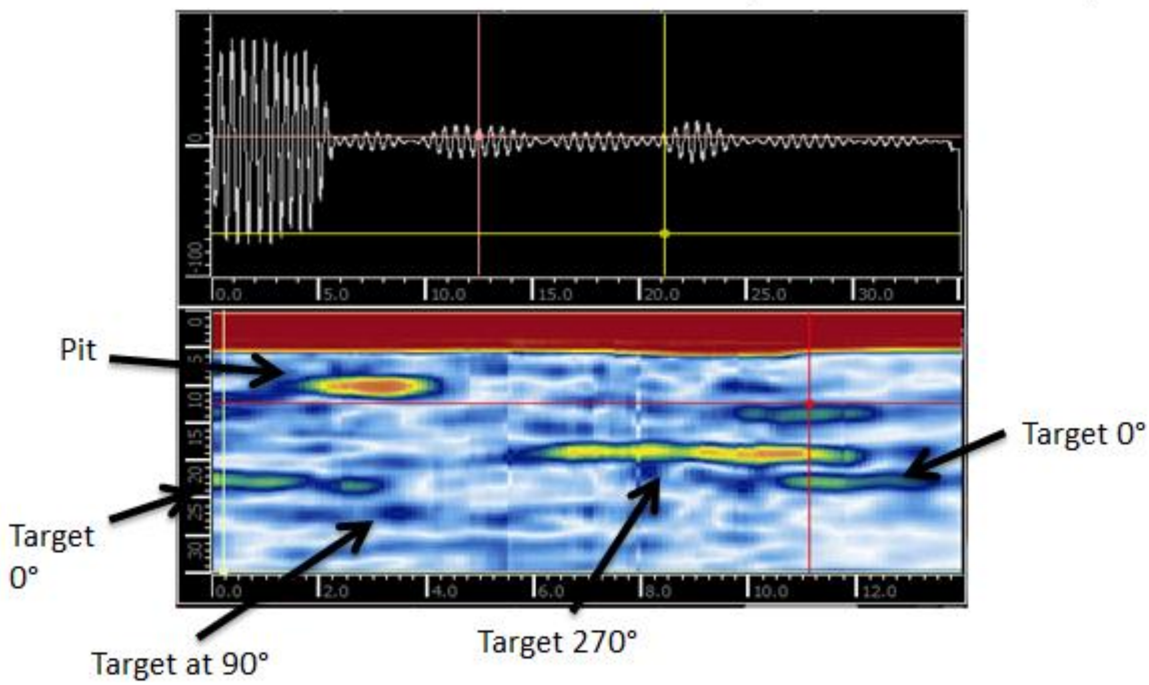

Figure 59: Scan of 4.5" pipe with tar wrap coating taken with 3.25" MsS circuit.

One way to overcome attenuation is to send and receive more energy by using a larger transducer. Since attenuation due to the tar wrap seemed to be limiting the performance of the 3.25" MsS circuit, the 6.5" linear circuit was tested next to see if it might provide better results. Impressively, the 6.5" circuit provided outstanding results. Both the 3rd and 4th targets, which were 16” and 20” deep into the tar region, respectively, were made clearly visible with the 6.5” circuit (see Figure 60). The scan is also less noisy than the scan taken with the 3.25” circuit, and the reflection from the target at 270° is less elongated.

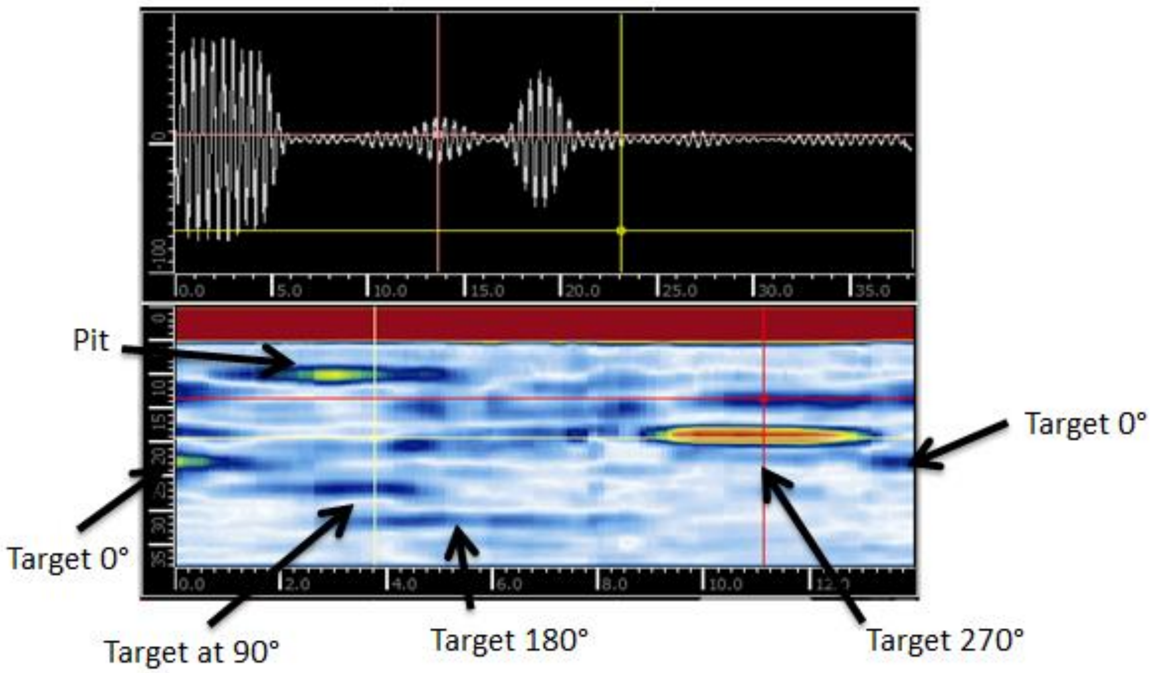

Figure 60: Scan of 4.5” pipe with tar wrap coating taken with 6.5" MsS circuit.

Chapter 7 Concluding Remarks

7.1 Summary

From the outset, the goal of this research was to determine what types of inspection problems may be studied using the prototype MRUT probe, Innerspec PowerBox H, and different magnetostrictive transducers. To that end, experiments were conducted on pipes with targets as well as pipes with pitting corrosion and a pipe with a viscoelastic coating. These tests yielded practical results, giving insight on the performance characteristics of MsS circuits and ribbon cables, as well as showing which MsS circuits are best suited to particular applications.

For the author, this research turned out to be a great learning experience touching on many subjects. Reviewing the literature provided background knowledge on the importance of nondestructive evaluation and structural health monitoring, the strengths and weaknesses of common NDE techniques, and the processes responsible for structural defects. Designing and conducting the experiments fostered a greater understanding of the magnetostrictive effect, comb transducer design, and general ultrasonic testing equipment and principles. Mode selection for the experimentation required an understanding of guided wave theory and dispersion, as well as the use of the finite element software ABAQUS to model elastic wave propagation. Besides the technical skills and knowledge gleaned, valuable lessons were also learned about project management, working both independently and in a team, sharing results, and overcoming the challenges that are frequently encountered during research and development.

7.2 Contributions

During this thesis, several discoveries were made with regard to the performances of the different transducers. This information could be very useful in designing an improved system or set of guidelines for medium range corrosion mapping using SH waves excited by magnetostrictive transducers. Initial testing on the control pipe showed that the "dead zone" of the MsS circuits is several inches shorter than that of ribbon cables, likely due to improved impedance matching. Since the MsS circuits have such a short dead zone, they could be used for inspection of inaccessible areas, i.e. where the transducer must be mounted close to the area of interest. It was also observed that the high voltage of the PowerBox system de-poles the FeCo, leading to progressively weaker signals unless the FeCo is re-poled regularly with a permanent magnet – this can be corrected by re-poling the FeCo frequently or possibly by modifying the PowerBox to reduce the voltage. Testing on the different pipes also showed that the MsS circuit designed for a 24" focal length performed very well for close range inspection of defects about 10" away. The testing on the 16" pipe with pitting and a hole in close proximity demonstrated that the focused MsS circuits could differentiate the two defects, while the other transducers could not. From the tests on the pipe with tar coating, it was also learned that using a larger transducer (6.5" vs. 3.25" aperture) can make tremendous improvement in the ability to detect defects hidden underneath an attenuative coating. Currently these insights may be useful for NDE inspectors who rely on magnetostrictive systems. In the future, this information could be incorporated during the design process of an improved PowerBox type system, and of new MsS circuits with different apertures and geometries suited to different applications. By providing this useful new information, this research could contribute to improvements in the reliability and affordability of pipeline NDE – leading to lower cost and improved safety for society at large. A short list of the major findings is given below:

- MsS circuits offer shorter dead zone than ribbon cables
- The high voltage of the PowerBox de-poles FeCo, this should be corrected
- The 24” focal length MsS circuit is superior for close range (~10”) inspection
- The focused MsS circuits have the best circumferential resolution for differentiating closely spaced defects
- Using larger aperture circuits improves inspection capability underneath attenuative coatings, targets up to 20” under the coating may be indentified

7.3 Suggestions for Further Research

A single thesis is inherently limited to what can be completed in a few months or years, and new questions are often uncovered during the course of research. For example, in this thesis it was discovered that the MsS circuit with 24” focal length works best for close range inspection – but why? This question could be the basis of further experiments leading to improved design of focused MsS comb transducers. This thesis gives insightful results for external corrosion mapping, and many more practical experiments could be conducted to expand upon this. Realistic experiments could be conducted using the same equipment to evaluate performance for other areas of pipe where corrosion is common. For example, a partially buried pipe could be tested to see if defects can be detected near the ground-surface interface, or a pipe could be tested to investigate detection of defects near supports. Although pipe elbows are a complicated wave guide, there is also the possibility to inspect for internal corrosion at elbows, and this would be valuable research as well.

Appendix A

A.1 MATLAB code for target cross sections with smoothing

The following code, used to generate the target cross section plots in Chapter 6.1, was originally developed by Cody Borigo and lightly modified by the author. A smoothing function was added.

```
%% Parameters
c = 3120;  %wave speed

Fs = 10e6;  %sampling frequency 10 MHz
N = 7503;    %number of samples
time = 0:1/Fs:(N-1)/Fs;

dx = 0.04*.0254;  %encoder pitch in inches converted to meters
Nx = 690;  %number of circumferential data points (length/pitch)
x = 0:dx:dx*(Nx-1);

folder = 'C:\Users\FBS014\Documents\PowerBox Data for MATLAB\';
files = {'325ribbon.csv','65ribbon.csv','65ufc.csv'};
filenum = size(files,2);

f1 = 100e3;
f2 = 150e3;
[b a] = butter(4,[f1 f2]/(Fs/2));  %bandpass filter between f1 and f2

%% Import Data
data = zeros(Nx,N,filenum);
filtdata = zeros(size(data));
hilbdata = zeros(size(data));
for fi = 1:filenum
    data(:,:,fi) = dlmread([folder files{fi}]);
    for xi = 1:Nx
        filtdata(xi,:,fi) = filter(b,a,data(xi,:,fi));
        hilbdata(xi,:,fi) = abs(hilbert(filtdata(xi,:,fi)));
    end
end

%% Measure Reflections
```

```
targetDist = [9.8 17.8 26.5 33.8; 11.8 19.6 28 35.8];  %axial length target
search area pairs
targetInx = round(targetDist*.0254/c*Fs*2);
target = zeros(Nx,size(targetDist,2),filenum);
targetrel = zeros(Nx,size(targetDist,2),filenum);
targetsmooth = zeros(Nx,size(targetDist,2),filenum);
peakinx = zeros(size(targetDist,2),filenum);
for fi = 1:filenum
    for ti = 1:size(targetDist,2)
        [~,inx] = max(max(hilbdata(:,targetInx(1,ti):targetInx(2,ti),fi)));
        target(:,ti,fi) = hilbdata(:,targetInx(1,ti)+inx-1,fi);
        targetrel(:,ti,fi) = target(:,ti,fi)/max(target(:,ti,fi));
        targetsmooth(:,ti,fi) = smooth(1:Nx,target(:,ti,fi));
        [temp,peakinx(ti,fi)] = max(target(:,ti,fi));
    end
    cmax(fi) = max(target(:,2,fi))/max(max(hilbdata(:,:,fi)))*100;
%#ok<SAGROW>
end

targetshift = zeros(size(target));
for fi = 1:filenum
    for ti = 1:size(targetDist,2)
        targetshift(:,ti,fi) = circshift(targetrel(:,ti,fi),[peakinx(ti,1)-
peakinx(ti,fi), 0, 0]);
    end
end

%% Plot Images
titles = {'3.25" Ribbon','6.5" Ribbon','6.5" unfocused FPCB'};
distances = {'8"','16"','24"','32"'};

figure(1)
set(gcf,'Position',[40 87 1818 877])
for fi = 1:filenum
    subplot(2,filenum,fi)

pcolor(c*time(1:10:end)/2/.0254,x/.0254,hilbdata(:,1:10:end,fi)/max(max(hilbd
ata(:,:,fi)))*100)
    xlabel('Distance (inches)')
    ylabel('Scan Position (inches)')
    shading interp
    caxis([0 cmax(fi)])
    title(titles{fi})
    colorbar

    subplot(2,filenum,fi + filenum)
    plot(x/.0254,target(:,:,fi)/max(max(hilbdata(:,:,fi)))*100)
    xlabel('Scan Position (inches)')
    ylabel('Reflector Cross-Section')
    ylim([0 cmax(fi)*1.2])
    title(titles{fi})
    legend(distances,'Location','Northeast')
end
```

```
figure(2)
set(gcf,'Position',[-1612 110 1531 838])
for ti = 1:size(targetDist,2)
    subplot(2,size(targetDist,2)/2,ti)
    plot(x/.0254,squeeze(targetshift(:,ti,:)))
    xlabel('Scan Position (inches)')
    ylabel('Reflector Cross-Section')
    ylim([0 1.25])
    title(distances{ti})
    legend(titles,'Location','Northeast')
end

figure(3)
set(gcf,'Position',[40 87 1818 877])
for fi = 1:filenum
    subplot(2,filenum,fi)

pcolor(c*time(1:10:end)/2/.0254,x/.0254,hilbdata(:,1:10:end,fi)/max(max(hilbd
ata(:,:,fi)))*100)
    xlabel('Distance (inches)')
    ylabel('Scan Position (inches)')
    shading interp
    caxis([0 cmax(fi)])
    title(titles{fi})
    colorbar

    subplot(2,filenum,fi + filenum)
    plot(x/.0254,targetsmooth(:,:,fi)/max(max(hilbdata(:,:,fi)))*100)
    xlabel('Scan Position (inches)')
    ylabel('Reflector Cross-Section')
    ylim([0 cmax(fi)*1.2])
    title(titles{fi})
    legend(distances,'Location','Northeast')
end
```

BIBLIOGRAPHY

[1] "Pipeline and Hazardous Materials Safety Administration -Pipeline Incident 20 Year Trends", 2015, from http://phmsa.dot.gov/pipeline/library/datastatistics/pipelineincidenttrends

[2] "About U.S. Natural Gas Pipelines," 2008, available from: www.eia.gov/pub/oil_gas/natural_gas/analysis_publications/ngpipeline/index.html

[3] Ritenbaugh, S., 2015, "Marcellus Shale Region To See Wave of Large Pipeline Projects," available from the Pittsburgh Post-Gazette

[4] Swartz, A., 2014, "San Bruno remembers: four years after PG&E explosion, Crestmoor neighborhood still being rebuilt," from The Daily Journal

[5] Togneri, C., 2014, "NTSB: Corroded pipe, lack of inspections led to gas explosion in W.V.," from the Pittsburgh Tribune Review

[6] "Pipeline Inspection," The NDT Resource Center, from www.nde-ed.org/AboutNDT/SelectedApplications/PipelineInspection/PipelineInspection.htm

[7] "Introduction to nondestructive testing," The American Society for Nondestructive Testing from https://www.asnt.org/MinorSiteSections/AboutASNT/Intro-to-NDT

[8] Rose, J., 2014, *Ultrasonic Guided Waves in Solid Media*, Cambridge University Press, New York, NY.

[9] Hellier, C., 2013, *Handbook of Nondestructive Evaluation, 2nd Edition*, McGraw-Hill, New York, NY.

[10] Papadopoulos, P., 2008, *Introduction to Continuum Mechanics Notes,* Department of Mechanical Engineering, University of California at Berkeley

[11] Biederman, R., 2005, *Physical Metallurgy Principles Applied to Steels and Other Ferrous Alloys,* Worcester Polytechnic Institute

[12] Callister, W., Rethwisch, D., 2010, *Materials Science and Engineering An Introduction, 8th Edition,* Wiley & Sons, Hoboken, NJ.

[13] "Fatigue Properties," The NDT Resource Center, from https://www.nde-ed.org/EducationResources/CommunityCollege/Materials/Mechanical/Fatigue.htm

[14] "Miner's Rule and Cumulative Damage Models," Issue 116, October 2010, Reliability Hotwire Magazine, from http://www.weibull.com/hotwire/issue116/hottopics116.htm

[15] Scholz, F., "Weibull Reliability Analysis," Boeing Phantom Works, from http://www.stat.washington.edu/fritz/Reports/weibullanalysis.pdf

[16] Jhung, M., Choi, Y., "Surge Line Stress Due to Thermal Stratification," November 5th 2007, Korea Institute of Nuclear Safety, from http://www.kns.org/jknsfile/v40/JK0400239.pdf

[17] Ahmed, W. *Flow Accelerated Corrosion in Nuclear Power Plants, Nuclear Power – Practical Aspects,* 2012, available from: http://www.intechopen.com/books/nuclear-power-practical-aspects/flow-accelerated-corrosion-in-nuclear-power-plants

[18] "Weld Types and Positions," 2015, The Weld Guru, available from http://www.weldguru.com/weldtypesandpositions.html

[19] Davies, A.C., 1972, *The Science and Practice of Welding, 6th Edition,* Cambridge University Press, New York, NY.

[20] Zhang, L., 2005, *Guided Wave Focusing Potential in Hollow Cylinders* (PhD thesis), Department of Engineering Science and Mechanics, The Pennsylvania State University

[21] "Manufacturing Processes," page 10, Catalog of JFE Steel Corporation, available from http://www.jfe-steel.co.jp/en/products/pipes/catalog/e1e-002.pdf

[22] Westin, E., Garrett, D., 2011 "Welded Stainless Steel Pipes & Tubes vs. Seamless," ACOM (a corrosion management and applications engineering magazine), available from http://www.outokumpu.com/sitecollectiondocuments/welded-stainless-steel-tubes-and-pipes-vs-seamless-acom.pdf

[23] Worman, J., 2011, "Liquid Penetrant Examination," The National Board of Boiler and Pressure Vessel Inspectors, available from http://www.nationalboard.org/index.aspx?pageID=164&ID=374

[24] "Penetrant Application and Dwell Time," The NDT Resource Center, available from https://www.nde-ed.org/EducationResources/CommunityCollege/PenetrantTest/MethodsTech/application.htm

[25] "Introduction to Magnetic Particle Inspection," The NDT Resource Center, available from https://www.nde-ed.org/EducationResources/CommunityCollege/MagParticle/Introduction/basicprinciples.htm

[26] Hayes, C., May 1997, "The ABC's of Nondestructive Weld Examination," The Welding Journal of The American Welding Society, available from http://www.ndt.net/article/0698/hayes/hayes.htm

[27] "Introduction to Radiographic Testing," The NDT Resource Center, available from https://www.nde-ed.org/EducationResources/CommunityCollege/Radiography/cc_rad_index.htm

[28] "Radiation Damage to Materials," CANTEACH, a public educational and reference library supported by the Canadian nuclear industry and Canadian universities, available from https://canteach.candu.org/Content%20Library/20040904.pdf

[29] Annila, L., "Nondestructive Testing of Pipelines," CERN, available from http://st-div.web.cern.ch/st-div/workshop/ST2001WS/Proceedings/Poster_3101/Annila.pdf

[30] Nelligan, T., Calderwood, C., "Introduction to Eddy Current Testing," Olympus NDT, available from http://www.olympus-ims.com/en/eddycurrenttesting/

[31] "Basic Principles of Eddy Current Inspection," The NDT Resource Center, available from: https://www.nde-ed.org/EducationResources/CommunityCollege/EddyCurrents/Introduction/IntroductiontoET.htm

[32] Revie, R.W., Reber, K., *Oil and Gas Pipelines: Integrity and Safety Handbook, Chapter 36: Eddy Current Testing in Pipeline Inspection*

[33] "Application Notes: Pipeline Surface Inspection Using Eddy Current Array Technology," Olympus NDT, available from http://www.olympus-ims.com/en/applications/stress-corrosion-crack-detection-pipelines-eddy-current-array/

[34] "NDT Materials Testing: The Story of the Wheeltappers and the Ancient Art of Crack Detection," Aerotech Laboratories, available from: http://www.aerotechlabs.co.uk/ndtmaterialstesting.html

[35] Krautkrämer, J., Krautkrämer, H., *Ultrasonic Testing of Materials, Third Edition*, 1983, Springer-Verlag, Berlin

[36] Rose, J., *Ultrasonic Guided Waves in Solid Media*, 2014, Cambridge University Press, New York, N.Y.

[37] Moore, P.O., Henneke, E., *Nondestructive Testing Handbook, 3rd Edition, Volume 7 Ultrasonic Testing,* Chapter 2, American Society of Nondestructive Testing, Columbus, OH

[38] Hellier, C., 2001, *Handbook of Nondestructive Evaluation,* McGraw-Hill, New York, NY.

[39] "Attenuation of Sound Waves," The NDT Resource Center, available from: https://www.nde-ed.org/EducationResources/CommunityCollege/Ultrasonics/Physics/attenuation.htm

[40] Bertoncini, F., Giunta, G., Raugi, M., Turcu, F., "Overview and Experimental Evaluation of Magnetostrictive Transducers for Guided Wave Inspection," University of Pisa, Italy

[41] Kropf, M., Tittmann, B., "Ultrasonic Magnetostrictive Transducers for Guided Ultrasonic Waves in Thin Wires," The Pennsylvania State University, Department of Engineering Science and Mechanics

[42] Van Velsor, J.K., Royer, R.L., Owens, S.E., Rose, J.L., 2013, "A Magnetostrictive Phased Array System for Guided Wave Testing and Structural Health Monitoring of Pipe," featured article in Materials Evaluation, Vol. 71, No. 11, pp: 1296-1301, The American Society for Nondestructive Testing

[43] du Tremolet de Lacheisserie, E., 1993, *Magnetostriction: Theory and Applications of Magnetoelasticity,* CRC Press, Boca Raton, Florida, USA.

ACADEMIC VITA

Matthew D. Waller
235 Overlook Road, Morgantown PA 19543
mdw5299@psu.edu
814-548-6576

Education

B.S. in Engineering Science, Minor in Engineering Mechanics
Honors in Engineering Science
The Pennsylvania State University
Schreyer Honors College

Honors and Awards

Frasier Merit Award (2014)
Semi-Finalist: NY Times Public Speaking Contest
President Sparks Award

Experience

Engineering Intern (2014-2015)
FBS Inc./Guided Wave
Development of medium range guided wave system for pipe inspection.
Supervisors: Dr. Joseph Rose, Dr. Cody Borigo

Membership

Society of Engineering Science
Phi Eta Sigma